UNIVERSITY OF BIRMINGHAM

MEASUREMENT OF RECOVERY AND RECRYSTALLISATION IN INTERSTITIAL FREE STEELS USING ELECTROMAGNETIC SENSORS

By

Russell Hall

A thesis submitted to

The University of Birmingham

For the degree of

DOCTOR OF PHILOSOPHY

School of Metallurgy and Materials

College of Engineering and Physical Sciences

The University of Birmingham (UK)

September 2016

Abstract

Interstitial free (IF) steel is used extensively throughout applications in the automotive, packaging and furniture industries due to its excellent formability and ductility. IF steel is produced in sheet form through the main processes of casting, hot rolling, cold rolling and annealing. The manufacturing process ensures excellent material properties for subsequent forming processes are developed through the formation of a fine equi-axed grain structure and desired crystallographic texture. Annealing processes for IF steels in modern steel making facilities are carried out in continuous annealing lines (CALs).

The annealing process improves the formability of the cold rolled IF sheet, whilst also reducing strength through the recovery and recrystallisation process. After the cold rolling process the grain structure is heavily deformed, the grains are elongated and possess a very high dislocation density. During the recovery process the dislocation density is reduced through annihilation and redistribution of dislocations to form sub grains. During the recrystallisation process new grains nucleate and grow into new, strain free, grains.

Magnetic properties of ferromagnetic material are known to be affected by microstructural phenomena such as dislocation density, grain boundaries, grain size and texture. It is therefore possible to monitor the recovery and recrystallisation processes using sensors that are responsive to changes in magnetic properties, in particular changes in magnetic permeability. The purpose of the research completed was to establish whether it would be possible to use electromagnetic (EM) sensors to monitor the recovery and recrystallisation processes in-situ during heat treatment, such that EM sensors could then be deployed in a CAL. EM sensors used within a CAL to monitor recovery and recrystallisation could then be used to provide feedback to the CAL control systems, improving the efficiency of the CAL and providing improved material property data.

Electromagnetic sensors have been used to investigate changes in inductance, which is related to permeability, caused by recovery and recrystallisation for IF steels. IF steel samples in the as-received, cold rolled condition (supplied by Tata Steel UK) were annealed at different temperatures (620^{o}C and

650oC) for different lengths of time to initiate recovery and recrystallisation, inductance for the samples was then measured at room temperature using a U-shaped EM sensor, the measurements were compared with hardness and microscopy data. U-shaped and high temperature cylindrical EM sensors were also used to investigate the significance of the effects that the primary textures ({111}<110>, {111}<123>, {111}<121>, {111}<011> and {111}<112>), which evolve during the annealing process, have on the measured inductance. Texture related measurements for IF steel were then compared with a grain oriented 3% Si steel, which has 95% GOSS texture {110}<001> to show the effects that strong texture has on measured inductance.

A high temperature cylindrical EM sensor was used to dynamically measure inductance during isothermal annealing in-situ. Different annealing temperatures were used, lower temperatures (365^{o}C and 420^{o}C) to investigate the effects that recovery only had on measured inductance. Higher temperatures (650^{o}C and 700^{o}C) were used to dynamically investigate the combined effects of recovery and recrystallisation during in-situ annealing. Following the in-situ inductance measurements interrupted in-situ experiments were conducted to link the measured inductance trends observed to specific changes in microstructure that are associated with the recovery and recrystallisation processes. The interrupted in-situ measurements were compared with hardness and microscopy data to support the changes in measured inductance that were recorded.

Permeability, and inductance, for ferromagnetic materials is known to be affected by external factors such as temperature and stress. In CALs strip temperature varies depending upon its position within the line, as does strip tension. Sensors used at different positions in a CAL will therefore operate at different temperatures and will be monitoring strip at different tensile stresses. Inductance measured by EM sensors must therefore take the changes due to external factors into account. The effect that temperature has on the measured inductance for IF steel was investigated using annealed samples of IF steel in a high temperature cylindrical EM sensor, inductance change was then compared with change in temperature to establish the relationship between measured inductance and temperature. To provide a comparison the same experiment was completed using a 430 grade ferromagnetic stainless steel sample.

Measurements using a U-shaped EM sensor (aligned with the direction of applied load) were completed for an as-received IF steel sample that was placed under tensile load (aligned in the rolling direction of the sheet) to investigate the effects that tensile stress has on measured inductance.

Experimental data from this research showed that the largest relative effects on EM sensor measurements were recorded for recovery, recrystallisation and temperature. The effects of stress on measured inductance were less significant. The relative effect of the starting and recrystallisation textures on the measured inductance were harder to distinguish amongst the effects of temperature, recovery and recrystallisation.

Experimental data recorded in this project shows that it is possible to monitor recovery and recrystallisation at room temperature and in-situ using EM sensors for IF steel samples annealed at different temperatures and times. It is shown that the recovery and recrystallisation processes have a significant effect on measured inductance and that with consideration to the effects of external factors it should be possible to use EM sensors within a CAL to monitor microstructural changes that can be related to recovery and recrystallisation.

List of Publications

R. Hall, M. Strangwood, L. Zhou, C. Davis. “Dynamic measurement of recovery and recrystallisation in interstitial free steel using a high temperature electromagnetic sensor”. La Metallurgia Italiana - n. 2 (35 – 42). 2016

Acknowledgements

The work presented within this thesis would not have been possible without the help and advice of my PhD supervisors Professor Claire Davis (University of Warwick) and Dr. Martin Strangwood (University of Birmingham). I am very grateful to them for their never running out of patience with me, providing training opportunities, always being willing to share their knowledge and for making the experience of my PhD so enjoyable.

Special thanks must also be given to Dr. Carl Slater and Dr Lei (Frank) Zhou who have been great companions and colleagues. They have put up with my endless questions and have always pointed me in the right direction when I’ve needed help.

This work could not have been completed without help from Professor Tony Peyton and Dr. John Wilson at the University of Manchester. Tony and John have a wealth of expertise in EM sensor design and application as well as magnetic measurement. Their advice has always been sage and they are both great fun to work with.

Finally this PhD would not and could not have happened without the help and support of my parents, Diane and Brian Hall. My gratitude to them, as I hope they know, is endless.

Contents

List of Figures

List of Tables

1. Introduction

Interstitial free (IF) steel is used extensively throughout applications in the automotive, packaging and furniture industries due to its excellent formability and ductility. IF steel has very low carbon content and nitrogen content, approximately 0.03 and 0.003 wt% respectively. Carbon and nitrogen are interstitial elements; the removal of interstitial elements from steels prevents age and bake hardening as well as preventing Luder's line formation during plastic deformation. IF steel is produced in sheet form, the main processes used to obtain the final product are casting, hot rolling, cold rolling and annealing. The manufacturing process ensures excellent material properties for subsequent forming operations through the development of a fine equiaxed grain structure and desired crystallographic texture.

The final phases of the manufacturing process are key to the production of IF steel, the steel is cold rolled and then either batch annealed or annealed in a continuous annealing line (CAL). Annealing improves the formability of the cold rolled sheets, whilst also reducing the strength, through recovery and recrystallisation processes. The initial phase of the annealing process, recovery, causes annihilation and re-distribution of dislocations within the cold rolled microstructure to form sub-grains. Recrystallisation is the reformation of the cold rolled grain structure by the nucleation and growth of new, strain free, grains. Nucleation can either occur randomly or it can occur at preferential sites such as grain boundaries or impurities [1].

Measurement of material properties currently takes place off-line after the IF steel strip has passed through the CAL and is completed using traditional intrusive methods such as tensile testing, with optical metallography and hardness as necessary. These procedures can be uneconomical and time consuming [2]. Development of an on-line non-destructive measurement system would be advantageous to steel manufacturers, offering efficiencies in terms of time and cost as well as providing direct feedback for the control of CALs.

IF steel is a single phase ferritic steel which maintains ferromagnetic behaviour up to the Curie temperature (Tc). It is known that the recovery and recrystallisation processes affect the magnetic

properties of ferromagnetic materials [3]. The change in magnetic properties is due to the rearrangement and annihilation of dislocations during recovery and then the nucleation and growth of new grains during recrystallisation. As each of these changes takes place the magnetic permeability of the IF steel changes; by measuring the permeability (or properties associated with the permeability) it should be possible to monitor recovery and recrystallisation dynamically and in-situ during annealing.

The purpose of the work presented in this thesis is primarily to show that it is possible to monitor recrystallisation in-situ for IF steel at recrystallisation temperatures using an electromagnetic sensor which responds to changes in permeability caused by changes in microstructure of ferromagnetic materials. Secondary aims are to show that the EM sensor is responsive to recovery as well as recrystallisation; that an EM sensor can be used to determine different stages of recovery and recrystallisation; to quantify the changes in EM sensor response due to changes in permeability caused by strain and temperature and to establish whether texture within IF steels has a significant effect on magnetic anisotropy and EM sensor measurement.

2. Background

This chapter covers the steel manufacturing process starting with primary steelmaking and moving onto the more complex processes involved in secondary steelmaking. An overview of the steel manufacturing process is useful as it gives a background to the manufacturing route for IF steel and describes the deployment locations for non-destructive technology (NDT) systems that are currently being used in steel manufacturing.

2.1. Steel Manufacturing Overview

Steel manufacturing plays a vital role in modern society, steel is used worldwide and is relied upon throughout various industries for its physical qualities such as formability, strength, toughness and ductility. Modern steel manufacturing can be split into two forms, primary and secondary steel manufacture. Primary steel manufacture involves converting liquid iron into steel using the basic oxygen steelmaking process or melting scrap steel in an electric arc furnace. Secondary steel making involves changing low carbon steel into steel of the required customer composition and cleanness before casting by adding alloying elements, lowering the amount of dissolved gases and removing or altering inclusions. A general overview of the steel making process is shown in Figure 1.

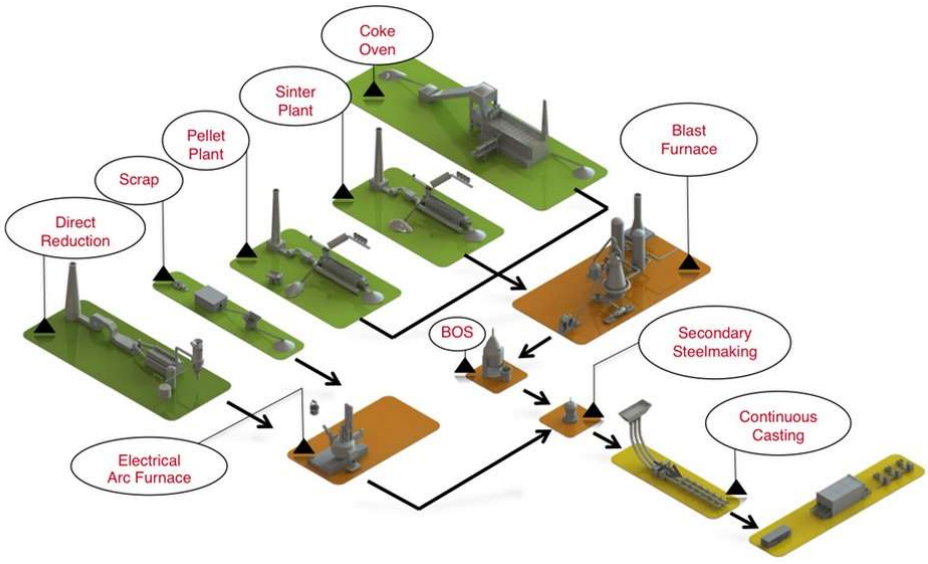

Figure 1: General overview of the steel making process [4]

2.2. Primary Steelmaking

Primary steelmaking includes blast furnace, basic oxygen steelmaking and electric arc furnace steelmaking. Essentially the basic oxygen process converts carbon rich molten pig iron, (produced from iron ore, limestone and coke) into steel. The electric arc furnace process is different to the basic oxygen process as it uses electrodes to melt scrap steel and directly reduced iron (DRI) to form molten steel ready for further processing.

The basic oxygen process involves blasting oxygen through the molten iron to lower the carbon content of the steel, making low-carbon steel. The processes also involves the addition of lime or dolomite to promote the removal of impurities and form a slag layer on top of the molten steel, which is tapped off before further processing. The steel produced at the end of the primary process is low in carbon content, high in oxygen but is not refined towards the exact customer requirements.

2.3. Secondary Steelmaking

Steel produced in the primary process is tapped off into a ladle, while the steel is in the ladle various processes can be employed before the steel is cast into slabs. The processes which take place in the ladle include de-oxidation, vacuum degassing, alloy addition, inclusion removal, inclusion chemistry modification, de-sulphurisation and homogenisation. Tight control of ladle metallurgy and processes are associated with the production of high quality steel grades.

The ultra-low carbon content of IF steel is achieved using a vacuum degassing process which removes carbon monoxide, nitrogen, hydrogen and other gases. Further reduction nitrogen and carbon is achieved through the addition of alloying elements such as niobium and titanium, which stabilise the residual interstitial elements [5].

2.4. Continuous Casting

At the end of the secondary steelmaking process the steel is cast into billets, blooms or slabs before final processing in finishing mills to produce the shapes and properties that are required by the customer. Large scale steel production employs the continuous casting process; the steel is poured from the ladle into a tundish, and then passes through the submerged entry nozzle into a water cooled copper mould which gives it the shape of a bloom, billet or slab, here it starts to solidify before going through a series of rollers. From here the steel may go directly to a hot rolling process or be stored, waiting for a reheating process before final rolling processes. As IF steels are used in a sheet form it is cast as a slab and then taken directly away for hot rolling into strip.

2.5. Rolling Processes

Rolling uses compressive forces to alter the cross sectional area of a work piece; the forces are applied by passing the material between two or more rollers. The distinction between the hot and cold rolling processes is made by considering the homologous temperature, in which the low end is at absolute zero and the high end is the material melting point temperature (T_m). When the process is performed at a temperature below $0.5T_m$, or the recrystallisation temperature, it is usually termed cold rolling [6].

2.5.1. Hot Rolling

Hot rolling takes reheated bloom, billets or slabs where the reheating temperature is typically 1200-1300°C. As hot rolling is performed at high temperature, the material being rolled is softer meaning less power is required and that it is easier to introduce large deformations [7]. Modern hot rolling takes place in rolling mills that are dedicated to the required end product. Strip is produced from slabs, which are reduced in cross section through roughing (reversing mill) and finishing (series of mills) rolling in the strip mill. An example of a production strip mill and the various stages is shown in Figure 2.

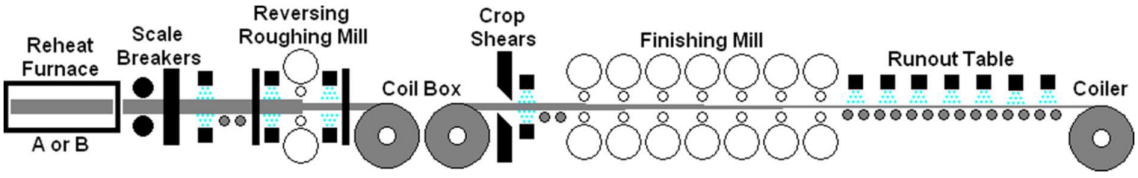

Figure 2: Schematic overview of a typical strip hot rolling mill [8]

Static recrystallisation occurs during hot rolling and takes place due to the combination of elevated temperatures and deformation [9], static recrystallisation occurs during hot rolling due to the strains imparted during rolling at elevated temperatures. Figure 3 shows the microstructural changes that occur due to hot rolling. The grain structure produced during hot rolling will be equiaxed if the rolling takes place at a temperature above the recrystallisation temperature and there is sufficient time between rolling passes for recrystallization to take place, equiaxed grains may develop during hot rolling below the recrystallisation temperature. Crystallographic direction (texture) developed during hot rolling can be significant and allows the basis of textures which support a materials drawing quality.

Texture and grain morphology developed in the hot rolling process has a "parental" effect on the final textures that are present in the microstructure after further finishing processes [10]. Texture development for IF steel is discussed in section 0. Hot rolled products have relatively poor surface finishes as they are covered in scale; the scale may or may not be removed before any subsequent steel processing is performed.

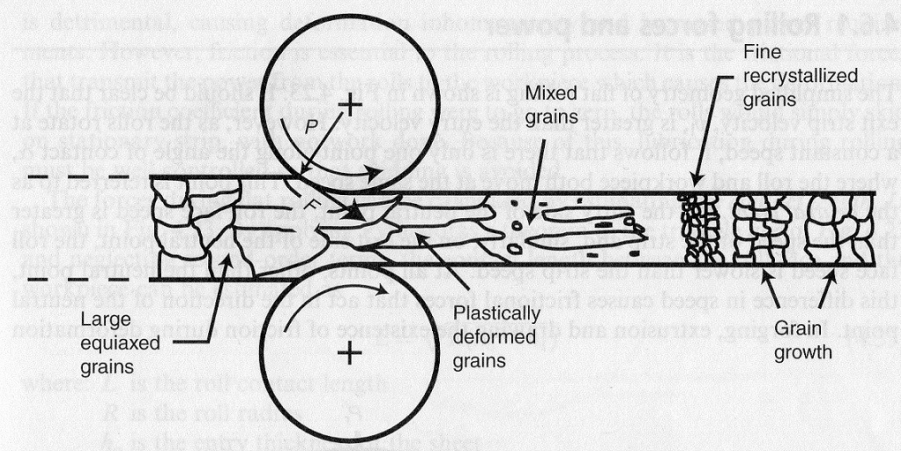

Figure 3: Schematic representation of grain structure produced during hot rolling [9]

2.5.2.Cold Rolling

Cold rolling causes severe plastic deformation and permanently alters the dimensions of the material being rolled. During plastic deformation dislocations are introduced into the atomic lattice, causing small changes in atomic position. The displacement of the atomic lattice is permanent and the amount of displacement is dependent upon the amount of plastic deformation applied to the material [11]. Deformation caused by cold rolling has a dramatic effect on both the physical properties and microstructure of the steel being rolled. In steels cold rolling reduces ductility while at the same time increasing yield strength, hardness and decreasing toughness [1]. It is unusual for any external heating source to be used during the cold rolling process, although cold rolling as a process will cause material heating due to friction, the amount of heat generated depends on the material thickness, rolling speed and applied forces. Rolling temperatures are typically in the region of 55^{o}C to 70^{o}C, peak temperatures of 300^{o}C are sometimes seen for rolling processes using very thick and slow moving material. The heat generated during cold rolling is not normally high enough to affect material properties [12]. After cold

rolling most sheet will go through annealing before processes such as deep drawing or stamping, although other processes (spinning, roll forming, bending and cutting) are sometimes used [13].

The advantages of cold rolling are:

- Tighter tolerances and better surface finish due to absence of cooling and oxidation
- Very thin products can be rolled
- Final properties of the work piece can be closely controlled, and grain size can be controlled before annealing

Cold rolling is an essential part of the production of IF steel. There are two main functions of the cold rolling process, to produce the required thin gauges and to increase the formability (r value) of the sheet through the introduction of a high energy deformed structure from which appropriate textures can be developed during recrystallisation [14].

The displacement of atoms from their original positions within the grains is caused by dislocations that are introduced during cold rolling. Dislocations are linear or one-dimensional defects within a grain's structure which cause misalignment of the atomic structure of the grain. During cold rolling dislocations move along slip planes and accumulate at grain boundaries which form barriers to their movement (discussed in more detail in section 3.1). Dislocations play an important role on the recovery and recrystallisation process and have direct influences on a materials strength, hardness, ductility and electromagnetic properties. Plastic deformation, the introduction of dislocations caused by cold rolling, also impacts other properties of the IF steel such as corrosion resistance, electrical conductivity and importantly for the work reported in this thesis, electromagnetic properties such as magnetic permeability [9, 10].

2.6. Annealing

Annealing refers to a process of heat treatment where a material is heated to an elevated temperature for a period of time and then cooled. Annealing is carried out to relieve residual stresses, decrease hardness, increase ductility and produce specific microstructures and textures through the instigation of recovery and / or recrystallisation [1].

Typically there are three stages to any annealing process, initial heating to a required temperature, holding (soaking) at temperature and cooling. Both time and temperature are key parameters in the annealing process as they are directly related to the formation of the required microstructure [1, 11]

IF steel is usually used in applications requiring gross plastic deformation, such as automobile body panels and complex structural components. In these applications deformation without fracturing or excessive energy consumption is required. Annealing is a key process in achieving the required material properties and microstructure to make this possible. Careful control of the annealing process is essential to obtain the necessary microstructure (usually fine grained) and to make sure that excessive grain growth is prevented [1, 15, 16].

2.6.1. Continuous Annealing Lines

Annealing in modern steel making plants takes place on continuous annealing lines. Continuous annealing lines have replaced the more traditional batch annealing process as they provide a more efficient and controllable annealing process. Continuous annealing lines are capable of annealing large quantities of steel strip quickly by moving steel strip at high speeds through a series of furnaces and processing equipment to obtain the correct material properties and dimensions. A typical continuous annealing line layout is shown in Figure 4.

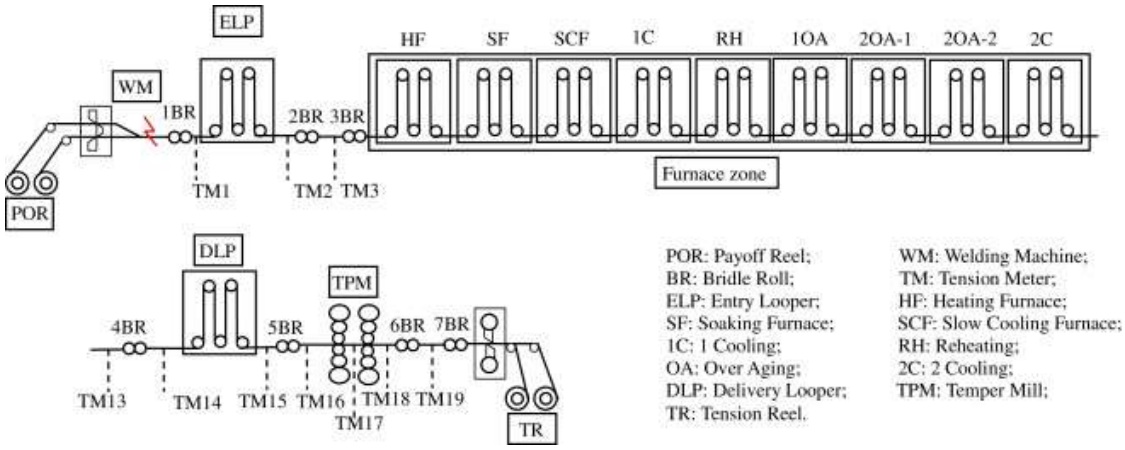

Figure 4: Typical layout of a continuous annealing line [17]

A continuous annealing line has the following sections:

- **Pay off reel and tension reel**. After cold rolling the strip is coiled, at the entry uncoiling station the cold rolled steel coil in unwound and the strip is joined to the strip already being processed by the welding machine. At the end of the annealing line the strip is coiled in its finished condition ready for shipping to the customer at the tension reel.

- **Entry and exit accumulators (entry and delivery loopers).** Accumulators provide storage areas between static steel coils and continuous strip running through the furnace sections. As the empty feed coil is stopped, replaced with a new full coil and both strips joined, the entry accumulator unwinds to provide continuous strip. Similarly, the exit accumulator winds up while the full take-off coil is unloaded at the exit end.

- **Furnaces**. Furnaces are required to heat treat the strip to achieve the desired properties. The heating furnace achieves the highest temperatures in the annealing line and holds around 400m to 500m of strip. To prevent contamination the furnace is heated using ceramic radiant tubes. The soaking furnace is used to maintain strip temperature and is electrically heated. The cooling stations between the furnaces control the cooling rates for the strip before subsequent heat treatment processes like overaging.

- **Atmosphere control**. To prevent oxidation of the strip as it passes through the furnaces, the furnaces are gas sealed (maintained using a slight positive pressure) and contain either hydrogen, nitrogen or a hydrogen / nitrogen mix. Different gases are used depending on the thermal transfer requirements from the heat sources to the strip.

Control of continuous annealing lines is currently a combination of traditional material batch sampling (hardness and microscopy), temperature measurements and statistical control methods. Statistical control processes such as SIROLL MSM [18] and CAQC [19] are used to estimate microstructural changes during the hot rolling process. SIROLL MSM and CAQC use data gathered through the hot rolling process, combined with chemical composition to calculate microstructural and material properties through computer based modelling.

Control of continuous annealing lines is mostly focused on monitoring strip temperature and furnace heating during annealing, these systems adapt the heating within the furnaces depending on the detected strip temperature using statistical algorithms during annealing [20-23], none of these systems use on-line microstructural condition as feedback.

Strip tension must also be carefully monitored to make sure that strip breakage is minimised, preventing downtime on the line. It is very difficult to estimate strip tension using first principles due to differing strip inertia, temperature, gas flow and different surface roughness [17]. Strip tension is controlled using algorithms which use feedback from loads on the strip rollers or strip load cells [24], as with the strip temperature controllers the tension systems do not use any feedback regarding the microstructural condition of the strip itself. Line tension varies depending on position within the CAL, peak tensile stresses when entering the heating and slow cooling furnaces are reported to be around 0.22 MPa with much smaller variations of up to 430 Pa [25, 26].

Strip temperature varies throughout a CAL. At the pay-off reels the strip is at atmospheric temperature, close to 30^{o}C. It is then typically heated to a temperature in the heating furnace of around 800^{o}C, it is held at 800^{o}C through the soaking furnace and then slow cooled to 750^{o}C before entering the overaging furnaces. During overaging the strip is held at a temperature of around 500^{o}C, before passing through

cooling furnaces at around 150°C [25]. The temperatures are not specific to a particular steel grade but are typical of CALs for steel strip. Recovery and recrystallisation will take place during the heating and soaking stages.

2.6.2. EM Sensor Positioning Within a Continuous Annealing Line

In principle an EM sensor technique capable of monitoring recovery and recrystallisation would be able to feedback information related to microstructural change of the strip as it passed through a CAL.

Use of an EM sensor technique in a continuous annealing line would require a series of sensors to be used so that change in signal for the strip is measured between the cold rolled and annealed conditions. Sensors would need to be placed in regions where EM measurements were possible without being compromised by strip temperature effects, readings at the highest line temperatures are not possible as ferromagnetic materials become paramagnetic beyond the Curie temperature (T_c), around 780°C (T_c is discussed in greater detail in section 4). Suitable positions for sensors would be at the entrance to the heating furnace (as long as the strip temperature at that point is known) and in the final cooling furnaces where the strip temperature has dropped back below T_c. Positioning of sensors in this manner would give readings before and after recovery and recrystallisation has taken place, the change in signal between the two sets of sensors as the strip passes them would indicate whether recovery and recrystallisation is complete.

EM sensor readings from a continuous annealing line would need to be corrected for temperature and strip tension as both temperature and tension are known to affect permeability, permeability variations due to different factors are discussed in section 4.4 [27]. EM sensors placed within a continuous annealing line would also need to be shielded from any environmental magnetic noise and ruggedized to withstand the continuous annealing line environment; this is outside the scope of the work presented in this thesis.

2.7. Chapter Summary

This chapter has reviewed the steel manufacturing process and described the different steps used in the production of steel products, with particular attention paid to the rolling processes and CALs. In later sections of this thesis the different areas of the steel making process are highlighted as sites for NDT processes and potential sites for EM sensor deployment.

3. Recovery and Recrystallisation

This chapter reviews and establishes an understanding of the mechanisms involved in recovery, recrystallisation and texture development within IF steels. As outlined, cold working (rolling) plastically deforms the microstructure of IF steel and produces changes in grain shape, introduces strain hardening and increases dislocation density. Annealing initiates recovery and recrystallisation reversing some of the changes in material properties caused by cold rolling.

3.1. Recovery

Recovery refers to changes in a deformed material which primarily occur before recrystallization. It is widely accepted that recovery and recrystallisation do not happen in isolation; however recovery can happen without recrystallisation at low temperatures. During recovery there is a release of stored internal strain energy; dislocations are able to move leading to rearrangement and annihilation of dislocations. Physical properties such as thermal conductivity and electrical conductivity are partially restored towards their pre cold worked levels. In this work the term recovery will be used primarily in association with plastic deformation caused by cold rolling. It is known that recovery is primarily due to changes in the dislocation structure in the material [1, 15, 28].

Dislocations are linear defects that are introduced into the crystalline structure of a material by the rupture and reformation of atomic bonds [1]. Cold rolling causes multiple dislocations to occur within single grains, atomic bonds are broken and reformed causing the grain's shape to change.

Plastic deformation is caused by dislocation motion and is called slip, the planes along which slip occur (and on which the dislocations travel) are called slip planes. Large scale plastic deformation relates to the permanent deformation which results from the movement of dislocations in reaction to an applied shear stress. Dislocations occur in two fundamental forms, edge dislocations and screw dislocations. An edge dislocation causes a localised distortion along the end of an extra half plane of atoms and also defines the dislocation line. Screw dislocations can be considered to be the result of a shear distortion; its dislocation line pass along the centre of a spiral or atomic plane ramp. It is common for crystalline materials to have dislocations with both edge and screw components; these are called mixed dislocations

(Figure 5). The magnitude and direction of the atomic distortion caused by dislocations is called the Burgers vector [1].

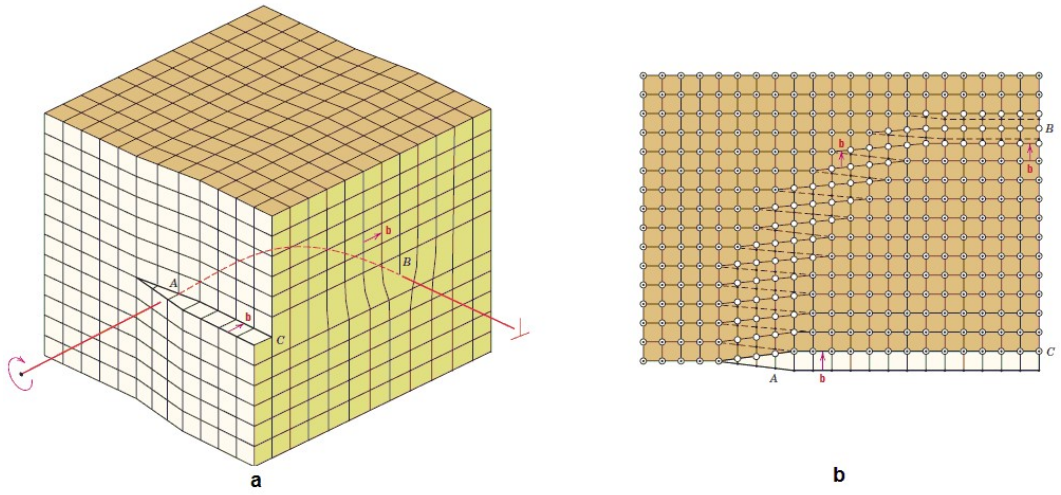

Figure 5: Representation of a dislocation that has mixed character, a combination of both edge and screw. (a) is a geometric view and (b) is the top view. In the top view, open circles denote atom positions above the slip plane, solid circles denote atom positions below the slip plane. At point A, the dislocation is pure screw while at point B the dislocation is pure edge. For regions in-between where there is curvature in the dislocation line (the red line running through points A and B) there is a mix of both edge and screw dislocation types. The Burgers vector is denoted by b. [1]

All metals have dislocations present in their structure, dislocations exist after solidification and the number of dislocations can be affected by processes such as plastic deformation or rapid cooling which causes thermal variations across the material, inducing thermal stresses. The amount of dislocations within a material is quantified by density. Dislocation density in a material is the number of dislocations present in a given volume, typical units for dislocation density are the number of dislocation per square millimetre (n/mm^2). After solidification dislocation densities can be as low as 10^3/mm^2. Heavy plastic deformation causes larger number of dislocations, and the amount may increase to as high as 10^9/mm^2 or even 10^{10}/mm^2 in the case of very severe plastic deformation [1].

Heating after cold working causes a release of stored energy within a crystal and allows the dislocations to move. As dislocations move two phenomena happen, rearrangement of dislocations into lower energy configurations and annihilation of dislocations. Both processes are achieved by glide, climb or cross-slip of dislocations [1, 28]. When two dislocations of opposite sign meet they are annihilated.

Dislocations that move but do not come into contact with another dislocation of opposite sign will align themselves into ordered arrays which have less stored energy. It is impossible to remove all dislocations from a crystal that has been plastically deformed by recovery [1].

3.2. Recrystallisation

When recovery is complete a deformed grain structure is still present, the grain structure still has a relatively high energy state. Recrystallisation is the formation of new, strain free, equiaxed grains with low dislocation densities that have material properties similar to, but not the same as, the grains that existed prior to cold working. The driving force in the creation of new grains is the stored energy that results because of the difference between strained and unstrained material [1].

3.2.1. Recrystallisation Temperature

Recrystallisation of a particular metal alloy can be specified in terms of its recrystallisation temperature, or the temperature at which recrystallisation is complete within one hour. Typically the recrystallisation temperature is between 30% and 50% of the absolute melting temperature of the metal alloy. The recrystallisation temperature depends on a number of factors; the amount of cold working, the grain size and the chemical composition of the alloy. Increased amounts of cold work enhance the rate of recrystallisation (the recrystallisation temperature is lowered) and approaches a constant or limiting value at high deformations [1, 28].

Recrystallisation is both time and temperature dependant. Complete recrystallisation will occur if cold rolled materials are heat treated (annealed) for longer time periods at lower temperatures. There is a limit to how low a temperature can be used for recrystallisation; if the temperature is too low then there is not enough energy for recrystallisation to take place. Recrystallisation will occur more quickly at higher temperatures.

Annealing temperatures to achieve recrystallisation in IF steels are reported to be at 550^{o}C and above [29]. Recrystallisation rates for IF steel that had been 90% cold rolled and subsequently annealed at 650^{o}C are shown in Figure 5. The figure shows that the IF steel was 70% recrystallised after 370s (6.2

minutes) and 97% recrystallised after 600s (10 minutes), full recrystallisation was not complete until around 3000s [30].

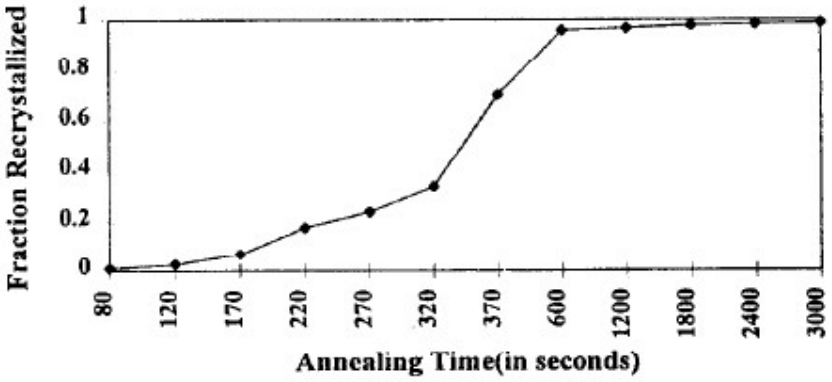

Figure 5: Recrystallisation fraction for IF steel at 650°C [30].

It has been shown that recrystallisation rates are dependent on both the amount of cold work (rolling) as well as temperature.

Table 1 shows recrystallisation data recorded for IF steels cold rolled to 70%, 80% and 90% reductions and shows the times taken to achieve full recrystallisation at different temperatures of 610°C, 630°C and 650°C [31]. The table also shows incubation times for the different amounts of cold rolling and annealing temperatures, the incubation time is a period where little or no recrystallisation takes place and after which recrystallisation occurs quickly. It can be seen that higher temperatures and larger degrees of cold rolling cause very short incubation periods, essentially recrystallisation happens much more quickly. The time to full recrystallisation for the sample annealed at 650°C shown in table 1 is 25 minutes, similar to the time reported in Figure 5.

Table 1: Full recrystallisation times for IF steel samples annealed at 610°C, 630°C and 650°C from cold rolling reductions of 70%, 80% and 90% [31]

Temperature (°C)	610			630			650		
Reduction (%)	70	80	90	70	80	90	70	80	90
Incubations times (min)	17	15	10	8	3-5	3	5	3-5	<1
Full Recrystallisation Time (min)	360	210	200	90	75	60	50	30	25

3.2.2.Grain Nucleation

The first appearance of new grains from a deformed microstructure is termed nucleation. The process whereby these new grains subsume the deformed microstructure can be defined as recrystallisation.

The driving force for nucleation and subsequent recrystallisation leading to the production of the new grain structure is the difference in internal energy between the strained and unstrained material. New grains form as small nuclei and develop until they wholly consume the parent material.

Grain nucleation and recrystallisation occur independently within a grain but can occur simultaneously across a number of grains. Progress of recrystallisation with time during isothermal annealing is usually plotted in terms of recrystallisation fraction (X_v) against log time, recrystallisation follows a sigmoidal pattern and typically shows a point where nucleation of new grains occur after an incubation time, then an increase in recrystallisation rate followed by a slowing of the recrystallisation rate once recrystallisation nears completion, Figure 6.

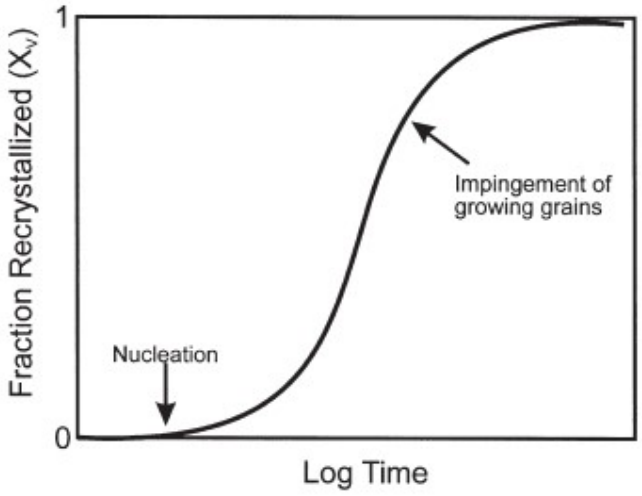

Figure 6: Typical recrystallisation behaviour during isothermal annealing [28].

There are several methods for the quantification of recrystallisation, these include stress relaxation, double hit, optical metallography and electron backscattered diffraction (EBSD) methods. The different methods can be divided into two categories, those which use direct observation (optical microscopy and EBSD methods) and those which rely upon mechanical properties (double deformation and stress relaxation). The methods involving direct observation rely upon statistical analysis of an optical micrograph from point to point across the 2D section, using micrographs and analysing them for different annealing times and temperatures gives different recrystallisation rates for annealing processes. The direct observation methods give data directly related to recrystallisation phenomena, however they are laborious and under some circumstances impossible to use. The double deformation technique relies upon the measured fractional softening between deformation passes which is related to recovery and recrystallisation, the technique struggles to distinguish between recovery and recrystallisation. The stress relaxation technique relies on the relationship between a material's stress relaxation rate with the amount of recovery and recrystallisation caused by annealing [32, 33].

Recrystallisation is a thermally activated process; the dependence on temperature for recrystallisation is illustrated in Figure 7 for a deformed C-Mn steel annealed at different temperatures varying from 850ºC to 1200ºC. Incubation periods are longer at lower temperatures and the rate of recrystallisation (shown by the steepest central part of the curve) is slower at lower temperatures [34].

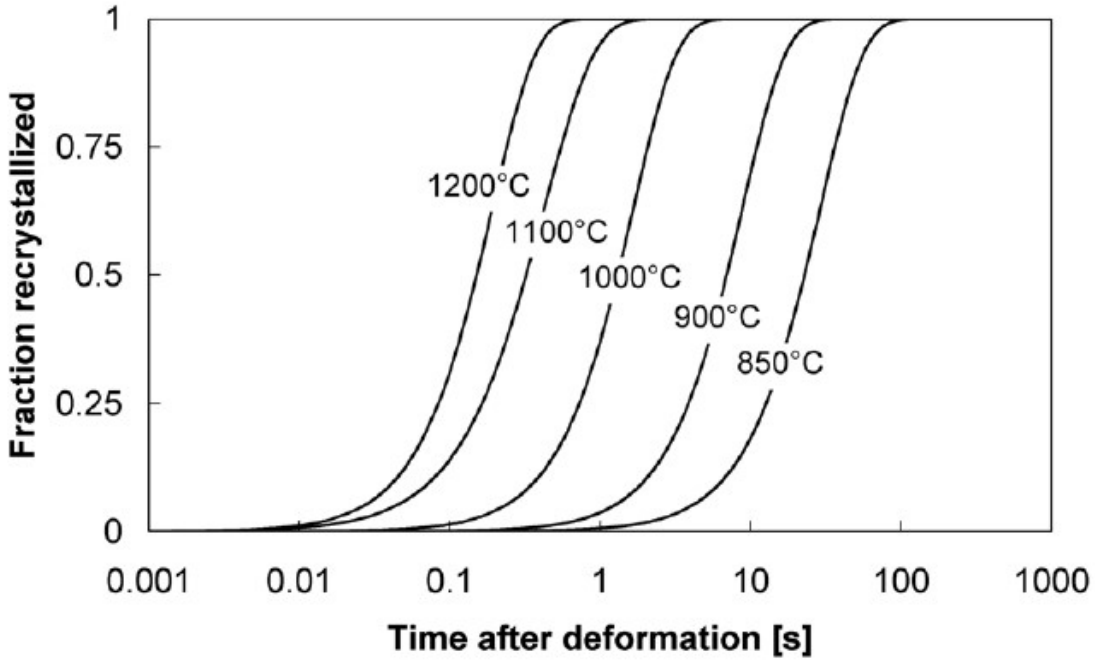

Figure 7: Recrystallisation curves for a deformed C-Mn steel which was annealed at different temperatures varying from 850°C to 1200°C [34]

Empirical models have been developed which can describe recrystallisation rates. The characteristic sigmoidal curve shown in Figure 6 can be well described by the Johnson-Mehl-Avrami-Kolmogorov (JMAK) equation:

$$X = 1 - \exp\left[-0.693\left(\frac{t}{t_{0.5}}\right)^{n}\right] \quad (1)$$

Where X is the recrystallisation fraction, t is time and n is a constant [34].

3.2.3.Grain Growth

On completion of recrystallisation grains will continue to grow if the sample being heat treated is left at high temperature, this is called grain growth. Recrystallised grain structures still contain a significant amount of stored energy within the grain boundaries; a material with fine grains has more stored energy than a material with large grains. Grain growth reduces the amount of stored energy within the material further by reducing the number of grain boundaries and therefore reducing the total amount of stored energy within the material.

Migration of grain boundaries allows grain growth to take place. Not all grains can expand and larger grains develop at the expense of smaller grains that reduce in size. Average grain size increases with time and at any given time there can be a range of grain sizes present with the material.

The rate of diffusion is dependent on temperature, at higher temperatures grain growth will occur more quickly than at lower temperatures. At very high temperatures grain growth will occur very quickly, with large grains developing immediately on the start of heat treatment [1, 3, 35].

For polycrystalline materials grain growth is dependent upon the time at which the material is left at elevated temperatures. The grain diameter (d) varies with time (t) according to the relationship:

$$d^2 - d_o^2 = kt \tag{2}$$

Where d_o is the initial grain diameter at t =0, d is the final grain diameter and k is a temperature dependent constant given by the exponential equation [1]:

$$k = k_o exp\left(\frac{-Q}{RT}\right) \tag{3}$$

Where k_o is a constant, Q is the activation energy, R is the gas constant (8.31 J/mol-K) and T is the temperature. Activation energy is considered to be the energy required to produce the diffusion of one mole of atoms, activation energies for IF steels are reported to be 180 kJ/mol [36].

In the same way as recrystallisation, grain growth has an effect on the mechanical, electrical and magnetic properties of the material [1, 3, 35].

3.2.4.Effects of Recovery on Material Properties

Recovery influences the mechanical, electrical and magnetic properties of polycrystalline materials such as IF steel. During recovery the stored energy within a material is reduced due to redistribution and annihilation of dislocations at elevated temperatures, the dislocation density within the material is reduced. Dislocation recovery is not a discrete microstructural process; it is a process which incorporates a number of steps. The various stages of recovery are shown in Figure 8.

Reduction of dislocation density affects several physical material properties including electrical resistivity and thermal conductivity. These parameters are difficult to follow and the progress of recovery is usually tracked using bulk measurements such as hardness, yield stress and electron back scatter diffraction (EBSD). Hardness measurement does not always track the recovery process with sufficient sensitivity to be accurate. The changes in yield stress and hardness are small compared to those caused by recrystallisation [28].

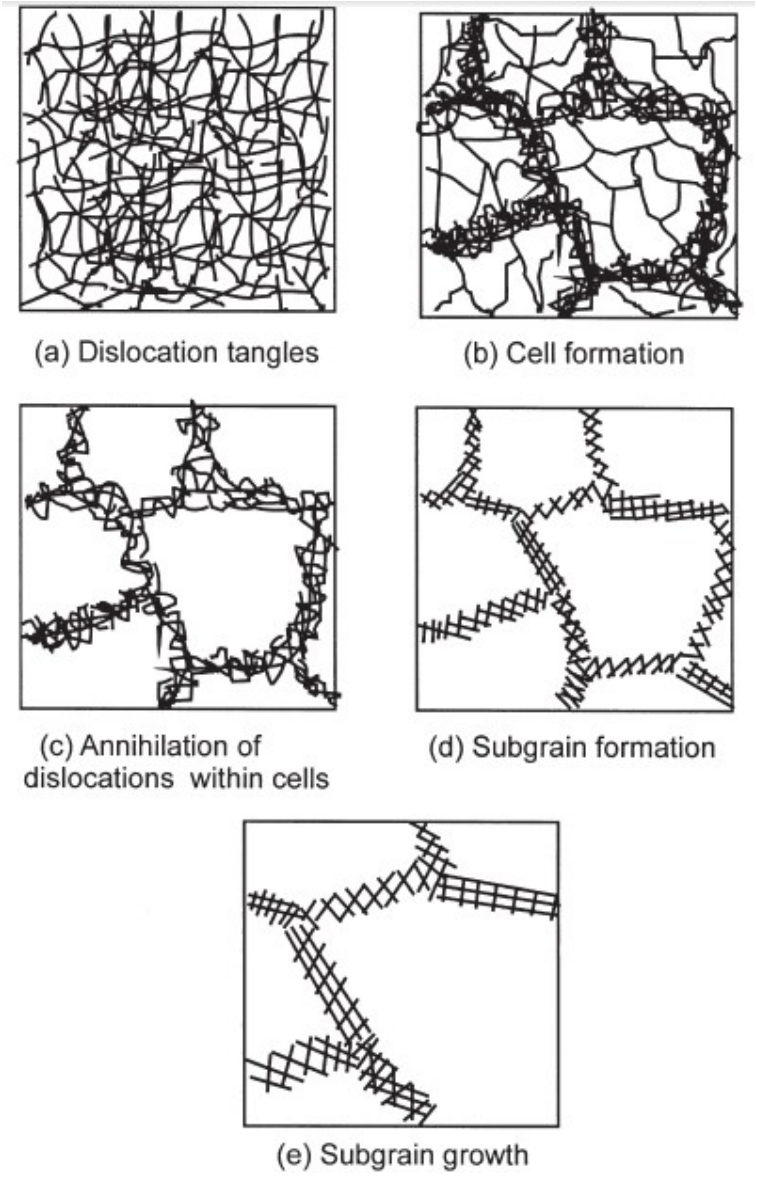

Figure 8: Various stages in the recovery of a plastically deformed material [28]

3.2.5.Recrystallisation Effects on Material Properties

Grain size influences the mechanical, electrical and magnetic properties of polycrystalline materials such as IF steel.

Mechanical properties affected by grain size are hardness, strength, toughness and ductility. Grains within a polycrystalline material have different orientations with grains boundaries between them. Plastic deformation causes the introduction of dislocations into grains, which move along slip planes and can under the right conditions cross grain boundaries. High angle grain boundaries (where there is a misalignment of greater than 10^{o} - 15^{o} between one grain and another [15]) act as barriers to the motion of dislocations along a slip plane because they require the motion to change direction and the boundary presents a discontinuity of slip planes from one grain to another. The barrier action of high angle grain boundaries causes dislocations to "pile up" at the boundary, rather than move across the boundary. Dislocation pile up causes stress concentrations ahead of slip planes, generating new dislocations in adjacent grains. Small angle grain boundaries are not as efficient at causing dislocation pile ups as dislocations are able to move between grains more easily due to the small misalignment. A representation of high and low grain boundaries is shown in Figure 9.

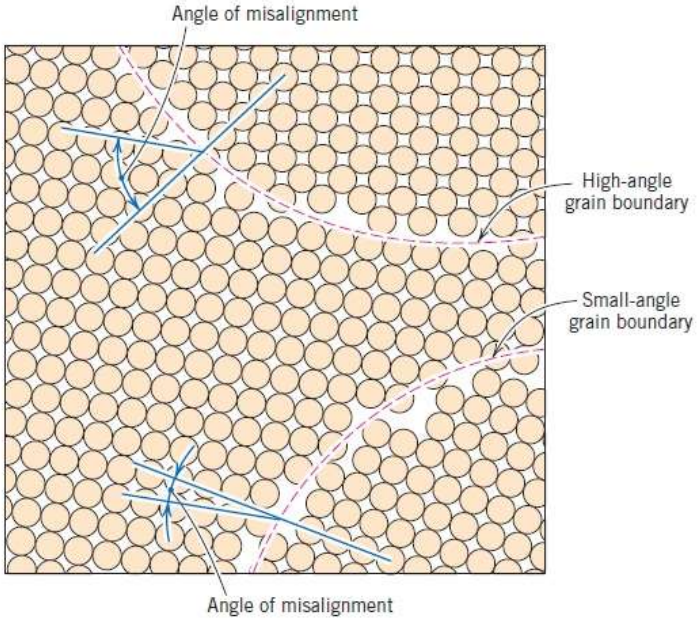

Figure 9: Schematic diagram showing high and low grain boundary misalignment from an atomic point of view [1]

Recrystallisation causes a refinement of grain size within the material and a reduction in the amount of dislocations. Both of these factors affect the material and magnetic properties of the material. It has been reported that grain size for recrystallised IF steel varies between 11 and 27 μm [37].

Materials with smaller and more refined grains are stronger than coarse grained materials as the greater number of grain boundaries within the more refined grain structure impede dislocation movement caused by plastic deformation. The relationship between yield strength (σ_y) and grain size is defined by the Hall-Petch relationship:

$$\sigma_y = \sigma_0 + k_y d^{-1/2} \quad (4)$$

Where σ_0 and k_y are constants for the particular material and d is the average grain diameter of the material [11].

Hardness is defined as a material's resistance to localized plastic deformation. Therefore if a material with smaller grains is stronger and more resistant to plastic deformation it will be harder [1]. As a material recovers and recrystallises, it will become less hard, initially due to reduction in dislocation density during recovery and then with the formation of refined grains during recrystallisation and then larger grains during grain growth.

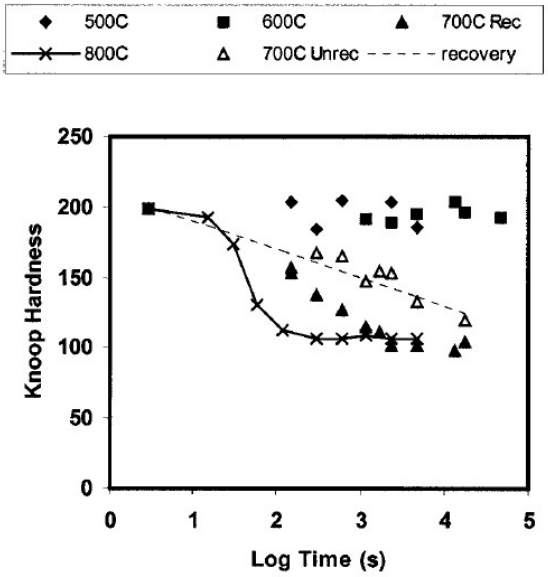

Figure 10: Knoop hardness measurements for IF steel rolled to 50% deformation at 500°C and subsequently annealed at different temperatures. The hardness measurements were taken at room temperature [38].

Figure 10 shows Knoop hardness values recorded for IF steel rolled to 50% deformation at 500°C and then subsequently annealed at different temperatures, the hardness measurements were taken at room temperature. Annealing at 800°C shows a significant drop in hardness over the total annealing time, decreasing from a value of 200 HK to approximately 100 HK. The initial drop in hardness at 800°C is small (approximately 5 HK at the first time step) and then a further decrease happens quickly before reaching a plateau at around 100 HK. The first initial decrease is attributed to recovery and the rapid drop in hardness is attributed to recrystallisation. Annealing at lower temperatures (500°C and 600°C) shows little or no decrease in hardness, attributed to limited recovery. The hardness changes for annealing at 700°C are reported as being more complicated, the initial stage shows an approximately linear reduction in hardness up to approximately 600 s, by which time the hardness is reduced from the initial value of approximately 200 HK to approximately 160 HK by recovery. The second stage corresponds with more rapid hardness reduction linked to recrystallised material. The hardness of un-recrystallised grains is also shown, confirming that the rapid reduction in hardness at 700°C is due to recrystallisation [38]. The data shows that recovery has little effect on hardness for IF steels and therefore that recovery is difficult to follow using hardness measurements. Recrystallisation however

has a large effect on the reduction of hardness and is much easier to follow using hardness values. The effects of recrystallisation on magnetic properties are discussed later in section 4.

3.2.6. Texture Evolution During Recrystallisation and Effects on Material Properties

The orientations of individual crystals of a polycrystalline material vary from one crystal to the next. The term "texture" is used to describe the distribution of orientations of a polycrystalline material sample. A material with strong texture has a lot of crystals with the same orientation, an example of a material with very strong texture is grain oriented electrical steel.

Initial texture is formed during solidification in the casting process; columnar grains grow in a preferred crystallographic direction affected by the heat flow direction. Crystals with a fast growth direction parallel to that of the heat flow will dominate the final structure after casting, therefore texture is more likely in thicker casts than in thinner casts where there is less heat flow through the material [39]. Secondary processes such as hot rolling, cold rolling and annealing also affect the amount of texture and texture orientation. Texture orientation after secondary processing is affected by the initial texture. As new grains nucleate during annealing (recrystallisation) they have a preferential direction and these preferential directions are referred to as fibres [40].

Formability is affected by texture; formability is plastic deformation of a material used to create shapes from the material. Manufacturing processes affected by a material's formability include deep drawing and pressing. Plastic deformation occurs in single crystals through the slip system, a process where permanent deformation of an atomic lattice is caused by the movement of dislocations due to applied force. Single crystals slip along planes (denoted using miller indices, e.g. {111}), slip occurs more easily in some planes than others. In polycrystalline structures deformation is more complex, slip in a single crystal can be obstructed by the crystal next to it. If crystals are aligned in similar orientations, there is a preferential texture, and the amount of obstruction is minimised making the material easier to deform [1].

Texture can affect the magnetic properties of cubic structures such as ferritic steels as the different cubic directions have different magnetic properties. For a single crystal [100] directions are said to be

magnetically easy; it is easier to magnetise a crystal if the applied field is aligned with the [100] cubic direction. [111] directions are magnetically hard; it is harder to magnetise the material with a field aligned in this direction. The effect of the different directions on the ability to magnetise a material is described as magnetic anisotropy and is caused primarily by spin-orbit interaction of electrons in neighbouring atoms [41]. Figure 11 shows the different cubic directions and the ease with which each direction can be magnetised.

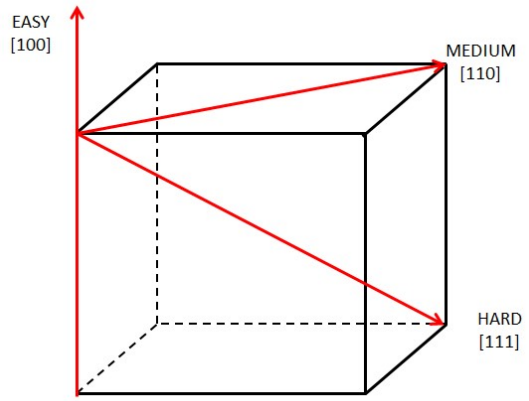

Figure 11: Magnetic anisotropy directions for a BCC crystal [27].

Magnetic anisotropy in ferromagnetic materials is dependent upon the alignment of neighbouring crystals within the structure. Where there is no preferential texture orientation, an applied magnetic field will have to cross multiple easy and hard magnetic directions; the net effect is no easily magnetised direction across the bulk of a material. However if there is a preferential texture within a material that can be aligned to an applied magnetic field it will be easier to magnetise the material in that direction [27]. An example of a material with defined texture which is easier to magnetise in one direction than another is grain oriented electrical steel; this is discussed in section 4.4.4.

Interstitial free steels are often used for applications which require significant deformation, texture control through the different manufacturing processes is very important to ensure good formability characteristics. Typical final textures for IF steels are {111}<110>, {111}<123>, {111}<121>, {111}<112> and {111}<011> [42, 43]. A detailed discussion of the expected magnetic anisotropy in IF steels is presented in section 4.4.4.

3.3. Chapter Summary

The purpose of this chapter has been to describe the steel making process, focusing on the areas where the EM sensor technique will be applied for this research (recrystallisation of cold rolled IF steel strip) and to look at the continuous annealing lines where an on-line EM sensor could be deployed to monitor recrystallisation.

The processes and mechanics of recovery and recrystallisation have been explained as a good understanding of the microstructural changes that occur during recovery and recrystallisation is essential when considering the experimental results recorded by an EM sensing system during annealing.

4. Magnetic Theory

IF steel is a single phase ferritic material with a body centred cubic structure at room temperature. Magnetic characteristics of IF steel below the Curie temperature follow the mechanism known as ferromagnetism. The magnetisation behaviour of IF steel is key to the research presented in this thesis. This chapter looks at the relevant magnetic characteristics that need to be understood in relation to the research presented.

4.1. Ferromagnetism

Materials which have magnetic properties and behaviour similar to iron are said to be ferromagnetic. Examples of ferromagnetic materials include iron, nickel, cobalt and many alloys of these materials. Ferromagnetic materials are not naturally magnetic on a macro scale, in that they do not generate their own magnetic field unless induced to do so. On a microscopic level ferromagnetic materials are formed of lots of magnetic poles and can be thought of as an assembly of lots of tiny permanent magnets, all of which are aligned in different directions, effectively cancelling each other out (magnetic poles are discussed later), Figure 12 (a).

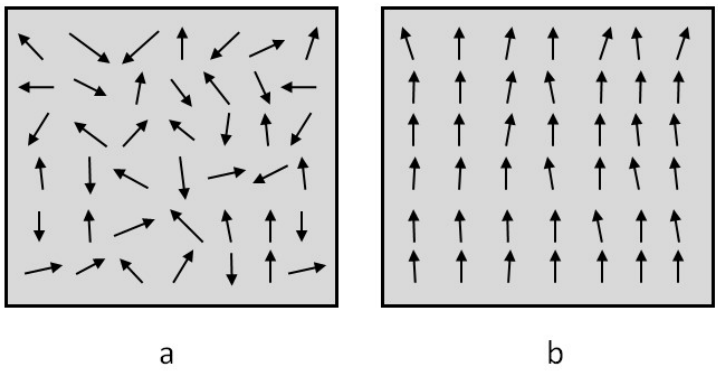

Figure 12: Distribution of directions of magnetic poles within a ferromagnetic material. (a) Ferromagnetic material with no magnetic field acting upon it, in a demagnetised state, (b) in a ferromagnetic material where an external field has caused the magnetic poles to align [41].

Ferromagnetic materials will be attracted to objects that have their own magnetic field such as permanent magnets and electromagnets; this attraction is caused by a magnetic field or force. Magnetic

fields may be produced by rare ferromagnetic materials which form permanent magnets. Naturally occurring permanent magnets are formed from magnetite or pyrrhotite. Of the two, magnetite produces the strongest magnetic field. Naturally occurring permanent magnets are unusual in that their magnetic fields do not diminish with time. The more usual sources of magnetic fields are either electromagnets or permanently magnetised ferromagnetic materials. Permanently magnetised magnetic materials are made when a ferromagnetic material is exposed to a magnetic field, causing alignment of magnetic poles. Electromagnets are created when an electric current is passed through a suitable material causing the generation of a magnetic field by forcing the alignment of disarrayed magnetic poles, both permanently magnetised ferromagnetic materials and electromagnets have magnetic poles that are aligned like those shown in Figure 12 (b) [27, 41].

Ferromagnetism is not caused by material chemistry; it is caused by its microstructure and atomic organisation. On an atomic level each electron within an atom has property called spin; the spin direction of the electron generates a magnetic moment for that electron. The spin of one electron can affect the spin of the electron next to it due to an overlap in the orbit of the electrons, this is called exchange interaction. Exchange interaction is relatively short range and is seen to become weaker if the atomic spacing and therefore spin separation is increased [41].

Generally electrons are paired and spin in opposite directions; the spins cancel each other out. There are electrons which are unpaired and if the spin directions of the unpaired electrons become oriented then a localised magnetic field is generated. Ferromagnetic materials in their natural state do not generate a magnetic field and this is due to the generation of magnetic domains on a granular scale within the material. Magnetic domains form naturally within a grain to reduce the magnetic energy within the grain to its lowest state (domain theory will be discussed later in this chapter) [41]. Magnetic domains are separated by boundaries called Bloch walls, the ease of movement of these walls is a very important factor in the use of magnetic non-destructive measurement techniques such as Barkhausen Noise [2] and EM sensors [44].

The ease with which a ferromagnetic material can be magnetised is related to its magnetic permeability, for most ferromagnetic materials it is easiest to relate the magnetic permeability of the material to the permeability of free space, this relationship is called relative permeability (μ_r). Materials that are easier to magnetise have higher relative permeability values. Permeability and the various different types of permeability are discussed later in this chapter. Relative permeability values for steel change with carbon content, the higher the carbon content the lower the permeability. Figure 13 shows the variation in permeability with carbon content for three different steels (0.11%, 0.99% and 1.8%), showing clearly that the measured permeability decreases with higher carbon content at different applied field levels [45]

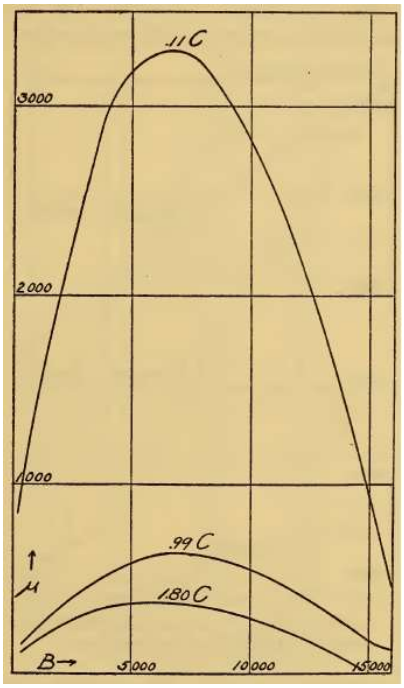

Figure 13: Variation of permeability with applied fields for steels of different carbon content [45].

The work presented in this thesis concerns IF steel which is a ferromagnetic material, however there are other types of magnetic behaviour which should be briefly mentioned as they have relevance under certain circumstances.

- Paramagnetism: Paramagnetic materials have very low permeability values, usually between 1 and 1.001. Permeability in paramagnetic materials is independent of applied field and temperature. Paramagnetic materials cannot be easily magnetised using an applied field. Examples of paramagnetic materials include potassium, sodium and ferromagnetic materials above their Curie point [27].
- Diamagnetism: Diamagnetic materials are those which can be magnetised with an applied field, but the direction of the magnetism is directly opposite to that of the applied field. Diamagnetic materials will be repelled from the poles of an electromagnet and will be attracted to weaker fields [27].
- Antiferromagnetism: Antiferromagnetic materials have no net total magnetic field but do possess ordered magnetic moments within their crystal structure. The magnetic moments align in antiparallel fashion, effectively cancelling out any overall magnetic field for the material as a whole [41].
- Ferrimagnetism: Ferrimagnetic materials possess ordered arrays of magnetic moments that are antiparallel in the same way as antiferromagnetic materials, however in ferrimagnetic materials the magnetic moments are not equal and spontaneous magnetisation still occurs as it does in ferromagnetic materials, albeit in much weaker manner [41].

All ferromagnetic materials become paramagnetic at high temperatures. The temperature at which a ferromagnetic material becomes paramagnetic is called the Curie Temperature (T_c). The effects of temperature on magnetic properties are discussed in detail later in this chapter [27].

4.2. Magnetisation and Permeability Curves (Hysteresis Loops)

When a piece of unmagnetised ferromagnetic material is brought near a magnet or subjected to the magnetic field of an electric current, magnetisation is induced in the material by the magnetic field. The magnetisation is described by a magnetisation curve obtained by plotting the intensity of magnetisation (I) or the magnetic induction (B) against the field strength (H). These curves are usually referred to as hysteresis loops and are a very important way of describing the magnetic characteristics of a material. An example hysteresis loop for iron is shown in Figure 14.

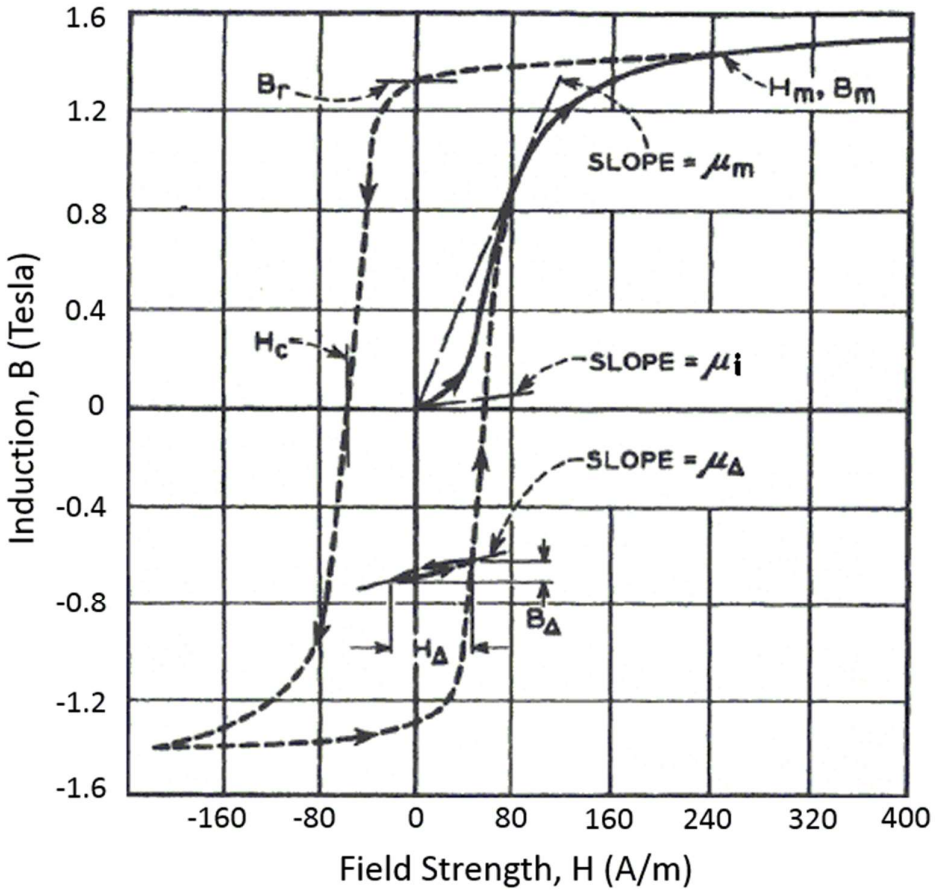

Figure 14: Hysteresis loop for iron. The dashed line shows the hysteresis loop and the solid line shows the magnetisation curve [27]. μi = initial permeability, μm = maximum permeability, μΔ = incremental permeability, H = field strength, B = magnetic flux, BΔ = applied incremental flux, HΔ = incremental field strength, Hm = field strength at maximum permeaility, Bm = applied flux at maximum permeability, Br = residual magnetic flux density, Hc = coercivity.

The ratio B/H is called permeability (μ) and is a representation of how the flux within the material changes in the presence of the applied magnetic field. A material's permeability changes depending on the amount of field that is applied, permeability can be measured by taking the slope of the magnetisation curve at a point relating to the field strength. Initial relative permeability (μi), represents the initial slope of the initial B/ H curve as the material is first magnetized from an unmagnetised state. For ferromagnetic materials after initial magnetisation caused by an increase in applied field the induction will not follow the same curve as the applied field is decreased (seen by the arrows in Figure 14, rather it lags behind the field as it is reduced. This gives rise to a characteristic curve for the material and is the reason why the curves are called hysteresis loops [27]. The lag of induction behind the reduction in applied field means that measurement of any magnetic property must first concern itself with the materials prior magnetic history, as it is possible for the material to still be magnetised even after the applied field has been removed altogether. This has particular implications for any electromagnetic non-destructive testing technique as the measurements that are taken can be misrepresentative. Depending on the types of measurements being taken and the prior magnetic history it may be necessary to demagnetise the specimen test sample.

If the applied field is increased indefinitely then the amount of magnetisation and the permeability will eventually reach a ceiling value, and the material is said to be saturated. Saturation is demonstrated in Figure 14 by the tips of the curve at the highest and lowest applied field values.

It is useful to define the terms coercivity and remanence at this point. Coercivity (H_c) describes the intensity of the magnetic field required to reduce magnetization to zero after a ferromagnetic material has been magnetised to saturation. Essentially coercivity measures a ferromagnetic materials resistance to demagnetisation. Coercivity is measured in Oersteds. Ferromagnetic materials with high coercivity are known as magnetically hard and can be used to make permanent magnets. Materials with low coercivity are known as magnetically soft and are used to make components which require rapid magnetisation or demagnetisation such as magnetic tapes or transformer cores. Remanence (remanant magnetisation) is the magnetisation that is left behind in a ferromagnetic material after a magnetic field

has been applied. Ferromagnetic materials with high remanence will maintain a magnetic field more easily after an applied magnetic field has been removed [27].

4.3. Magnetic Domain Theory

Iron and ferromagnetic steels in their natural state appear to be unmagnetised, they are both attracted by magnetic fields and can be magnetised under the application of a magnetic field. Explaining why this happens is possible through magnetic domain theory. Magnetic domains are formed when the spin directions of groups of electrons within individual crystals are aligned in a particular direction. If the electron spins are all aligned in the same direction then the magnetic energy state of the crystal is very high and unstable. To satisfy the need to reduce the magnetic energy state of the crystal magnetic domains form naturally, dividing the crystal up into areas with groups of electrons whose spins are aligned in widely different directions. Magnetic domains are separated by boundaries called domain or Bloch walls. This is represented simply and schematically in Figure 15 [41].

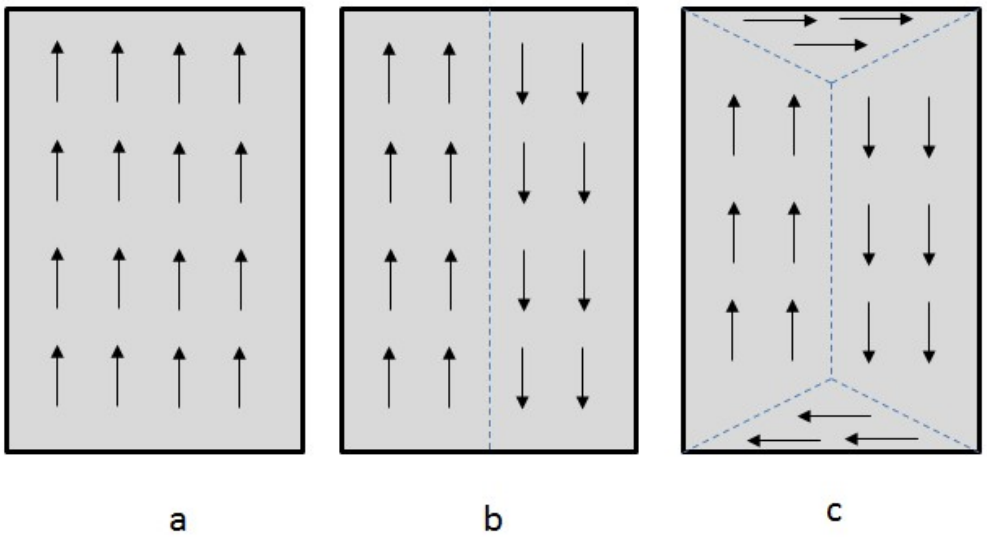

Figure 15: Representation of ferromagnetic crystal in three different states. Ferromagnetically ordered crystals can reduce their magnetic energy state by breaking up into complex structures of domains: (a) represents a crystal with a single domain which is in an unsustainable high energy state (this could be thought of as a single bar magnet). Reduction in magnetic energy can be achieved by the division of the single domain into multiple domains, (b) consists of a two domain structure (similar to having two bar magnets next to each other) which are of a lower energy state than (a). The magnetic energy state can be reduced still further by further division and the addition of further domains, known as closure domains (c) [41].

Magnetic domains in ferromagnetic materials are much more complex than that shown in Figure 15. A more realistic image of magnetic domains within a polycrystalline ferromagnetic material, such as IF steel, is shown in Figure 16.

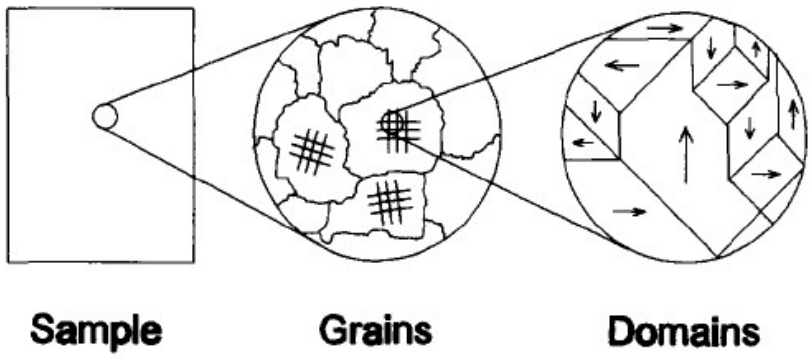

Figure 16: Magnetic domains in a polycrystalline steel [46].

The domain wall forms the boundary between two domains and plays an important part in how easily a ferromagnetic material can be magnetised by an applied field and how easily the material will lose its magnetisation once the field is removed. When a field is applied to a ferromagnetic material the domains that are aligned in the same direction as the applied field will become stronger and will grow at the expense of the other domains which are not aligned with the applied field. The number of electrons whose spin is aligned with the applied field becomes larger within the growing domain and the domain expands at its edges. To do this the domain walls must move to allow the domain to grow in size. The motion of the wall movement is smooth and demonstrated in Figure 17. On initial application of an applied field only the domains aligned in the direction of the applied field will grow, domains that are perpendicular may change shape but their polar direction will not change. If strong fields are applied then domains that are perpendicular to the applied field will start to rotate and shrink, eventually being destroyed once the material reaches saturation [41].

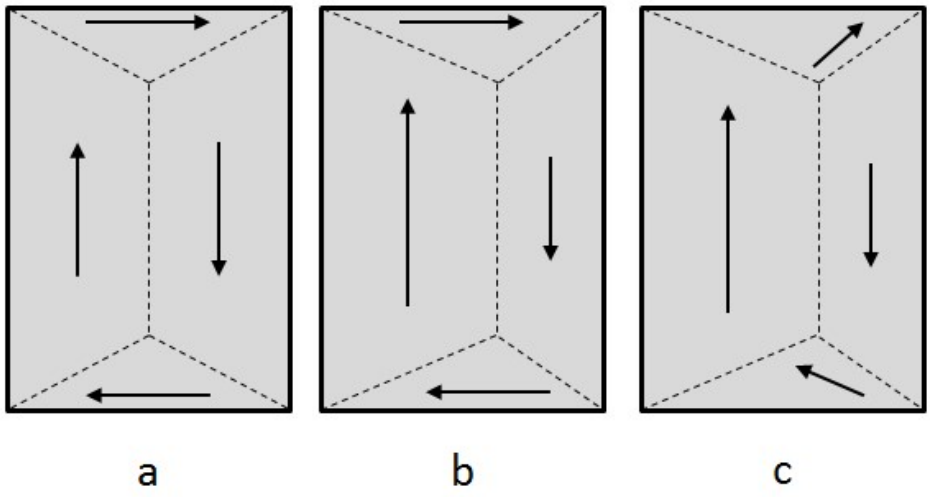

Figure 17: Magnetisation process in a ferromagnetic material: (a) shows an unmagnetised sample; (b) shows a sample that is being magnetised by a weak applied field that is aligned vertically, the domain that is aligned with the applied field has grown as the number of electrons with aligned spins grows; (c) shows the same sample under the influence of a strong magnetic field applied in the vertical direction, as the field is stronger domain rotation has started to take place.

If the applied field causing magnetisation is weak then the process is reversible and the domain walls will return to their original position. If the applied fields are strong enough the domain wall movement may be large enough that returning to their original position is not possible. Strong magnetic fields may have enough energy to move domain walls past crystalline imperfections such as dislocations, precipitates and even crystal boundaries so that domains join up across the material as a whole (the effects of crystalline imperfections on domain wall movement and permeability are discussed later in this chapter). When the field is removed these defects may prevent the domain walls from returning to their original position, causing magnetisation of the material as a whole. To return the material to its original state would require the application of a field in the opposite direction to that used for magnetisation [27, 41].

Figure 15 represents a simple two dimensional view of the magnetic domains in a single crystal and has no consideration of crystallographic orientation, or texture, of the ferromagnetic material being magnetised. Texture plays an important part in the alignment and movement of domains. It is known from magnetisation experiments that smaller applied fields are required to magnetise a ferromagnetic material in some directions than in others. For body centred cubic (BCC) ferromagnetic materials (such

as IF steel) it is easier to magnetise the material the more closely the field is aligned to the [100] direction of the crystal lattice as shown in Figure 11.

Magnetic domains will naturally try to align with the magnetically easy [100] direction. Texture is a product of the various rolling and heat treatment processes that are used in the steel making process. Texture development is important in the production of IF steel strip as optimum textures are required to achieve the best r-values for the strip to give it the best drawability [47]. R-values (Lankford coefficient), are a measure of plastic anisotropy for a rolled sheet material and give an indication of the ease of a materials formability [1]. Texture direction is associated with rolling and can mean preferential alignment of texture in different directions, the bulk texture in the rolling direction of a strip will be different to that in the transverse and normal directions. Therefore if there is preferential texture in a steel, there must be a degree of magnetic anisotropy associated with domain alignment in the magnetically easier directions [48]. Observation of domain alignment with texture in IF steels is difficult as the preferred texture aligns the {111} planes of the grains with the rolling direction and also because the grain size is very small [49]. Observation of domain alignment with texture is most easily made in grain oriented (GO) silicon steels which have a primary texture where the [001] direction is aligned with the rolling direction and the grains are very coarse. Figure 18 shows domains observed in GO silicon steel, the domains are magnetised parallel and antiparallel with the rolling direction, forming a distinctive striped pattern [50].

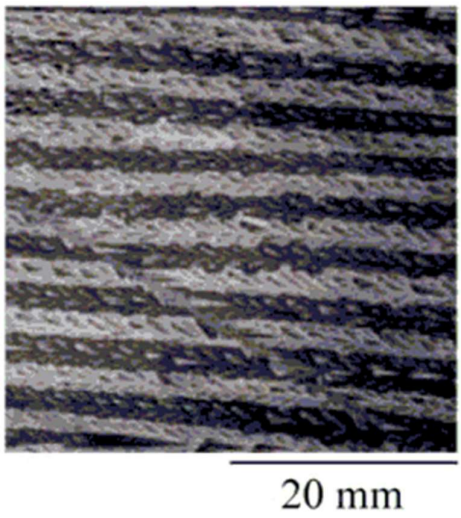

Figure 18: Magnetic domains observed using in a single grain of GO silicon steel. The rolling direction is left to right across the page [50]

Alignment of domains to texture causing magnetic anisotropy means that any bulk magnetisation measurement or electromagnetic measurement will require acknowledgement of the texture within the sample being tested [48], this is discussed in greater detail in section 4.4.4.

4.4. Permeability

The electromagnetic sensing technique chosen for an application is dependent on the magnetic property being measured. Different electromagnetic sensors are effective at measuring different parameters than others. The project work presented in this work is concerned with changes in permeability that are caused by recovery and recrystallisation, the sensors used are designed to measure changes in initial permeability at low fields. Different sensors are available that can measure changes in permeability. It is therefore important to understand what permeability is, the various factors that govern permeability values and how permeability will change during annealing and as a result of the microstructural changes caused by annealing.

The different types of permeability are defined by the slope of B/H taken from different points of a magnetic hysteresis loop. Permeability is effectively a measure of the ease with which a material can be magnetised. The different types of permeability are initial permeability, incremental permeability, maximum permeability, differential permeability and relative permeability. The value of the permeability change depends upon the amount of field applied and it is useful to consider the three different types of permeability that can be obtained from a hysteresis loop, each type is highlighted in Figure 14.

Initial permeability (μ_O) is the ratio of B/H as the applied field and inductance approach zero for the initial magnetisation curve. Initial permeability will increase or decrease in line with the relative permeability of the material. Initial permeability is particularly important for the research presented in this thesis as the applied field from an EM sensor is very small and the samples have no prior magnetisation history [27].

Maximum permeability (μ_m) is used to describe the largest ratio of flux to magnetic field that is generated during a magnetisation cycle. Maximum permeability is calculated using the steepest slope of the initial magnetisation curve. [27].

Incremental permeability (μ_Δ) is the permeability measured for a given field strength and induction. For a given field strength if the amplitude of the applied field is cycled between two values greater than zero after either initial magnetisation or during initial magnetisation, a permeability value for that cycle will be obtained. This is seen in Figure 14 by a smaller hysteresis loop (called a minor loop) within the full hysteresis loop that has its own ratio of B/H [27].

Differential permeability is simply the ratio of B/H for the magnetisation curve (dB/DH) [27].

Relative permeability is a special term which is very useful in classifying the permeability of one material in comparison with another. Relative permeability considers the permeability of a material for a given field in relation to the magnetic constant, otherwise known as the permeability of free space (μ_0), 12.6 x 10^{-7} T/m. Relative permeability is calculated by dividing the measured permeability (μ) of a material at a given field strength by μ_0. Most materials are paramagnetic and will have a relative permeability of close to 1, whereas ferromagnetic materials can have relative permeability's that are very high [51].

4.4.1. Variation of Permeability with Temperature

Temperature is one of the biggest factors that affect a ferromagnetic materials magnetisation. The greatest influence of temperature upon magnetisation occurs at high temperatures approaching the Curie temperature. As temperature increases ferromagnetic materials become more responsive to applied magnetic fields, that is to say that their permeability increases with temperature. The increase is permeability is not linear with temperature increase and the rate of permeability change as temperature increases varies with applied field strength. At low applied fields, permeability only increases with temperature until the Curie temperature (T_c) [27]. The effects of temperature on permeability at different applied field strengths for iron are seen in Figure 19.

In steels, when low fields are applied, permeability increases with temperature up to T_c in a similar way to iron. It has been reported that permeability increases with temperature for different steels and that the rate of increase varies between different grades of steel [45, 46]. When high applied fields are used the effect is reversed and permeability decreases as temperature increases. The tests were completed

using ring specimens of four different steels SPCC and SS400 construction grades as well as 6.5% Si (grain oriented) and 35A250 (non-grain oriented) electrical grade steels. The results reported show different permeability responses to temperature for different applied fields Figure 20 [52, 53]. Literature data looking into the effects of temperature on initial permeability for steels is sparse, the majority of the research considers the application of field strengths approaching magnetic saturation.

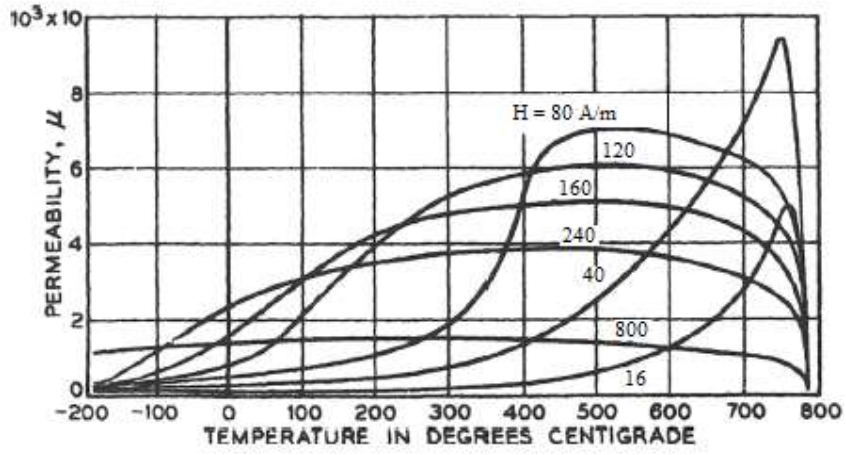

Figure 19: The effects of temperature on permeability for iron at varying constant field strengths [27].

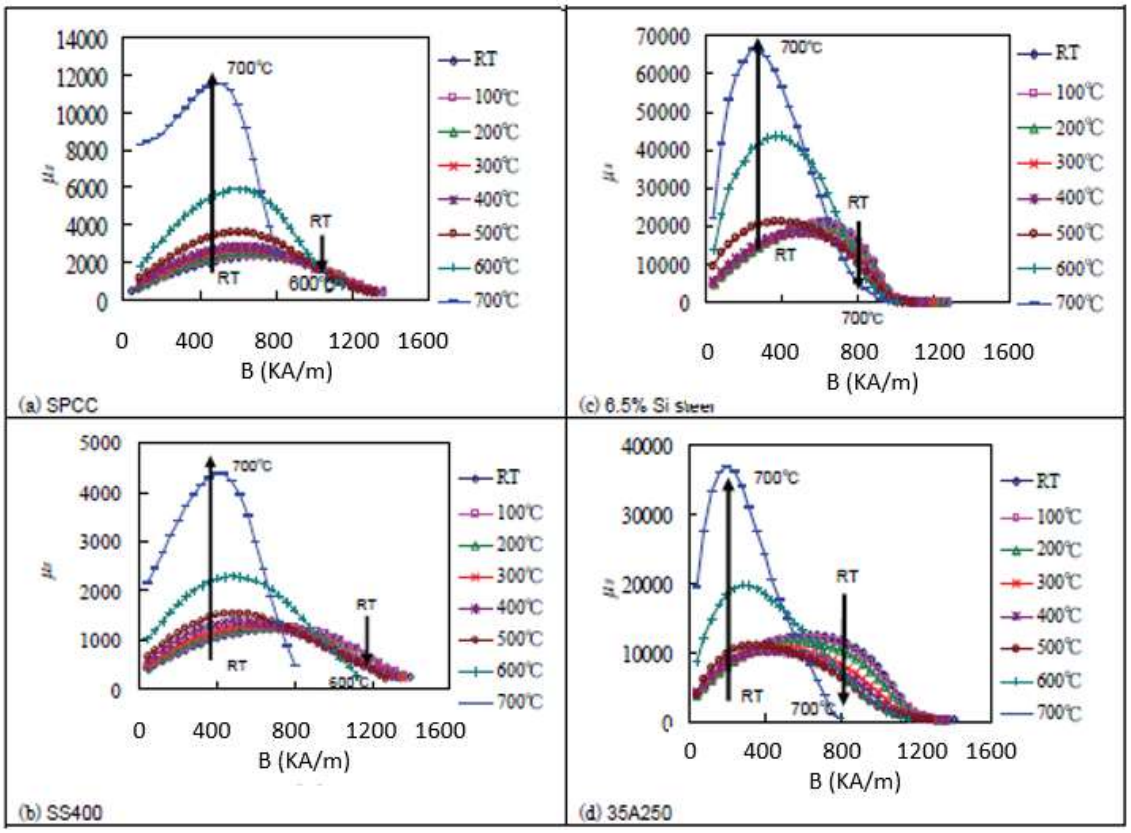

Figure 20: Comparison of permeability at different applied fields for varying temperatures (0°C to 700°C) for 4 different steel grades. (a) SPCC, (b) SS400, (c) 6.5% Si Steel, (d) 35A250 [53].

T_c varies depending on the material chemistry, T_c for pure iron is 780°C, pure nickel is 354°C and for pure cobalt is 1120°C. Different types of steel alloys will have different values of T_c depending on alloying elements, values of T_c for different grades of ferromagnetic stainless steels have been measured at 670°C to 750°C [27, 41, 54].

When the temperature of a ferromagnetic material exceeds T_c its permeability drops to a value of 1 very quickly. Once the temperature of the material exceeds T_c the material changes from ferromagnetic to paramagnetic. A combination of exchange energy and internal thermal energy changes cause the magnetic moments within the material to become misaligned and cancel each other out [27, 41].

4.4.2. Variation of Permeability with Stress and Strain

Magnetic properties in ferromagnetic materials are affected by changes in stress. The effects of stress on ferromagnetic properties can be very large. In iron based alloys (such as IF steel) tension causes increases in permeability at low fields [27]. Figure 21 shows magnetisation curves for iron with varying applied elastic tensile stresses ranging from zero applied stress to 4 kg/mm^2 (data derived from literature), it can be seen that permeability increases with stress at constant field strength. The amount of increase with applied stress is not linear as the applied field increases, permeability increases by a greater amount at higher fields for the same stress increase.

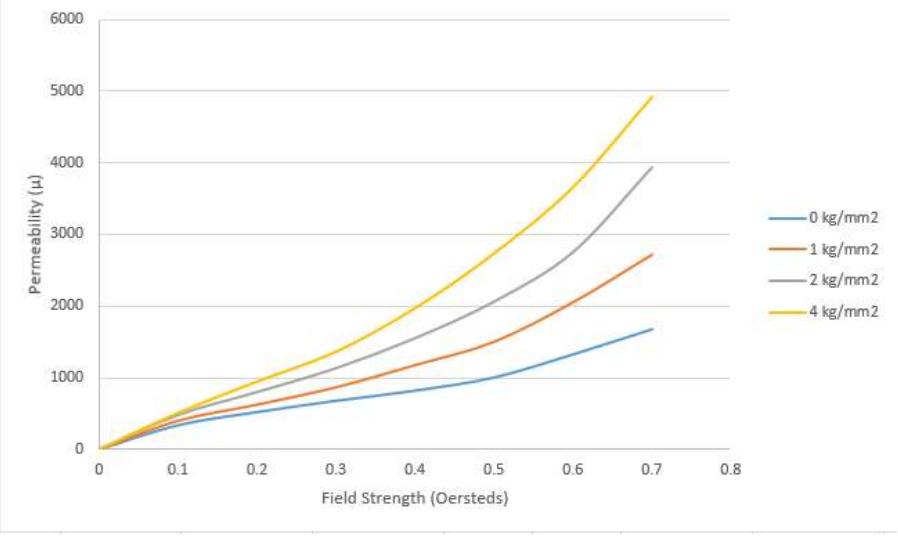

Figure 21: Magnetisation curves for iron with applied stresses ranging from 0 to 4 kg/mm^2 (data derived from literature) [27].

The magnetic induction required for saturation remains unchanged for tensile stresses within the elastic region. Application of stresses beyond the elastic limit will usually decrease permeability of annealed materials due to the introduction of dislocations with plastic deformation [27]. Figure 22 shows the effect that plastic deformation has on initial permeability for 7090 grade carbon steel (0.17% carbon content) samples, each sample has undergone a different heat treatment. The data shows that plastic deformation has a dramatic effect on initial permeability, with the largest decrease in initial permeability taking place in the first 2% of plastic deformation [55].

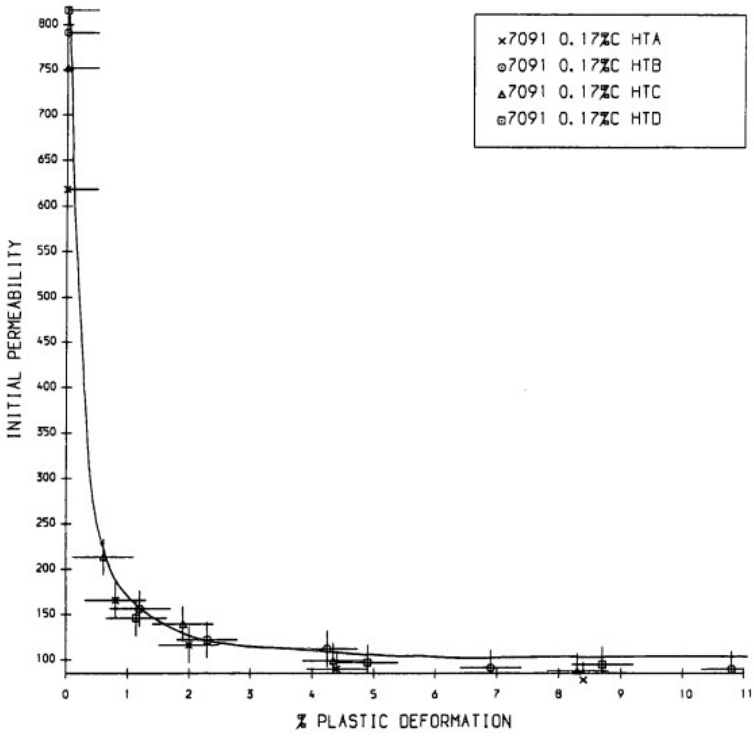

Figure 22: Variation of initial permeability (μ_i) with plastic deformation for annealed samples of 7091 grade steel (0.17% carbon content) [55].

Changes in permeability caused by applied stress are due to a phenomenon called reverse magnetostriction. Magnetostriction is defined as the change in a materials shape caused by an applied magnetic field, reverse magnetostriction is the change in magnetic properties caused by shape change (when stress is applied to a material). Changes in permeability caused by reverse magnetostriction must therefore be directional, at low applied fields tensile stresses will cause an increase in permeability below the elastic limit in the direction of the applied stress and a decrease in permeability in the direction perpendicular to the applied stress (which is in compression). Below the elastic limit the changes in permeability are closely linked to the orientation of magnetic domains to the applied stress and the applied field. Domains will tend to elongate in the direction of the applied tensile stress, making it easier to magnetise the material with a field aligned in the direction of the applied stress, a simple representation of this effect is shown in Figure 23. In reality only some of the magnetic domains within

the material are reoriented due to the introduced stress, and as a result the application of stress introduces no permanent magnetisation in the material [27, 46, 56].

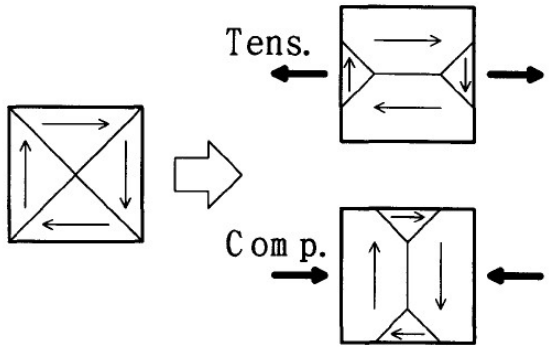

Figure 23: Domain reorientation caused by applied stress [46].

Electromagnetic techniques have been used to measure both residual stresses and applied stresses. Details of these techniques are discussed in section 5.4.5.

4.4.3.EM Methods for Measurement of Stress and Strain

As steel strip moves through a continuous annealing line the tension in the strip will fluctuate. Any EM sensor that is deployed will need to be able to account for strip tension changes during on-line measurement and it is important to show that EM sensing systems can account for changes in strain caused by changes in strip tension.

Jagadish et al. investigated uniaxial elastic stress in pipeline steels using Magnetic Barkhausen Noise (MBN) and showed that Barkhausen noise is affected by both tensile and compressive stresses. Rms MBN voltage was shown to increase with tension and decrease with compression, Figure 24, MBN voltage is the voltage outputted by the sensor (Hall effect probe, outputting a voltage measurement from the instrument) at any given time during MBN measurement. It was explained that the realignment of magnetic domains with the applied stress combined with the direction of the applied field (which was in the same direction as the applied stress) increased the MBN output. The opposite was true for compressive stress as the magnetic domain realignment was not in line with the applied stress or field [57].

A study by Stefanita et al. which was completed on mild steel plates showed a similar trend for elastic tensile stress, MBN energy increased during the application of elastic tensile stress. MBN energy measurements are directly related to the energy required for domain walls to overcome pinning sites. Stefanita et al. continued the work into plastic strain and showed that the effect of plastic strain on MBN energy was much smaller, and possibly, inverse to that of elastic loading [58]. In both cases the change in MBN output due to elastic loading was linear to the applied tension.

Krause et al. investigated the output for MBN on pipeline steels during elastic loading and unloading above 200 MPa (the steels yield stress was 600 MPa). The results show an increase in MBN energy under elastic tension and that there was a decrease in MBN energy when the samples were unloaded, Figure 25. Three samples were tested, each of the same composition but cut from different parent samples. Each sample displayed a degree of hysteresis in the measured MBN energy on unloading, but the work showed that the effects of elastic loading on MBN energy output is reversible under elastic loading conditions [59]

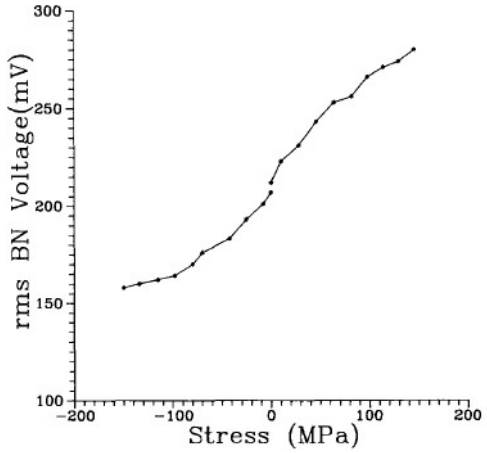

Figure 24: rms Barkhausen noise voltage output for tensile and compressive elastic strains [57].

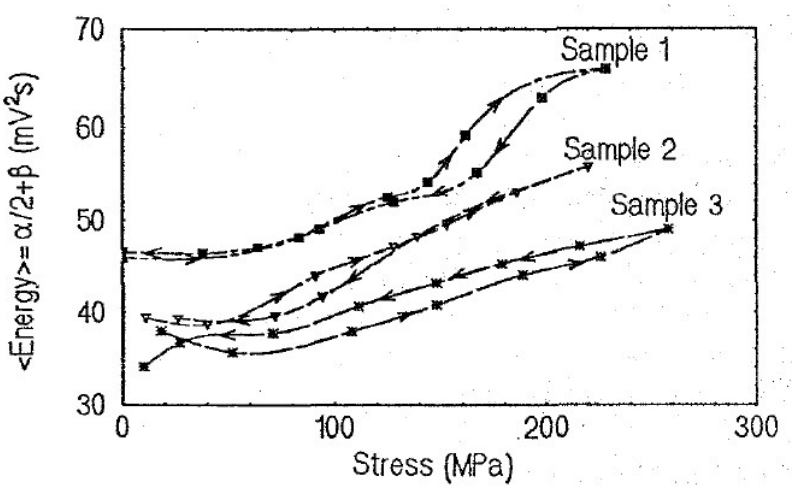

Figure 25: MBN energy for elastic tensile loading and unloading of pipeline steel [59].

Kwun and Burkhart looked at the effects of tensile and compressive stresses on magnetic hysteresis loops in ferromagnetic stainless steel. Their work showed that the hysteresis loop shapes were significantly changed by the application of tensile and compressive stresses, an example of the changes are shown in Figure 26. For all of the samples tested it was found that tensile stress increased the magnetic induction (B) and that compressive stress decreased B. The increase of induction under tension represents an increase in permeability under tension [60]. Similar results were obtained by Sipeky and Ivanyi in an investigation into grain oriented silicon steels. They found that permeability, H_c and the gradient of hysteresis curves all increased with applied tensile stress. They also found that energy losses decreased for hysteresis loop measurements as tension was applied to the samples. Their work concluded that hysteresis loop measurement was an accurate method of measuring tensile stress within grain oriented electrical steels [61].

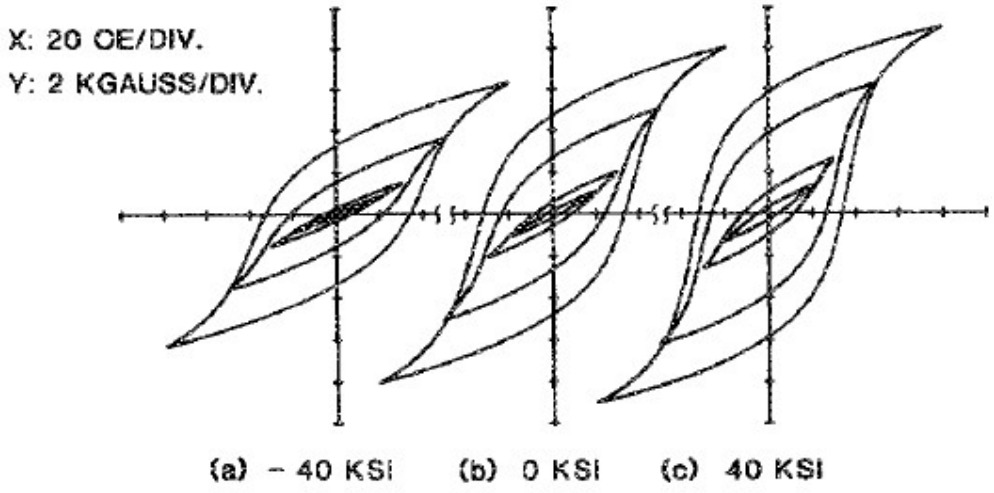

Figure 26: Hysteresis loops for AISI 410 ferritic stainless steel in both compression and tension (1 KSI = 6 MPa) [60].

Wilson et al. studied changes in residual magnetic fields in samples of flat drawn steel [54]. The measurements were taken in both the direction of applied stress and perpendicular to the direction of the applied stress. Magnetic field increases were found to be larger in the direction of applied stress, measurements were taken in several different positions across the sample and all returned the same trends, Figure 27. No changes in field were recorded for low applied stresses, increases only became apparent at stresses of over 50 MPa [62]

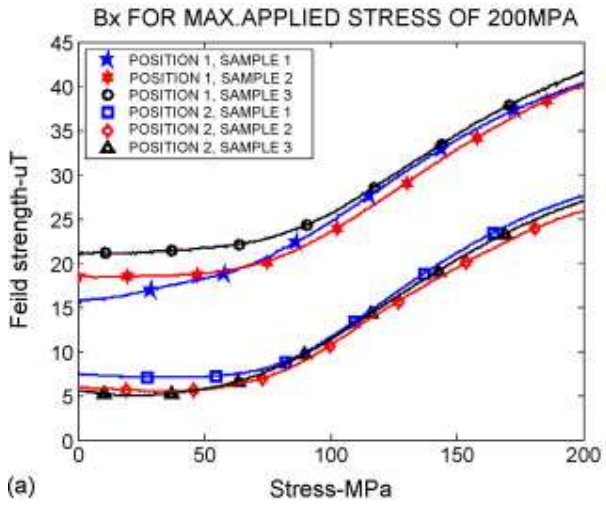

Figure 27: Residual magnetic field measurements in the direction of applied tensile stress for flat drawn steel samples [62].

4.4.4. Variation of Permeability with Texture

During steel manufacturing processes such as cold rolling and annealing texture develops due to rotation of the crystal lattice. As the crystal lattice reorients the magnetically easy [100] and hard [111] rotate with respect to the rolling direction. The development of crystallographic texture can lead to magnetic anisotropy within a ferromagnetic material, meaning that it will be easier to magnetise in one direction than it is in another. Anisotropy will occur if there is a preferred texture which develops during cold rolling and recrystallisation, whichever direction has a primary alignment of [100] cube axes will be more easily magnetised than any other axis [63].

Texture for IF steel after cold rolling is weak and dominated by texture developed during hot rolling. These textures are {111}<110>, {111}<121>, {111}<123>, {001}<110> and {112}<110>. Recrystallisation textures are dominated by grain orientations where <111> is aligned with the rolling direction (RD), the most commonly reported recrystallised textures are {111}<110>, {111}<123>, {111}<121>, {111}<011> and {111}<112> [64-66]. These textures form up to 70% of the bulk texture in recrystallised IF steels. No single texture dominates the overall microstructure, {111}<110> and {111}<121> are reported to be at around 15% of the volume and {111}<123> texture has higher volume, up to 20%. The rest of the microstructure is formed of more random textures [47, 65, 67]. Tata Steel Europe have confirmed that the reported textures for IF steel in the literature are the same as those contained within the commercial IF steels produced at their Port Talbot steel mill [68].

As there are a variety of textures within cold rolled or recrystallised IF steel it is not obvious that there will be any strong degree of magnetic anisotropy. Table 2 lists the orientations of the magnetically easy cube axes ([001], [010] and [100]) for the deformed (as-received) condition and Table 3 lists the orientations of the magnetically easy cube axes in relation to both the RD on the RD plane (first number in brackets) and RD in the ND plane (second number in brackets) of IF steel strip. The primary recrystallised textures in IF steel do not have any magnetically easy cube axes lying in RD plane.

Table 2: Orientations of magnetically easy cube axes for the primary textures within deformed IF steel.

Texture	Orientation of (100)	Orientation of (010)	Orientation of (001)
{111}<110>	(45.0°, 30°)	(75.0°, 45°)	(15.0°, 45°)
{111}<123>	(74.5°, 30°)	(44.5°, 45°)	(5.5°, 45°)
{111}<121>	(66.0°, 30°)	(6.0°, 45°)	(36.0°, 45°)
{001}<110>	(45.0°, 30°)	(45.0°, 0°)	(45.0°, 0°)
{112}<110>	(45.0°, 26.6°)	(45.0°, 26.6°)	(45°, 63.4°)

Table 3: Orientations of magnetically easy cube axes for the primary textures within recrystallised IF steel.

Texture	Orientation of (100)	Orientation of (010)	Orientation of (001)
{111}<110>	(45.0°, 30°)	(75.0°, 45°)	(15.0°, 45°)
{111}<123>	(74.5°, 30°)	(44.5°, 45°)	(5.5°, 45°)
{111}<121>	(66.0°, 30°)	(6.0°, 45°)	(36.0°, 45°)
{111}<112>	(19.5°, 30°)	(10.5°, 45°)	(49.5°, 45°)
{111}<011>	(35.3°, 30°)	(65.0°, 45°)	(5.30°, 45°)

Grain oriented (GO) silicon steel, which is used in transformer cores, is designed to have very high magnetic anisotropy. Magnetic anisotropy in GO silicon steels is obtained by careful control of texture. GO silicon steel possesses "cube on edge" or GOSS texture ({110}<001>), which aligns the [100] easy axis with the rolling direction of the sheet [69, 70], Figure 28. Table 3 shows the orientations of the magnetically easy cube directions ([100], [010] and [001] and the magnetically hard cube direction [111] for GO silicon steel. The orientation nomenclature used in Table 4 is the same as Table 3.

Table 4: Orientation of magnetically easy and hard directions for GO silicon steel

Texture	Orientation of (100)	Orientation of (010)	Orientation of (001)	Orientation of (111)
{110}<001>	(0º, 0º)	(90º, 45º)	(90º, 45º)	(54º, 0º)

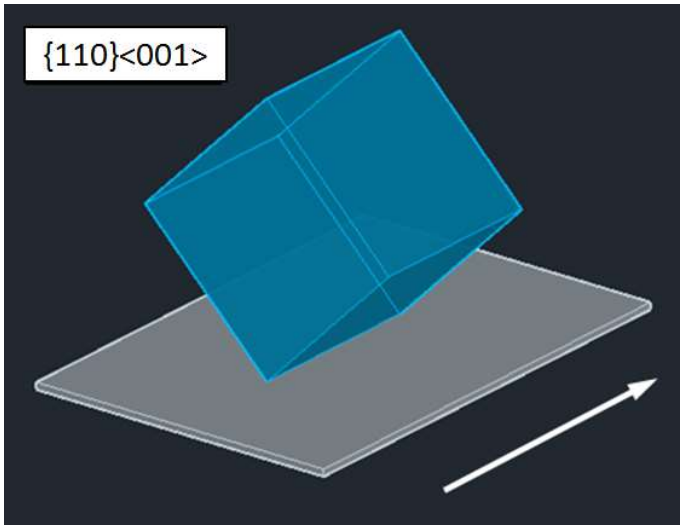

Figure 28: Single cube oriented to [110]<001> texture (cube on edge). Rolling direction is shown by white arrow.

Figure 29 shows the affect that texture has for GO electrical steel, the highest induction (and therefore the highest permeability) is aligned to the rolling direction (0º) which is aligned to the [100]<001> texture. The lowest induction values are shown between 45º and 60º from the rolling direction, and intermediate induction values are shown at 90º to the rolling direction [71].

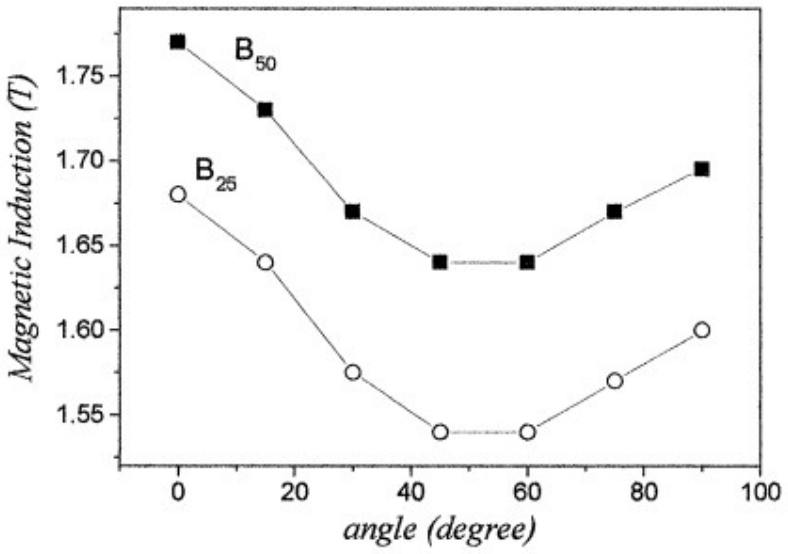

Figure 29: Magnetic Induction at applied field values of 2500 A/m (B25) and 5000 A/m (B50) as a function of the rolling direction [71].

4.4.5.Permeability, Microstructural Features and Grain Growth

A material's permeability value is associated with the different microstructural features within ferromagnetic materials. The types of features which effect permeability are dislocations, grain boundaries, precipitates and phase balance. Understanding the effects of these features on permeability is essential in explaining the responses of any magnetic measurement system which is being used to monitor recovery and recrystallisation. Microstructural features effects on permeability are closely linked with magnetic domain theory as the features act as restrictions to the free movement of domain walls and domain size [27, 72].

Magnetic domain alignment with an applied magnetic field requires domain wall movement in order that the domains can move, grow and rotate. If domains can move easily without restriction, then the materials permeability will be higher than in a material where the domains are not free to move. Microstructural features prevent free movement of domain walls since they act as pinning points. At low fields domain walls may not be able to move past the pinning points, higher applied fields will force the domain walls to overcome the pinning points and move past them.

When the applied field is removed the domain walls will try to move back to their original positions, this may not be possible if pinning points were overcome during magnetisation and the domains walls may become pinned as they move back toward their original position. Pinning of domain walls after magnetisation causes permanent magnetisation, in order to return the domain walls back to their original positions a field needs to be applied in the opposite direction to the original applied field. Domain wall pinning is illustrated in Figure 30 [27, 73].

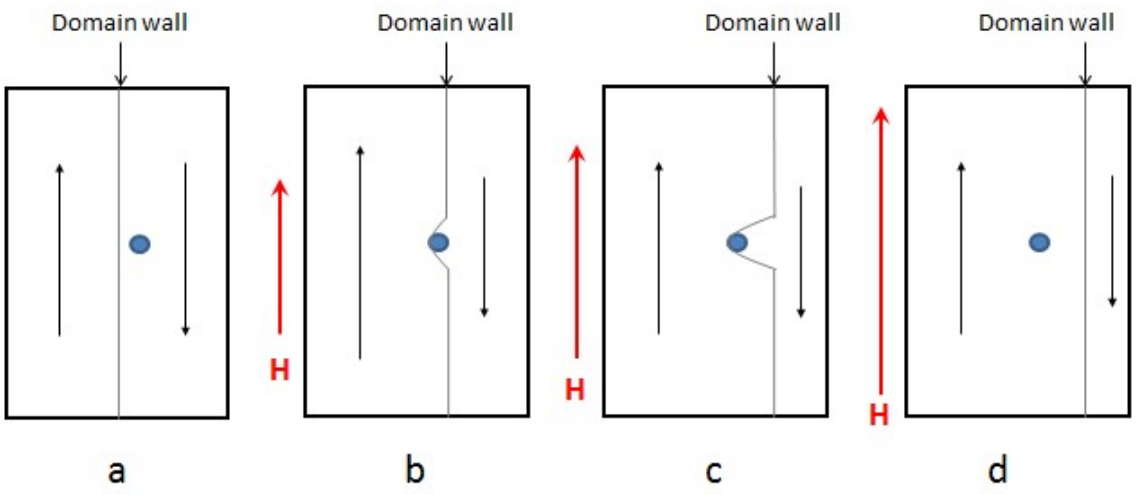

Figure 30: Illustration of domain wall movement and pinning. (a) Sample in an unmagnetised state, domains are evenly sized; (b) low magnetic field H applied to the sample, domain parallel with the applied magnetic field grows at the expense of the domain which is antiparallel to the applied field, domain wall becomes pinned; (c) stronger magnetic field H is applied, further movement of the domain wall takes place but the pinning point cannot be overcome; (d) high magnetic field H is applied and the pinning point is overcome, the domain wall is now free to move.

At low fields the magnetisation process is primarily governed by the domain wall movement, the greater the number of pinning points the harder it is for the domain walls to move [73]. The heavily deformed microstructure of cold rolled IF steel has a high dislocation density (pinning points) and the EM sensor technique used in this project operates at very low fields, so it follows that changes in dislocation density of IF steel will be a key factor affecting permeability.

Precipitates form in steels during heat treatment processes, precipitation is an important parameter to control in steel manufacture as it can affect hardness and yield strength. Precipitates act as pinning points and hinder the free movement of domain walls.

The amount of pinning caused by precipitates is related to the size of the precipitate, precipitates that are the same width as the domain wall cause the greatest amount of pinning [74]. Precipitates play an important role in the control of both texture and grain size during recrystallisation. Typical precipitates that form in IF steels during heat treatments are TiS, TiC_4S_2 and TiN. Precipitates are formed during the casting and hot rolling processes, it is reported that very little precipitant growth occurs below 800ºC (higher than the recrystallisation temperatures used in this project) [75] [76].

Grain size plays an important role in the permeability of ferromagnetic materials. The relationship between grain size and permeability has been studied in detail for silicon steels, where it is of particular importance, and shown to be a factor in the permeability of low carbon steels [3, 77, 78]. Coercivity (H_c) reflects the amount and pinning strength of a material as it is related to the density of grain boundaries. Both theoretical [79, 80] and experimental [81] work have related H_c to grain diameter (d_k):

$$H_c \propto \frac{1}{d_k}$$

Grain boundaries act as pinning points for domain wall movement due to the presence of defects at the grain boundary as well as the misalignment of texture between two grains [82]. Investigation of recovery and recrystallisation using an EM technique will be heavily affected by reduction in dislocations density and the grain size [72, 83].

4.5. Chapter Summary

The recovery and recrystallisation process will cause changes in relative permeability in IF steel through a combination of changes in dislocation density, grain size and texture. Each of the parameters will affect the change in permeability by a different amount, potentially with one parameter being more dominant than another. It is known that changes in dislocation density and grain size will have a direct effect on relative permeability as they change the degree of magnetic domain wall pinning [84]. Texture does affect material permeability when there is a single dominant texture, as seen in GO silicon steels, however there is no reported effect of texture on permeability for IF steels which may be due to the weaker reported textures. It has been shown that permeability in ferromagnetic materials will change with variations in stress and strain.

5. NDT Techniques for Measuring Recovery and Recrystallisation

Several non-destructive testing techniques have been developed which are capable of measuring recovery and recrystallisation. A review of these techniques and the relevant strengths and weaknesses are presented in this chapter.

5.1. Ultrasonic Techniques

Ultrasonic non-destructive measurement uses high frequency sound waves to conduct examinations of materials. Ultrasonic measurements can be used to characterise materials, measure dimensions, assess material properties and look for internal inclusions or flaws in a material. To initiate a measurement a pulse of ultrasonic sound is introduced into the test subject. The pulse will be reflected from the back surface of the test sample, the amplitude of the reflection and the time taken for the reflected pulse to be received will be dependent on the sample's microstructural characteristics, secondary reflections will be received from defects (such as inclusions or cracks). An illustration of the general principle of ultrasonic measurement is shown in Figure 31.

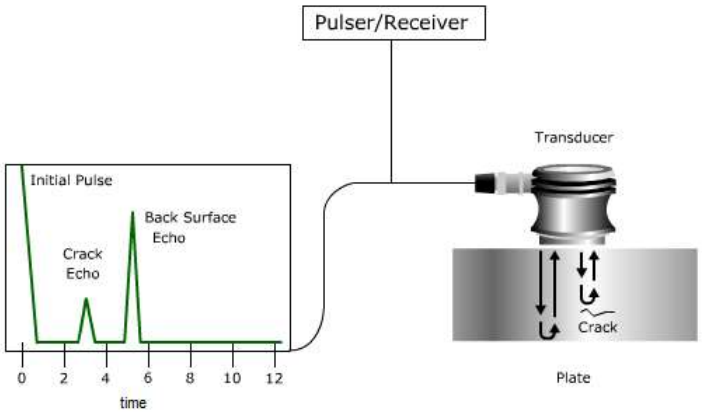

Figure 31: Basic principle of ultrasonic inspection [85]

Many different ultrasonic techniques exist; including laser ultrasonics, electromagnetic acoustic resonance (EMAR) and basic ultrasonic testing. Each different technique has its own requirements, basic ultrasonic inspection requires good surface preparation and a couplant to ensure good sound transmission into the sample. EMAR systems do not require couplant, making them easier to deploy,

although they suffer from lower efficiency and require careful electronic design. Laser ultrasonic systems use lasers to generate and receive ultrasonic sound waves, laser ultrasonics measurement does not require contact with a sample but is limited by needing a clear line of sight to the test sample as well as restricted access to test samples due to the hazards if working with lasers [86].

Propagation of sound waves through a material is affected by microstructural properties or defects such as grain size, deformation and crystallographic texture [87, 88]. Moro et al. [89] showed that ultrasonic pulse-echo measurement could be used to distinguish between different amounts of cold working in stainless steel, with a correlation between the amount of deformation and wave velocity. The work showed that the more deformed the grain structure becomes (greater amount of dislocations), the slower the velocity of the sound wave through the material, Figure 32.

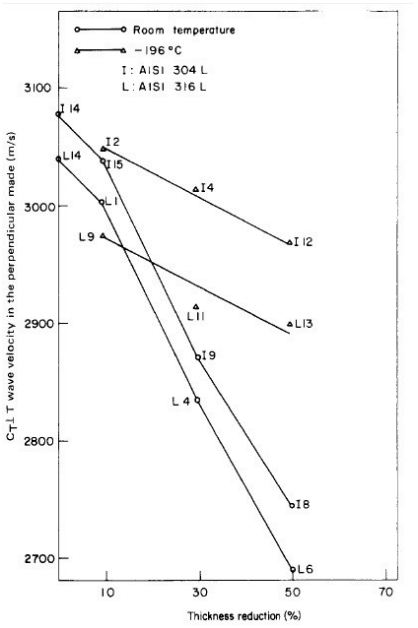

Figure 32: Wave velocity (T wave) against deformation for AISI 304L and 316L stainless steels, the different numbers on the chart (I9, I8 etc.) are sample numbers [89].

Ogi et al. showed that ultrasonic attenuation could be used to investigate grain size using the EMAR system on low carbon steels. Application of the EMAR system showed that grain size could be evaluated and that there was good agreement between the EMAR system and grain sizes estimated by microscopy, Figure 33. In samples where there was a broad distribution of grain size the EMAR system was shown to give an estimate of average grain diameter that was within an error band of 6 μm when compared with optical microscopy. Some outliers can be seen and this is because of a difference between what is optically viewed as a grain boundary and what the EMAR system defines as a grain boundary. The EMAR system views elastic discontinuities as grain boundaries, and this causes confusion in the EMAR measurements, particularly for martensitic steels. Phase boundaries in dual phase steels can also be seen as grain boundaries by the EMAR system adding to the error margins [88].

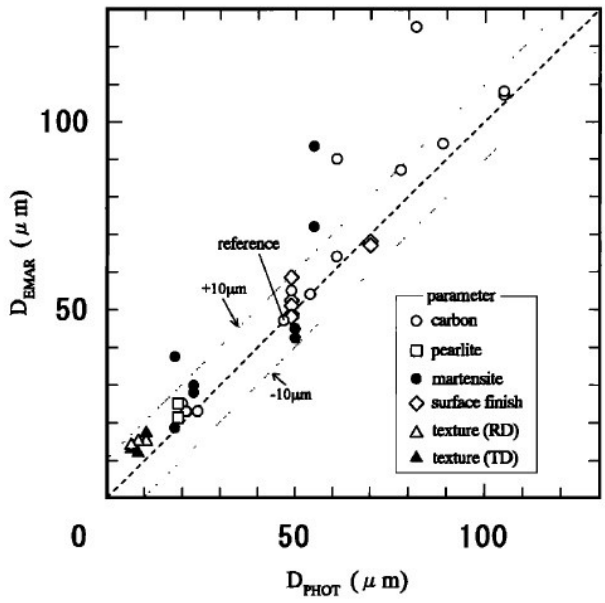

Figure 33: Relationship between average grain diameter measurements made using the EMAR system and measurements made by optical microscopy. Different low carbon steel samples were tested, each with a different initial microstructural parameter such as carbon content, pearlite fraction, surface finish or texture. Grain diameter was measured for the samples of each different parameter type [88].

Grain growth in austenitic AISI 316 stainless steel was analysed using laser ultrasonics at both room and high temperatures. Room temperature measurements of samples with different grain sizes were shown to return different fast Fourier transform (FFT) spectra for coarse and fine grained conditions, Figure 34. Details of the technique used to obtain the FFT ratios are in reference [90]. Laser ultrasonic measurements looking at the fast Fourier transform ratio for AISI 316 samples heat treated for different times showed an almost linear relationship between ASTM grain size and FFT ratio, Figure 35. This ratio was then used to look at dynamic measurements of grain growth in samples held isothermally at 1000°C and 1050°C using induction heating. The results showed that grain growth could be monitored using laser ultrasonics as heat treatment occurred [90].

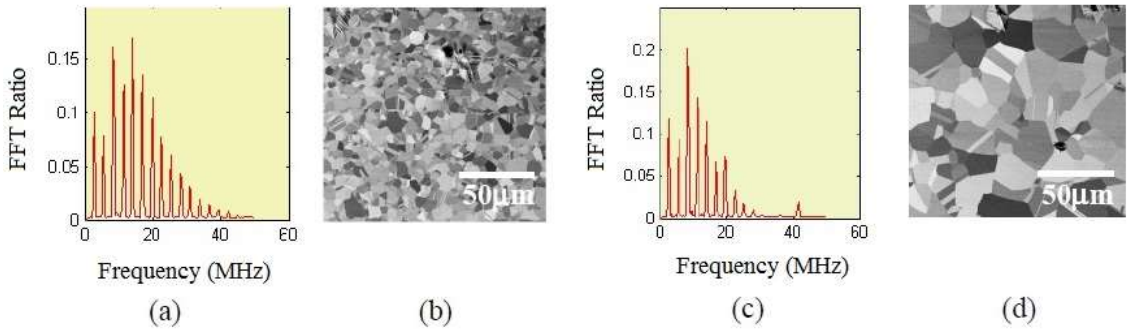

Figure 34: FFT spectra and microstructures for 316 steel in fine grained condition,(a)+(b), and coarse grained condition, (c)+(d) [90].

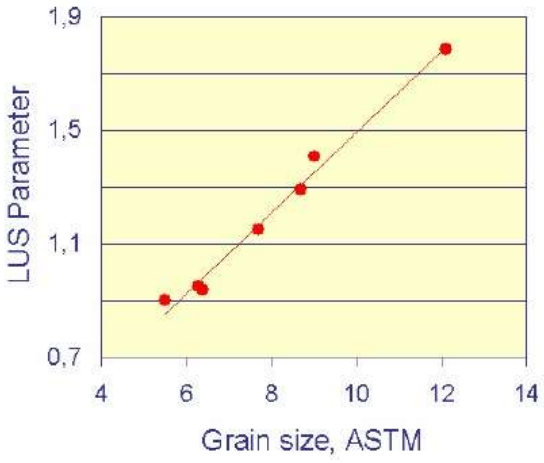

Figure 35: Relationship between the FFT ratio and grain size for 316 stainless steel [74]

Studies of recrystallisation at room temperature for IF steels were completed by Pandey et al [91]. The work reported a relationship between IF steel samples annealed for different times at 650°C in order to initiate different amounts of recrystallisation and surface wave velocity. Recrystallisation was assessed using hardness measurements and optical microscopy which were correlated against ultrasonic measurements. The results from the tests show an increase in wave velocity as recrystallisation takes place which is matched against a drop in hardness associated with recrystallisation, Figure 36. The data reported concluded that the ultrasonic technique used was sensitive to changes caused by recrystallisation but not recovery [91].

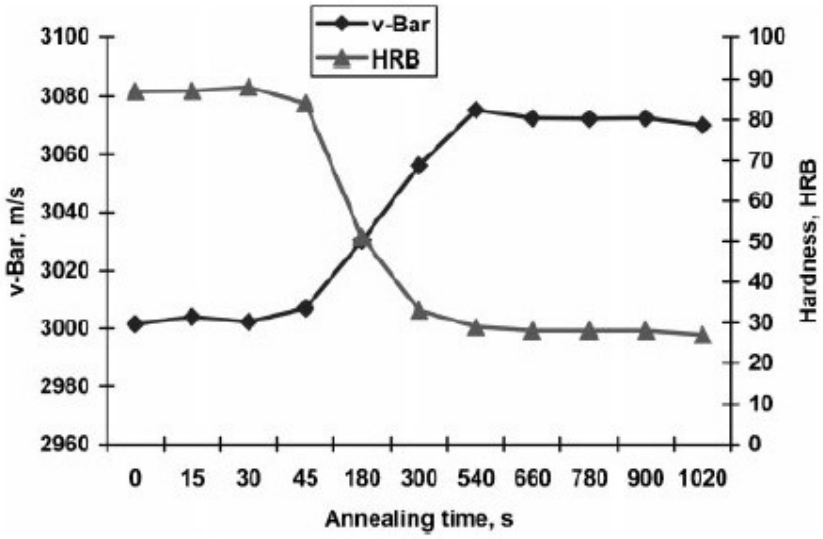

Figure 36: Relationship between surface wave velocity and hardness for IF steel with different annealing times at 650°C. The increase in surface wave velocity corresponds with the decrease in hardness associated with recrystallisation [91].

Laser ultrasonics have been used to monitor recovery and recrystallisation for different materials. Kruger et al. used laser ultrasonic spectroscopy to monitor recrystallisation for two different compositions of cold rolled aluminium alloy (AA5754 and AA6111) that were annealed in a Gleeble thermomechanical simulator by considering texture changes that took place during the recrystallisation process at different temperatures. The work concluded that ultrasonic measurement of recrystallisation agreed well with traditional metallographic and softening mechanisms that are used for measurement of recrystallisation [92].

Characterisation of steel transformation in a hot strip mill environment was performed by Hutchinson [93], the work recognising the importance of being able to monitor the condition of a material throughout its processing in order to maintain quality and uniformity of properties. In this respect the work was very similar in its target to the work presented in this thesis for an EM sensor (a comparison of NDT techniques is presented in section 5.5), the difference being that the ultrasonic measurement equipment was deployed to look at characterisation of hot strip rather than recrystallisation in continuous annealing of sheet steel. The hot strip mill presents similar problems to a continuous annealing line in terms of environment, high temperatures with moving steel and so it is a useful comparison system for any EM sensor research with in-situ measurement as the end goal. The research found that different behaviour was observed for different chemistries of steel and that it was possible to deduce phase transformation from austenite to ferrite in-situ at high temperature [93].

In-situ laser ultrasonic measurement of low carbon steels annealed in a Gleeble at temperatures between 590^{o}C and 610^{o}C showed that ultrasonic measurements were very sensitive to recrystallisation. The velocity of ultrasound measurements was found to first decrease and then increase as recrystallisation took place, this was linked to a combination of both texture evolution and magnetomechanical damping during the recrystallisation process. The work concluded that ultrasonic velocity measurement was a promising tool for the characterisation of recrystallisation and annealing in low carbon steels, although further work was required due to changes in velocity still taking place after recrystallisation had finished [94].

Investigation of recovery in ferritic ultra-low carbon steel using in-situ laser ultrasonics has shown that ultrasound wave velocity is sensitive to the recovery process and is attributed to dislocation damping whereas attenuation of ultrasound waves remains constant throughout recovery. Ultrasound velocity was seen to decrease as recovery occurred, recovery in the test samples was confirmed by the measurement of stress relaxation in the sample. Recovery was monitored at three different temperatures (550^{o}C, 730^{o}C and 800^{o}C), the results can be seen in Figure 37 [95].

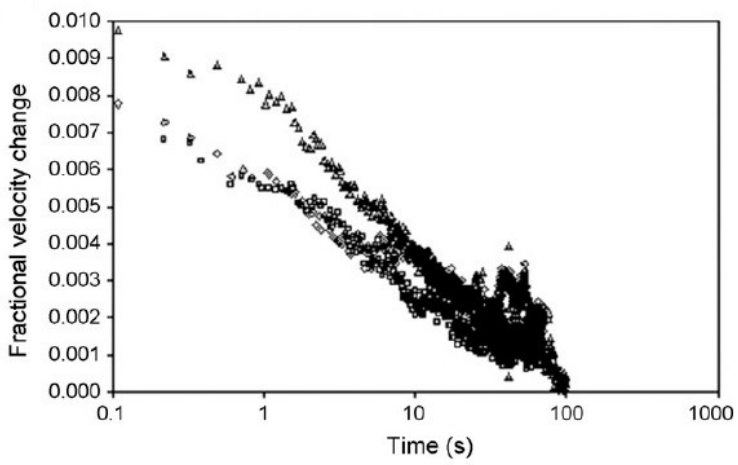

Figure 37: Fractional velocity change during recovery in ferritic ultra-low carbon steel. Open triangles = 550°C, open diamonds = 730°C and open squares = 800°C [95].

In 2003 experiments were conducted with laser ultrasonic measurement in a continuous annealing line at SSABTunnplåt. It was found that it was possible to assess strip thickness accurately using ultrasonic measurement data, which was correlated against an already existing X-ray measurement device. Laser ultrasonic data was also used to assess the (grain size dependant) tensile strength of the material using comparisons of high and low frequency responses, the results were successful showing a good correlation between frequency measurement and tensile strength. Further work carried out at the continuous annealing step at Outokumpu Stainless exposed some of the weaknesses of using laser ultrasonics for in-situ measurements in continuous annealing lines. Measurements taken there were compromised by the presence of steam and dust from oxide scales, as well as high air temperatures which meant extra cooling for the laser head of the sensor. It was thought that these problems could be overcome with the use of better optics for the lasers [96].

Laser ultrasonics has been shown to be sensitive to microstructural features in the laboratory as well as in industrial applications. Laboratory based laser ultrasonics has been used on various steel grades including low carbon steels and stainless steels. While laser ultrasonics can be used to detect changes in microstructure, there are several limitations.

Industrial application of laser ultrasonics is limited by the need for a clean line of sight to the material being assessed, parameters such as scale, dust and steam can effect or prevent laser ultrasonics from providing useful data. There are health and safety concerns around the deployment of laser ultrasonics as the lasers used are often relatively powerful and can cause harm to skin and eyes, therefore they must operate in a closed environment, or be disabled before any maintenance or human interaction can be performed (this is not an issue for most electromagnetic systems which operate at very low power and magnetic field strength). A comparison of different NDT techniques used to analyse recovery and recrystallisation is shown in Table 5.

5.2. X-Ray Diffraction

X-Rays are a form of electromagnetic radiation which has high energy and a wavelength of the order of the atomic spacing for solid bodies. When a beam of X-rays contacts a solid material (the incident beam), some of the beam will be diffracted by the electrons associated with each atom or ion that is in the beams path. By measuring the pattern and spacing of the diffracted X-rays it is possible to determine the atomic or molecular structure of the material being analysed since the grouping of electrons causing the diffraction within the measured structure will provide a specific signature. This signature can be analysed to determine the mean atomic spacing and disorder within a single crystal or polycrystalline structure [1]. Figure 38 shows the incident and diffracted beams used in X-ray diffraction and their interaction with the test sample on an atomic scale.

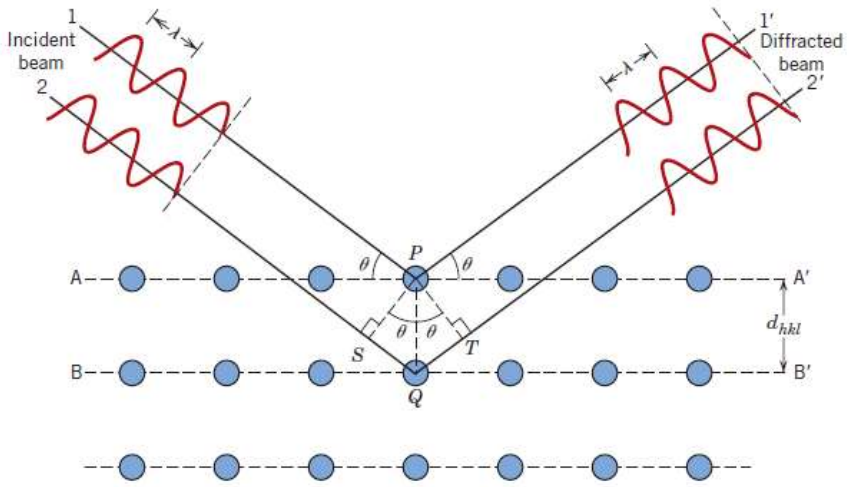

Figure 38: Diagram showing x-ray diffraction technique [1]

X-ray diffraction can be used to measure the development of precipitates in steels [97, 98] during heat treatment processes. Estimation of dislocation densities within steels has been completed using the X-ray diffraction technique in both single and multiple grains [99, 100]. Grain nucleation, rolling texture and recrystallisation texture measurement has been analysed in great detail using X-ray diffraction in different steels including IF steels [43, 101-103].

The sensitivity of X-ray diffraction to changes on an atomic scale have meant that it can be used to measure changes in stress and strain as well as residual stresses [104, 105].

X-ray diffraction can be either a reflective technique or a transmission technique which takes averages over an area which has been targeted, generally X-ray diffraction measurement is lab based although some industrial applications have been developed which examine texture development as part of the strip manufacturing process. Hoersch-Stahl AG (Germany) have developed an industrial system which has been used for round the clock texture measurement of low carbon steels at room temperatures, the system has shown to be reliable and able to measure r values with an accuracy of +/- 0.1 (where typical measurements have a magnitude of 2.0) [106, 107]. Laboratory based X-ray diffraction has been used to track the evolution of texture in IF steels which has undergone 90% cold rolling, although it was not used to directly measure recrystallisation [30].

X-ray diffraction has been used to study recrystallisation in 90% cold rolled aluminium samples, where it was possible to track both grain nucleation and growth using three dimensional X-ray diffraction with a special resolution of 5µm x 5µm x 1µm [108]. Grain nucleation and growth for individual ferrite grains in carbon steels during cooling from 900^{o}C to 600^{o}C was also studied using three dimensional X-ray diffraction. The accuracy and resolution of the three dimensional X-ray measurements was compared to the classical Zener model for grain nucleation and further used to describe the complicated nature of grain growth [109].

For laboratory based applications sample preparation is very important and samples are usually required to be very small (less than a 10mm cube). Sample penetration is typically very shallow in laboratory based techniques, typically tens of microns.

Where X-ray diffraction techniques have been deployed to analyse strip during manufacture it has been reported to be successful and uses a transmission technique which analyses texture to predict the r_m-values for strip which is going to be used for deep drawing applications [106, 110]. It is reported that the transmission X-ray technique used was relatively unaffected by environmental issues such as dust, however like all beam techniques a clear view to the material being measured is important.

X-ray systems are disadvantaged for industrial deployment due to health and safety risks, X-rays are generated during the measurements which have enough power to cause radiation burns (ionisation) and therefore X-ray NDT systems have to be carefully housed and shielded to prevent exposure of workers to stray X-rays generated during measurement [111].

5.3. Electromagnetic Techniques

There are several competing electromagnetic techniques which are being used to assess microstructural characteristics in ferromagnetic materials, this section will discuss the theory behind the different types and look at the systems that have been developed.

5.4. Electromagnetic Measurement Theory

5.4.1. Magnetic Barkhausen Noise (MBN)

When a magnetic field is applied to a ferromagnetic material and smoothly increased the magnetisation of the material does not take place continuously, rather it happens in a series of steps or jumps. The steps or jumps are very small and magnification of the magnetisation curve is required in order that the steps can be seen (Figure 39), they can however be heard with the use of a microphone as they produce a crackling noise. The steps are caused by the abrupt movement of the magnetic domains within the material. As the domains grow, shrink or rotate in accordance with the applied field the domain walls become pinned and unpinned as the applied field increases or suddenly rotate. The combination of domain walls overcoming the pinning points and abruptly changing orientation at higher fields causes a release of energy which is called magnetic Barkhausen noise (MBN) [112, 113].

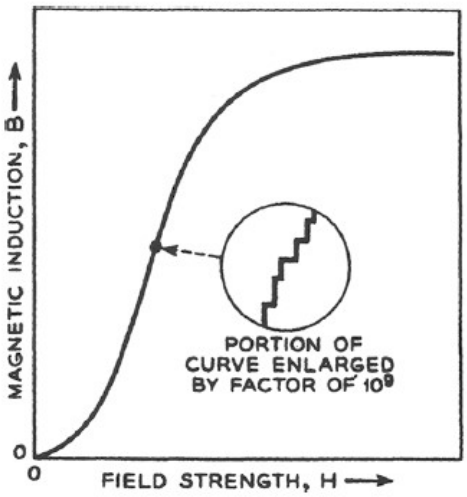

Figure 39: Discontinuous steps of magnetisation responsible for the Barkhausen effect [27].

The degree of Barkhausen noise that is produced during magnetisation of a sample is related to the density and type of pinning points. Some pinning points will be harder to overcome than others, theoretically allowing Barkhausen noise to be used to measure different microstructural characteristics of a material. Use of Barkhausen noise in this way is in reality difficult due to the stochastic nature of domain wall movement and the inclusion of competing types of pinning points with a sample [112].

Barkhausen noise is generated either by a physical change in the material which causes a change in the magnetic domain formation, such as stress or strain, or by magnetisation. Magnetisation of samples in different conditions, for example at different stages of recovery and recrystallisation, will cause different amounts of Barkhausen noise to be generated as the microstructural conditions change.

Barkhausen noise is most effective when there is no lift off between the Barkhausen noise sensor and the sample; a reasonable amount of surface preparation is required for contacting measurements. Rust and loose scale should be removed before any Barkhausen measurement is completed and areas of the sample where surface roughness and pitting occur need to be avoided as they can cause distortion of flux which causes errors in the response [114]. Barkhausen noise measurements can be non-contacting, however careful calibration for lift off is required as even small variations in lift-off can have significant effects on magnetisation amplitude and speed [115].

The equipment required to complete Barkhausen noise measurements is a magnetic yoke, search coil and signal amplification equipment [116]. The layout of a typical MBN system is shown in Figure 40.

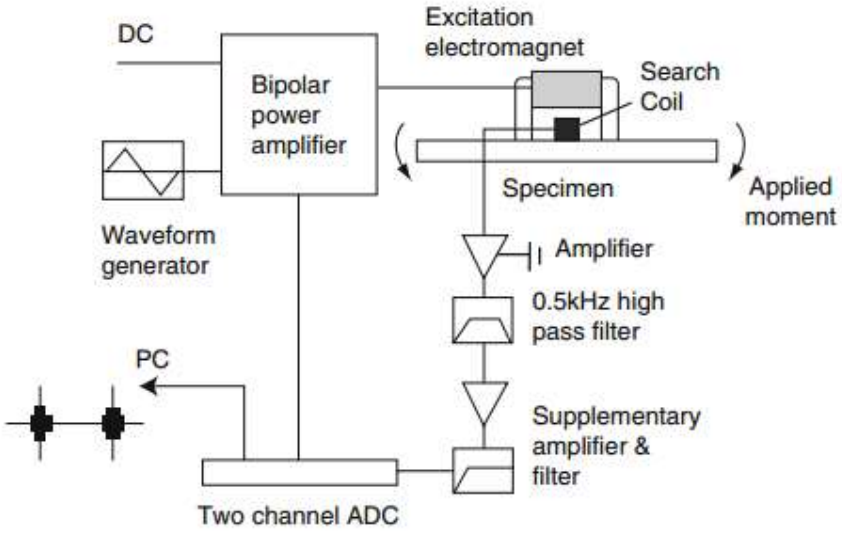

Figure 40: Typical magnetic Barkhausen apparatus [117]

Barkhausen noise systems have been used to investigate variations in grain size, where the intensity of Barkhausen noise is related to the number of grain boundaries, smaller grained samples have more grain boundaries (pinning sites) and give a larger Barkhausen noise response. Sample composition and phase change also have effects on Barkhausen noise, it has been found that the presence of different phases, precipitates and intergranular impurity segregation cause variations in Barkhausen noise. [117]

Barkhausen noise measurement systems are commercially available for measurement of residual stresses and defects caused during the manufacturing process. Barkhausen measurement sensors have to be tailored to the geometry being measured to avoid variations in measurement signals caused by lift off [114, 118]. Further discussion of the use of Barkhausen noise measurement techniques are carried out later in this chapter.

Barkhausen noise has several advantages, it can operate in a non-contacting manner (as long as lift off is accounted for), it is sensitive to several microstructural parameters and is relatively easy to deploy. A major disadvantage of the Barkhausen noise measurement process is that it uses high magnetic fields and causes significant magnetisation of the sample, without demagnetisation between measurements

Barkhausen noise readings have poor repeatability, if demagnetisation is not possible then multiple readings in different positions must be made [119].

5.4.2. Multi-frequency Electromagnetic (EM) Sensors

Electromagnetic sensors use an AC current to drive an excitation coil, which generates a magnetic field around the coil. When the coil is brought near to a conductive test sample the magnetic field will be affected. The changes in the generated magnetic field can be measured using a separate sensing coil; a voltage difference is induced across the sensing coil. The voltage induced in the sensing coil is related to the relative permeability (μr) of the material being tested. As discussed in section 3.4, ferromagnetic materials μ_r is affected by microstructural features [44].

Various shapes and types of electromagnetic sensors have been developed including circular air cored sensors, C shaped ferrite cored sensors and H shaped ferrite or air cored sensors. The use of the different sensor type is dictated by the sample being examined. The use of multi-frequency measurements allows the sensors to see through the depth of the plate as lower frequencies will penetrate more deeply than higher frequencies [120].

As a Non-Destructive Testing (NDT) method, EM sensors have several benefits – they are non-contacting, can measure several parameters at once, can be used online due to a fast response during measurement and are relatively cheap as sensor heads are inexpensive to manufacture [120].

A detailed discussion of the sensors and sensor design used in this research is presented in section 5.5.

5.4.3. EM Methods for Recovery and Recrystallisation

The end goal of the research in this thesis is to show that EM sensors have the potential to monitor recrystallisation on-line in a steel plant's continuous annealing line. It is important to consider other electromagnetic systems that have been used to monitor recrystallisation as they provide credence to the idea of using EM sensors online as well as showing the strengths and weaknesses of competing systems.

MBN, hysteresis loops and EM sensor techniques have all been used to examine the effects of recrystallisation in steels, although all measurements have been made at room temperature on samples that have been rolled and then heat treated to give different amounts of recovery and recrystallization. No in-situ EM measurements of recovery or recrystallization have been reported.

MBN has been shown to be sensitive to changes in recovery and recrystallisation in carbon steels. The amplitude of the MBN response was shown to increase with recovery, but decrease with recrystallisation (Figure 41), the samples used for the experiments were annealed at different temperatures and times, all measurements were completed at room temperature [2]. The overall energy of the MBN response was shown to increase during recovery and decrease in response to recrystallisation. During recovery, dislocation density decreases as the dislocations rearrange themselves into cell/sub-grain walls with some dislocation annihilation, and the amplitude of Barkhausen noise increases, this is considered to happen as domain walls travel further as they unpin, releasing more energy and causing a greater Barkhausen noise measurement amplitude (Figure 42) [2, 121, 122]. During recovery dislocation density changes are the dominant feature affecting Barkhausen noise. As recrystallisation takes place, grain boundaries become the more dominant parameter affecting Barkhausen noise. At the start of recrystallisation there is no mean growth in grain size; new grains are initially smaller than the recovered deformed grains (the sub-grains) and when recrystallisation is complete the recovered and deformed grain structure is replaced with a finer recrystallised grain structure. The distance moved by domain walls therefore diminishes as recrystallisation takes place, leading to a drop in measured Barkhausen noise [2].

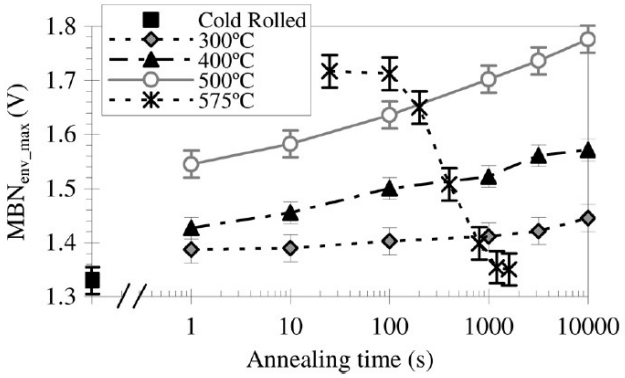

Figure 41: Amplitude of the peak of the MBN envelope as a function of time for different annealing temperatures in extra low carbon steel. Recrystallisation occurred in the 575ºC sample after 100s, this was verified by optical microscopy whilst recovery only was seen at the lower temperatures [2].

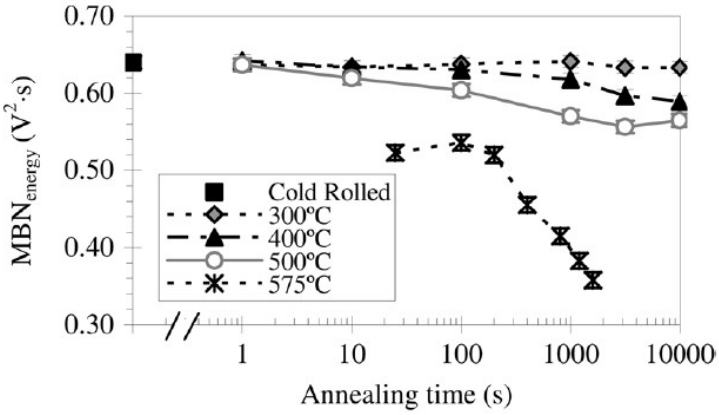

Figure 42: MBN energy as a function of time for different annealing temperatures [2].

Magnetic hysteresis loop measurements have been used to examine the effects of recovery and recrystallisation of low carbon and IF steels. Gurrachaga et al. have considered the different parameters that can be extracted from a hysteresis loop that are sensitive to recrystallisation, these include the coercive field (H_c), hysteresis loss (W_h) and remenant magnetisation (B_R). It has been observed that H_c is sensitive to recovery and recrystallisation with H_c dropping as the amount of time for recovery increases. As recrystallisation takes place at higher temperatures the drop in H_c is more severe than for recovery, Figure 43 [37].

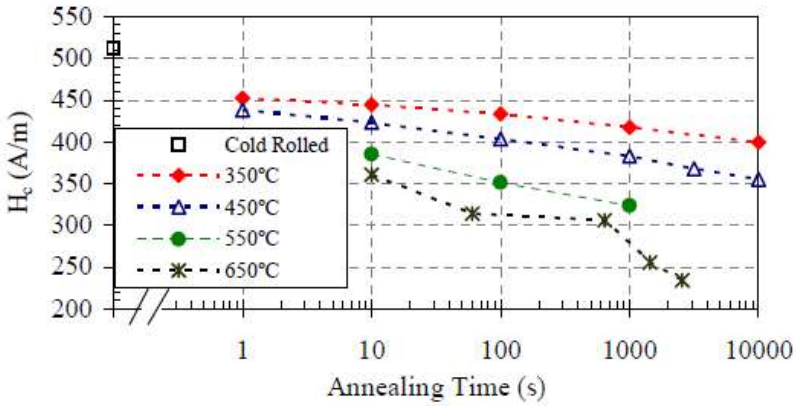

Figure 43: Evolution of coercive field H_c as a function of annealing time for different temperatures in IF steels. The decrease in H_c for the 650°C annealed sample after 1000s was due to the onset of recrystallisation [37].

A change in the shape of the B/H curves was also measured as a result of recovery, when a sample of IF steel was heat treated at 450°C for different lengths of time it was observed that the B/H loops became steeper, showing less hysteresis, Figure 44 [37]. This is in agreement with annihilation of dislocations during recovery allowing domain walls to move more freely.

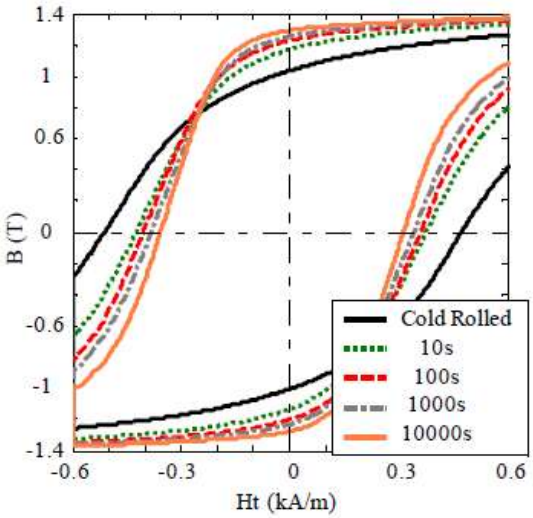

Figure 44: B/H loops for a sample of IF steel heat treated at 450°C for different lengths of time [37].

Further work by Ansaripour et al. looked at low carbon steel samples that were heat treated at 500°C and 640°C correlating hardness changes against changes in H_c, showing that as hardness dropped so did H_c, Figure 45. The work also found that there was less magnetic hysteresis as the samples were heat treated.

The increase in H_c for the 640°C test at 2000s was attributed to a combination of decreased grain size due to the start of recrystallisation and a softening of the effect caused by reduction in dislocation density, at 3800s H_c for the 640°C sample H_c begins to drop again as the recrystallised grains start to grow [123].

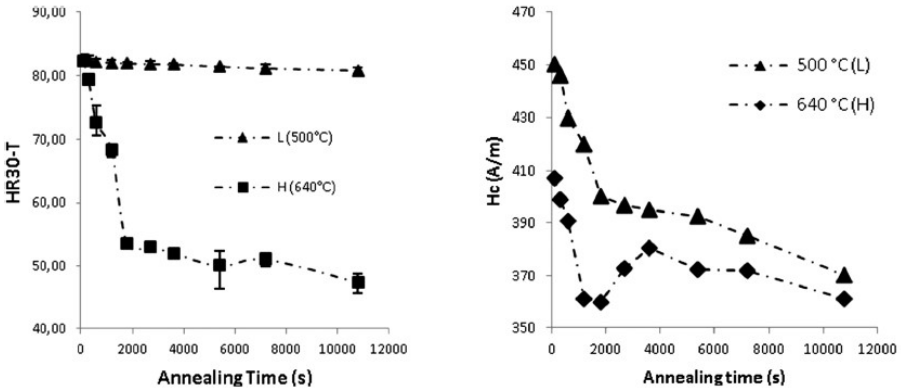

Figure 45: Rockwell hardness (left) and Hc evolution (right) for low carbon steel samples annealed at 500°C and 640°C for different lengths of time [123].

A study completed by Lukin et al. on IF steel showed that there is an inverse relationship between grain size and H_c (in agreement with Gurruchaga et al.) and they used the relationship to suggest that it is possible to estimate grain size in IF steels using H_c measurements during steel manufacturing, although the paper does not suggest a solution to the practical problems of taking H_c measurements on moving steel at high temperature. Also the work was only completed on samples at room temperatures, not for samples at high temperatures [124]. Similar relationships of H_c against grain size are reported by Landgraf et al. for non-oriented electrical steels [81] and by Degauque et al. for high purity iron [125].

Work completed by L. Zhou et al. showed that the low field relative permeability increased with grain size. Figure 46 shows the relationship between relative permeability and the grain size for grains that varied in size from 14 to 74μm for an extra low carbon steel, the data shows good agreement with an inverse square root type relationship (fitting parameter R^2 of 0.99) although it also fits well with an inverse relationship (fitting parameter R^2 of 0.98). Permeability increases as the grain size increases as the pinning effects on domain walls due to the number of grain boundaries decreases [126]

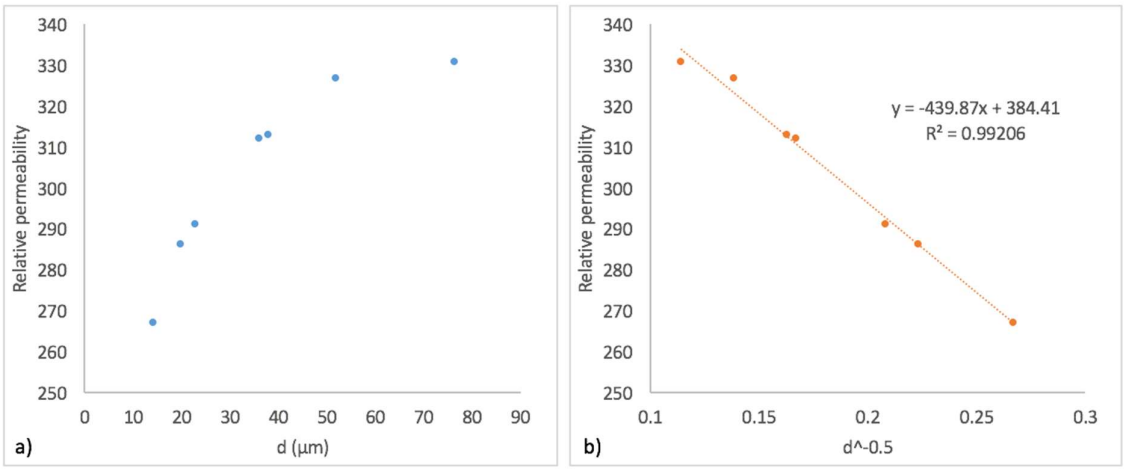

Figure 46: Relationship between the grain size (d) and low field relative permeability in extra-low carbon steel samples with grain size of 14-74 µm [126].

5.4.4. On-Line EM Sensor NDT Systems

Suitability of systems for deployment into industrial settings is very important in terms of the longer term goals of this project work. While the research presented in this thesis aims to provide the theory and confidence that an on-line EM sensor system for the measurement of recrystallisation in a continuous annealing line is possible it is important to show that the system already has pedigree of working in a real industrial setting.

A low field EM sensor system (EMSpec) has been developed to operate in the run out table of Tata Steel's IJmuiden hot strip mill [127]. The sensor is an H type sensor which was developed to sit in-between the rollers of the hot strip mill's run out table. The sensor is not designed to monitor recrystallisation, but is designed to monitor phase transformation as the hot steel passes over the run out table. The sensor at the Ijmuiden plant measures phase angle changes since inductance measurements are affected by the distance between the sample being tested and the sensor (called lift off). Phase angle measurements are relatively independent to the varying distance (at larger lift off values, approximately 40 mm is used in the mill) between the steel and the sensor that occurs on run out tables. Measurements completed with the system to date have confirmed that the system can monitor phase changes on-line and can provide an accurate method for analysing phase transformation by analysis of the steel's electromagnetic properties [127, 128].

Impulse Magnetic Online Controller (IMPOC) systems have been developed which are capable of monitoring changes in magnetic properties and correlating them to tensile strength and yield strength within steel strip online [129]. The IMPOC system was initially developed by the Institute of Applied Physics, Minsk and further developed by ThyssenKrupp Steel, it is now used in steel plants world-wide. IMPOC systems have been developed for use online in pickling lines, continuous annealing lines (near the accumulator / strip exit point operating at ambient, not high, temperature) and hot dip galvanising lines. IMPOC systems use a pulsed magnetic field to periodically magnetise the steel strip and measure the amount of residual magnetisation, the amount of residual magnetisation is then used in a mathematical model to calculate the material properties. High speed IMPOC systems are capable of making measurements on strips that are running at speeds of 900 m/s. The IMPOC system is sensitive to lift off effects between the sensor head and the surface of the material being measured, this is accounted for by having a sensor on both sides of the strip and balancing the sensor outputs. The IMPOC system uses high energy magnetic fields and is very sensitive to edge effects caused by the proximity of the sensor head to the strip edge, IMPOC system sensors need to be at least 500mm from the edge of a strip to account for this. The IMPOC system's reliability is also affected by variations in strip speed and strip tension which cause decreases in signal, therefore compensation factors are used to account for varying line speed. The IMPOC system has not been adapted to measure the effects of recrystallisation [130, 131].

Harmonic analysis (HACOM) systems have been developed to measure changes in microstructural parameters, and is a type of magnetic hysteresis loop measurement [130]. HACOM uses sinusoidal magnetisation at low fields at frequencies between 20Hz and 5KHz, the magnetisation is completed at 4 frequencies. Magnetisation is induced into the sample using air cored coils. The magnetisation of the sample runs through hysteresis loops; the magnetic hysteresis induces field changes into receiving coils which is analysed using fast fourier transform. HACOM has been used to analyse cold rolling in IF steels and was shown to be sensitive to small amounts of reduction.

Figure 47 shows HACOM data recorded for 2% incremental elongations in a high strength IF steel caused by cold rolling, the different charts show the cosine (a) and sine (b) harmonic amplitudes recorded for the samples at base frequencies. The largest change in harmonic amplitude was recorded in the first 2% reduction, with smaller variations for further reductions up to 8% [130].

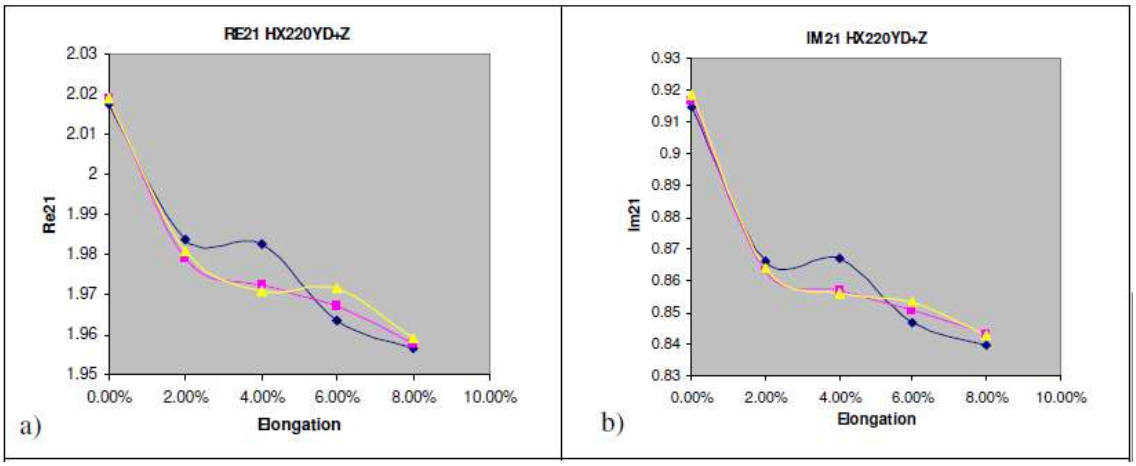

Figure 47: HACOM data for different IF steel samples reduced in 2% steps from 0% to 8% cold rolled elongation, (a) shows the cosine part and (b) shows the sine part of the base frequency harmonics. Each line represents a repeat measurement for the same material [130].

HACOM was found to be extremely sensitive to external electromagnetic noise, lift off and the residual stress state of the material. The lift off variable was overcome by using two sensor heads, one on each side of the test sample, with the mean value of the two sensor readings used. This would not be an ideal solution in a continuous annealing line due to the amount of disruption required to place the equipment within the line. At this time HACOM has not been used in an industrial application to monitor grain size or recrystallisation [130].

The 3MA system measures Barkhausen noise parameters, it has been shown to be responsive to changes in microstructure through annealing for a limited number of steels in laboratory trials. The system was seen to match data produced by the HACOM system for 51CrV4 grade steel but was not seen to be sensitive in changes due to cold rolling in IF steels for the same sample sets shown in Figure 47. Stress (residual) levels in the materials tested are considered to dominate 3MA measurements and are considered to over write the effects of other parameters in the signal [130].

It is worth noting that all of the systems mentioned in this section will be heavily influenced by any previous magnetisation. In the case of 3MA and HACOM prior magnetisation effects can be caused by earlier measurements, any effect of prior magnetisation reducing the usefulness of the signal [130].

5.5. Critique of NDT Methods for Recovery and Recrystallisation

Different types of NDT techniques that can be used for recovery and recrystallisation have been discussed in this chapter, this section will summarise the techniques in terms of their applications, strengths, weaknesses and suitability for deployment into continuous annealing lines for in-situ measurement of recovery and recrystallisation. Table 5 provides a summary of the techniques discussed in this chapter.

EM sensor technology is suitable for deployment into CALs to monitor recovery and recrystallisation as it is non-contacting, unaffected by strip speed and has been shown to be robust when deployed into hazardous environments such as hot-strip run out tables. However, the effect of line tension and temperature on the magnetic properties, specifically low field permeability for the EM sensors being considered in this work, compared to the effect of recovery and recrystallization, has not been assessed and is required before determining if the sensors can provide a dynamic in-situ method for monitoring recrystallization.

Table 5: Review of NDT techniques, applications and suitability for deployment into a CAL

NDT Type	Structural Parameters	Applications	Strengths	Weaknesses *	Suitability for Deployment into a CAL
Ultrasonics	Grain size Dislocations Atomic spacing Phase Texture	Homogeneity Recovery / Recrystallisation Stress / Strain Phase transformation Assessment of material properties LUS systems already deployed in industrial applications	Penetrates through the whole medium Phased array allows ultrasonic beams to be focused LUS can operate at a significant stand off LUS can be deployed with line of sight into hot environments	High degree of surface preparation Surface (or very close) contact required unless LUS Environmental conditions (steam, dust, air turbulence) affect LUS Laser safety requirements for LUS	LUS system already deployed into hot strip mills so the technology already exists. LUS sensitivity to dust and steam reduces reliability.
X-Ray Diffraction	Texture Dislocations Precipitates Atomic spacing Phase balance	Texture measurement Dislocation density measurement Grain nucleation analysis Residual stress Assessment of material properties Estimation of r_m values X-ray diffraction systems deployed in industrial application for estimation of residual stress levels Thickness measurement	Provides information on a range pf scales from atomic to through thickness	Cannot measure microstructure features on fast moving surfaces, though through thickness (averaged) measurements can be completed on moving strip Highly polished surface finish required Residual or dynamic stresses can confuse measurement Significant health and safety protocols have to be in place for the system to be used	Not suitable for deployment into CAL due to high speed movement of the strip through the mill and difficulties with application in a hot environment.

NDT Type	Structural Parameters	Applications	Strengths	Weaknesses *	Suitability for Deployment into a CAL
MBN	Grain size Dislocations Precipitates	Homogeneity Recovery / Recrystallisation Stress / Strain Assessment of material properties MBN measurement systems deployed for industrial applications for static measurements	Sensitive to multiple parameters Can practically measure up to depths of 1.5mm for low frequency systems	Cannot measure above Curie point Contacting measurement system Prior magnetic history can affect results Surface contact required Surface preparation required	Not suitable for deployment into CAL as MBN measurements cannot be performed on a fast moving surface
Magnetic Hysteresis Loops	Texture Grain size Dislocations Precipitates Atomic spacing	Homogeneity Recovery / Recrystallisation Stress / Strain IMPOC systems already deployed in industrial applications (although it should be noted that IMPOC does not use the full hysteresis loop)	Multiple parameter output	Cannot measure above Curie point High power requirements Prior magnetic history can affect results Can leave test material magnetised Hysteresis loop measurement generally required good surface contact, although IMPOC can operate up to 25mm away from material surface Sensitive to test subject geometry Readings affected by line speed Sensitive to prior magnetisation	Systems such as IMPOC show that the technology is available to deploy magnetic hysteresis loop measurement systems into hazardous areas such as CALs. High speed of strip movement within the CAL could prove to be a limitation. Would require compensation for both strip temperature and tension as well as development to operate at high temperatures

NDT Type	Structural Parameters	Applications	Strengths	Weaknesses *	Suitability for Deployment into a CAL
Multi-frequency low field EM Sensors (such as EMSpec system)	Grain size Dislocations Atomic spacing Phase balance Precipitates Texture	Phase fraction Grain size Recovery / Recrystallisation Stress / Strain EM Sensor system already deployed in industrial applications	Low field strength Multi-frequency measurement Can measure at large stand-off distance using phase angle measurement (non-contacting)	Cannot measure above Curie point Sensitive to multiple parameters Prior magnetic history can affect results Affected by environmental EM noise	Multi-frequency EM sensors have already been deployed into run out tables in hot areas. EM sensor measurements are unaffected by dust, steam and changes in line speed. Would require compensation for strip temperature and tension and development for a system that can operate at high temperatures. Sensors need to be shielded against external EM noise.

* Knowledge, understanding and control of the microstructure being analysed is important for all NDT techniques so that any measurements can be attributed to a particular parameter change.

6. Material Data

6.1. IF Steel

IF steel sheet of 1 mm thickness in the cold rolled condition was supplied by Tata Steel UK. The chemical composition of the IF steel supplied by Tata Steel UK is shown in Table 6 [132].

Table 6: IF steel chemical composition.

Element	C	Si	Mn	P	Cr	Mo	Ni	Nb
% by weight	0.0027	0.004	0.109	0.011	0.016	0.001	0.009	0.001

6.2. 430 Grade Ferritic Stainless Steel

An annealed 430 grade ferritic stainless steel sheet of 2 mm thickness, manufactured by Thyssenkrupp Stainless UK and supplied by Wild Manufacturing Group Ltd, was investigated. The chemical composition specified for the 430 grade stainless steel is shown in Table 7 [133].

Table 7: 430 grade stainless steel chemical composition.

Element	C	Si	Mn	P	S	Cr	Ni	N
% by weight	0.035	0.220	0.290	0.021	0.001	16.080	0.180	0.043

6.3. Grain Oriented (GO) Silicon Steel

A 3% silicon GO steel sheet of 0.3 mm thickness was used for some experiments, provided by Tata Steel UK, the chemical composition specification for the grade is shown in Table 8 [134].

Table 8: 3% grain oriented silicon steel chemical composition.

Element	C	Si	Mn	P	S	Cu	Ni	N
% by weight	0.001	3.0	0.200	0.001	0.001	0.100	0.001	0.001

7. Sample Preparation, Experimental Equipment and Methods

This chapter discusses how samples were prepared for experimentation, the equipment used for experiments and the experimental methods that were employed.

7.1. Metallography Sample Mounting, Grinding, Polishing and Etching

Where samples were required for optical microscopy, sections were cut in the appropriate direction (rolling direction or transverse direction) from parent material. The sections were mounted in non-conductive Bakelite using an OPAL 460 hot mounting press.

Samples were ground using grinding papers with increasing levels of refinement. Initial grinding was completed using 240 grade grinding paper until the sample and Bakelite surface was planar. Subsequent grades of paper used were 400, 800 and 1200. All grinding was completed using water as a lubricant.

Polishing was completed using Struers polishing discs of different types along with corresponding diamond polishing suspensions in accordance with guidelines from the Struers Metalog Guide [135]. All polishing was completed using Struers Labopol automatic polishing machines.

IF steel samples were etched using Nital 2% etchant. Stainless steel samples were etched using Kallings etchant. No etching was carried out for the 3% silicon GO steel.

7.2. Microscopy

Sample microstructures were viewed using a Zeiss Axioscop 2 microscope. Images were recorded using Axiovision 4 software, which was on a dedicated PC linked to a camera on the microscope.

7.3. Hardness Measurement

Hardness measurements were recorded using an Indentec 5030 SKV Vickers hardness testing machine, with a 5kN load. Samples for hardness tests were mounted in Bakelite as they were for optical microscopy. All hardness values presented are the average of five hardness readings taken from different positions on a sample. Errors presented are a combination of machine error (+/-0.1 HV) [136] and repeatability errors caused by repeated measurements.

7.4. Grain Size Measurement

Grain size measurement was completed using the mean linear intercept method. Micrographs of the desired areas were obtained. Test lines were drawn in different directions across the micrograph (a minimum of 5 lines per micrograph). The number of grain boundaries along each test line was counted. An average of the number of grain boundaries to line length was then calculated, giving a mean linear intercept value for grain size [137].

7.5. Heat Treatment and Quenching

Samples were heat treated using Elite Thermal Systems laboratory based muffle furnaces. Sample temperature was monitored using K type thermocouple wire which was spot welded to samples or K type thermocouples that were placed so that they touched the EM sensing apparatus and sample where welding thermocouple wires to samples was not appropriate because of space constraints.

Furnace temperature was set using furnace controls and was monitored using K-type thermocouples connected to an RS components thermocouple reader and datalogger. Furnace temperature settings were altered until the correct furnace temperature was achieved. Furnaces were allowed to heat up to target temperature before samples were placed into the furnace for heat treatment. Heat treatment times were measured using a stopwatch or software clock.

Samples required for subsequent U-Type EM sensor measurements were wrapped in stainless steel foil to minimise oxidation during annealing. Any rough scale or oxidation was removed before any measurement work was completed.

Samples were either allowed to air cool or were water quenched. Samples that were water quenched were removed as quickly as possible from the furnace and immersed into a water bath for approximately 1 minute, the samples were moved around in the water and then immediately dried.

7.6. EM Sensors

EM sensors were used for both room temperature and high temperature in-situ measurements. This section discusses the type of sensor used, the design of the EM sensor used and the experimental procedures used for the different types of experiments that were conducted.

7.6.1. EM Sensor Design

Two types of EM sensor were used; initial experiments were conducted using a U-shaped sensor placed on the surface of the samples. Later experiments were conducted using a cylindrical EM sensor capable of high temperature measurements within a furnace.

The U type EM sensor design is formed of a U-shaped ferrite core (sourced from Magdev Ltd.) and windings around the core, enamel coated copper wire (0.25mm diameter) was used to make the windings. An excitation coil is wound around the bridge of the sensor and two flux sensing coils are wound in series from a single wire around the legs of the core. The excitation coil induces an alternating current magnetic field into the sample; the frequency of the applied field is varied from 10Hz to 65000Hz. The flux sensing coils pick up changes in the magnetic field caused by the test sample [120]. The excitation coil is driven by either a 1250 or 1260A Solartron multi-frequency impedance analyser, the impedance analyser also receives and processes the signal from the sensing coils. Figure 48 shows a schematic diagram of a U-shaped EM sensor. U type EM sensors used for the work in this project were encased in a transparent resin block; this ensured that the sensor was stable when placed onto a test sample.

The base of the resin block was ground flat. A protective plastic layer of 0.25mm thickness was applied to the base of the sensor, providing a sensor lift off to any sample of 0.25mm. Example U shape EM sensors are shown in Figure 49. The ferrite cores dimensions are 15.5mm long, 6mm wide, 11mm high. The bottom of each leg of the ferrite core, where contact with the test sample is made, has dimensions of 5mm x 6mm.

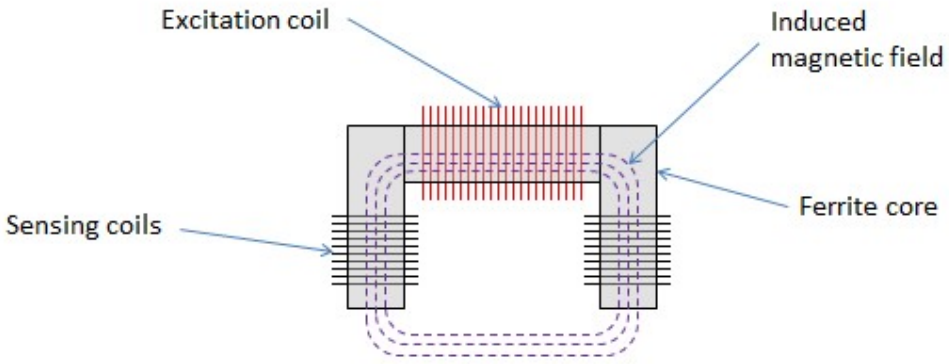

Figure 48: Schematic diagram of a U-shaped EM sensor.

Positioning of samples under a U-shaped sample is very important. The EM sensor signal is affected by proximity to the edges of the sample (edge effects) as well any gap between the bottom of the sensor and the sample (lift off effects). The magnitude of U shape EM sensor responses decreases when in range of the edge of a sample, and decreases as lift off increases [138]. Section 7.7.2 discusses control of these variables as part of experimental procedure.

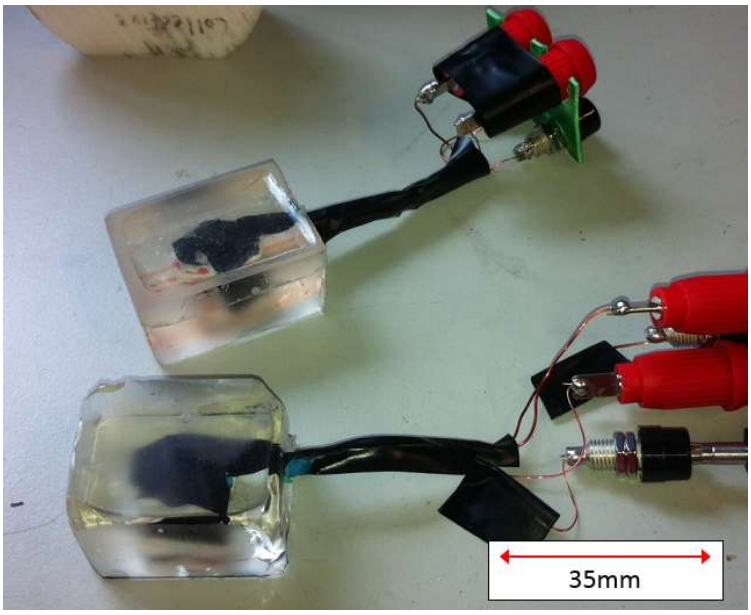

Figure 49: U type EM sensors. Ferrite core and windings are contained within the transparent resin outer block.

U-type sensors induce electromagnetic fields into the surface of the test sample. The depth of the sample measured by the sensor is affected by frequency of the applied field, the permeability and conductivity of the sample and the sensor design (distance between sensor feet). The depth (δ) penetrated by a mutually induced electromagnetic field is called the skin depth and is given by:

$$\delta = \sqrt{\frac{\rho}{\pi f \mu_R \mu_o}} \tag{5}$$

Where ρ is the resistivity of the material in Ω/m, f is the frequency in Hz, μ_o is the permeability in a vacuum (4.7×10^{-7} Henry m^{-1}), σ is the conductivity in the sample and μ_r is the relative permeability [139].

For high temperature (and room temperature) in-situ measurements air cored cylindrical sensors were used. Whereas U type EM sensors are placed onto the surface of a test sample, samples are placed within the cylindrical sensor body. The cylindrical sensors were manufactured using an alumina former, with generating (outer) and receiving (inner) coils wrapped around the former. The sensors were encased in a high temperature solid silica coating, which both protects the sensing and receiving coils as well as holds them in place. Cylindrical sensors have some advantages over U type sensors,

they can be used where ferrite cores are not suitable (high temperatures), they are easier to model and are not affected by edge effects or lift off. Cylindrical sensors are affected by the volume of the sample placed into the sensor and by sample position within the sensor. Cylindrical sensors cannot be used to measure large samples such as sheets.

The high temperature sensor was formed around an alumina former, the receiving coil had 54 turns and the generating coil had 50 turns. To withstand the high temperatures of measurements taken in-situ in furnaces the coils are made from K-Type thermocouple wire. Images of the high temperature cylindrical sensor during construction are shown in Figure 50; Figure 51 shows the cross section and dimensions of the high temperature cylindrical sensor.

Figure 50: High temperature in-situ cylindrical EM sensor in different stages of construction, with only inner windings in the left most picture, with both inner and outer windings in place in the middle picture and coated in silica outer in the right most picture.

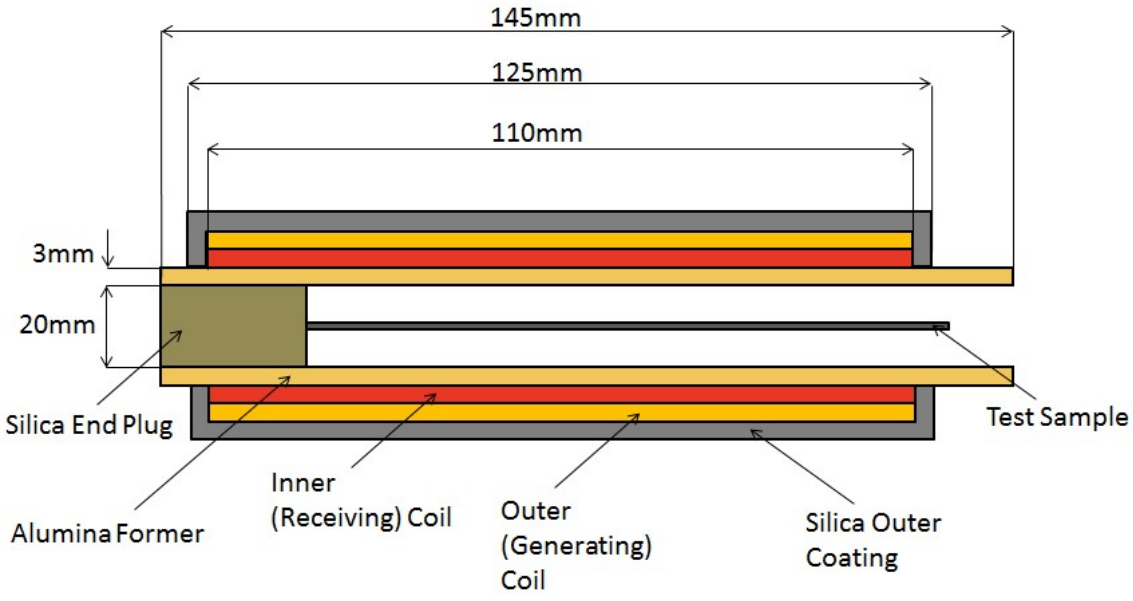

Figure 51: Cylindrical high temperature EM sensor cross section

Test samples are placed inside the cylindrical sensor and inductance measurements are affected by:

- Sample position – movement of the sample along the axis of the sensor affects the inductance measurements and is a variable that must be controlled. Sample placement consistency during experiments was controlled by inserting the samples into the sensor until they butted up against the silica end plug. Sample position is demonstrated schematically in Figure 51.
- Sample volume – the magnetic field induced into the test sample is affected by the overall volume of the sample contained within the coils, larger samples return higher inductance values. It is therefore very important that any samples inserted into the sensor for comparison are the same size. IF steel sample preparation for in-situ measurement is discussed in section 7.7.1.

7.6.2.EM Sensor Control

Both cylindrical and U-type EM sensors are controlled via a computer or lap top which is connected to a Solartron 1260A multi-frequency analyser. The computer communicated with the multi-frequency analyser using either SMART or FRA control software [140]. The software enables the multi-frequency analyser to be programmed to conduct multi-frequency or single frequency measurements for set time periods.

7.6.3.EM Sensor Output

EM sensors measure inductance at set frequencies; typically there are two ways of presenting data from an EM sensor measurement. The first is inductance plotted against frequency for a multi-frequency measurement at a given time and the second is a plot of inductance at a set frequency against time (when in-situ material changes are being recorded).

A typical EM sensor multi-frequency response curve is shown in Figure 52. The multi-frequency response curve is sensitive to the electromagnetic parameters (resistivity and permeability) of the material being tested depending on which part of the curve is being interpreted. At low frequencies, on the plateau of the curve, the inductance measurement primarily responds to changes in sample permeability. At high frequencies the inductance readings are also affected by the samples resistivity due to the generation of eddy currents in the sample [141]. Materials with high permeabilities are easier to magnetise and return higher inductance values at lower frequencies than those with lower permeability values. Example curves for materials (same size samples and lift off) of different permeabilities are shown in Figure 53.

An error budget for EM sensor measurements is presented in Appendix 1.

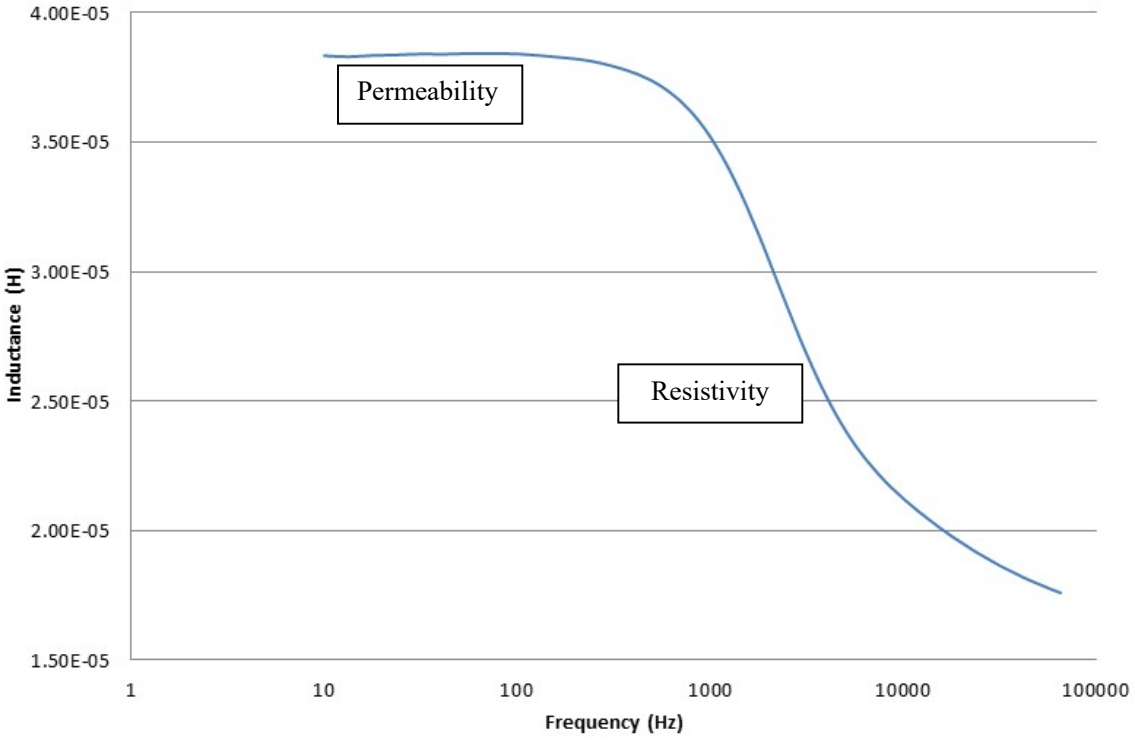

Figure 52: Typical EM sensor multi-frequency measurement for an as-received IF steel sample. At lower frequencies the inductance readings are sensitive to the samples permeability and at higher frequencies the readings are affected by the test samples resistivity.

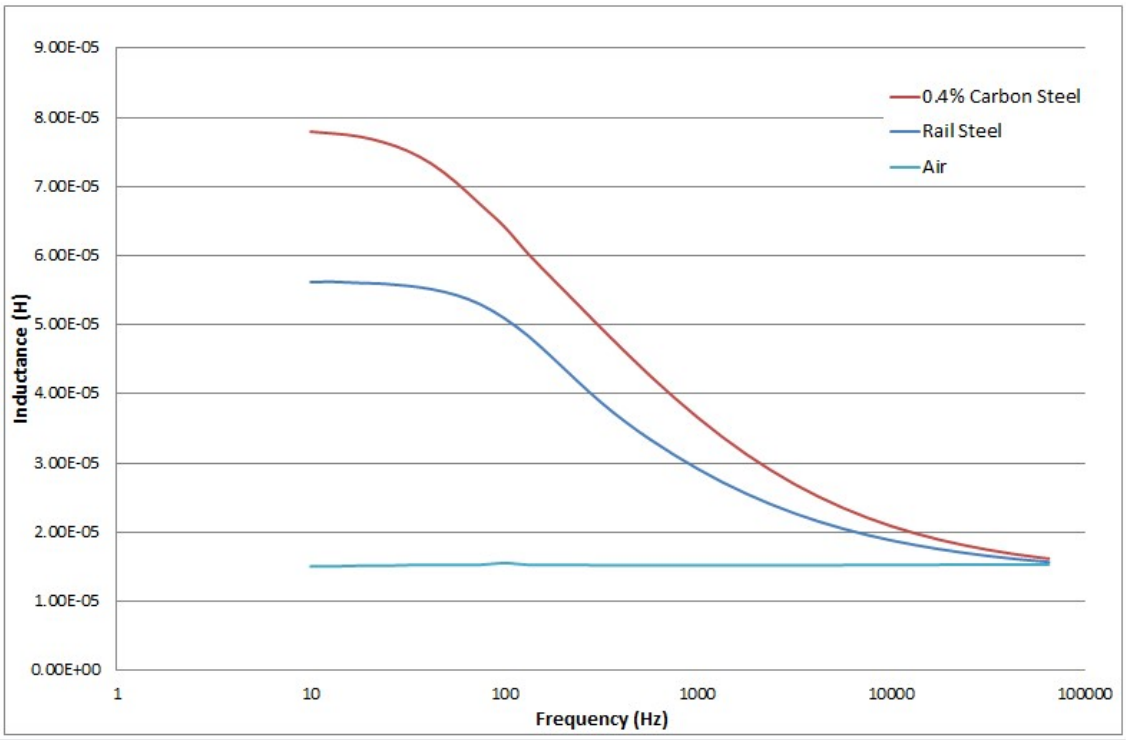

Figure 53: Example multi-frequency EM sensor measurements for samples of the same size but different permeability and resistivity and a measurement taken for air. Rail steel (0.6% C) has μ_r of 56 and 0.4% C steel has μ_r of 140 [138] Rail steel has typical resistivity values of 0.25 to 0.27 μΩm (depending on position of measurement on the rail) [142] and 0.4% C has a resistivity of 0.23 μΩm [143].

When a series of multi-frequency measurements are completed, as Figure 53, it is possible to extract single frequency measurements from the multi-frequency data to show trends at a single frequency. The inductance response to materials of different permeability shown in Figure 53 can also be represented by the data points in Figure 54 which uses inductance values recorded at 100Hz to show the change of inductance with steel grade. It is important to note that while the measurements shown in Figure 54 are predominantly affected by differences in permeability they are also affected to a lesser extent by the materials resistivity (as at 100Hz the inductance values are not in the plateau region); as the measurement frequency increases the importance of resistivity also increases. Values are shown at 100Hz in Figure 54 to illustrate the effect of material properties on inductance as this is the same frequency as that used in high temperature experiments. 100Hz frequency was chosen for the high temperature measurements as measurements as lower frequencies were shown to be less reliable and measurements at 100Hz were more repeatable.

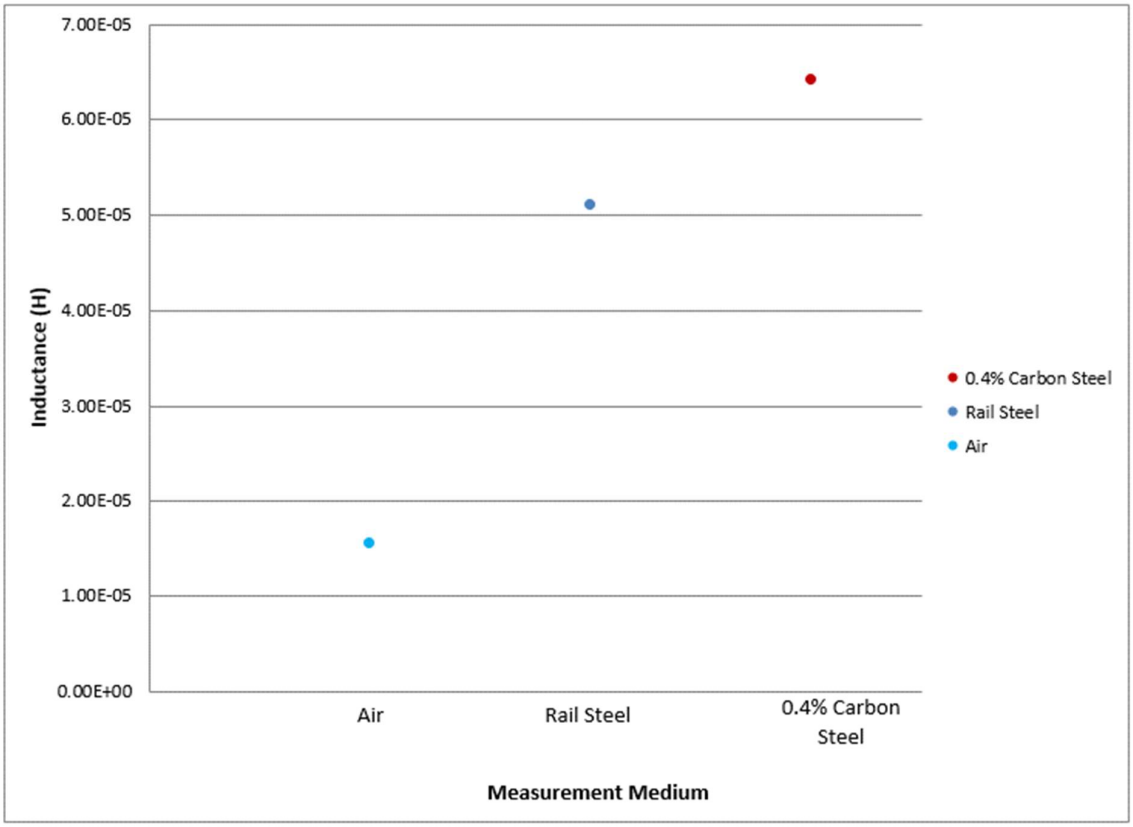

Figure 54: Single frequency (100Hz) data points extracted from multi-frequency curves for different permeability samples shown in Figure 53.

EM sensors can also be used to measure inductance at a single frequency at chosen time intervals. Using a low frequency, corresponding to the plateau of the inductance versus frequency curve, it is possible to measure changes in inductance that are related to permeability against time.

The basic relationship between inductance and permeability for an EM sensor can be described by:

$$L = \frac{N_1 N_2 \mu_o \mu_r A}{l} \quad [6]$$

Where L = Mutual inductance (H), N_1 = number of turns in sensing coil, N_2 = number of turns in exciting coil, μ_o = permeability of free space (1.26×10^{-6}), μ_r = relative permeability of the sample, A = area of the coil and l = length of the sensing coil. The equation shows that inductance and relative permeability are proportional to each other and that sensor geometry and design are important features when using measured inductance to establish permeability values. However, this equation is not a perfect descriptor

of the relationship between permeability and inductance for the sensor, as it suggests a linear relationship between permeability and inductance. The U-shape EM sensors used in this work are ferrite cored and are driven by alternating current, the cylindrical sensor is driven by alternating current but is air cored. It is known that the measured sensor signal is also affected by the eddy currents in the sample, which is more significant when measuring higher permeability materials. In these experiments low frequency measurements have been used as they are less affected by eddy current effects. Therefore at high permeabilities the applied field will not penetrate though the thickness (as shown by the skin depth equation, equation 5), which will result in a non-linear inductance increase. Equation 6 does not take this effect into account. In order to determine the relative permeability of a material accurately from an EM sensor measurement finite element method modelling can be used, where the Maxwell equations are applied to calculate local field and coil inductance from relative permeability and resistivity, this approach still requires calibration and fitting for a particular sensor. FE modelling for sensor performance was not performed as part of this thesis as the focus was on the experimental measurements for in-situ material microstructure changes.

7.7. EM Sensor Experimental Procedures

7.7.1. IF Steel Sample Preparation for EM Sensor Measurements

Samples used for U-type EM sensor readings were prepared by cutting rectangular sections of IF steel from parent sheets. The pieces had dimensions of 100 x 80 x 1mm, the longest direction aligned with the rolling direction of the sheet. The centre of the sample was marked with a line in the rolling direction to allow reproducible sensor positioning.

Samples used for high temperature measurements were prepared by cutting rectangular pieces from parent sheet. Sample dimensions were 110 x 19 x 1mm, the longest side of the sample aligned with the rolling direction. The samples thickness (1mm) was consistent as it is the sheet thickness. The sample width and length was cut to +/- 0.5mm in each direction. Figure 55 shows the variation between 5 different samples measured at room temperature in the high temperature cylindrical EM sensor. The variation between samples at low frequencies (10 Hz to 200 Hz) is 0.1×10^{-5} H which is less than 3 % of the low frequency inductance value showing little signal sensitivity to sample size for the samples tested.

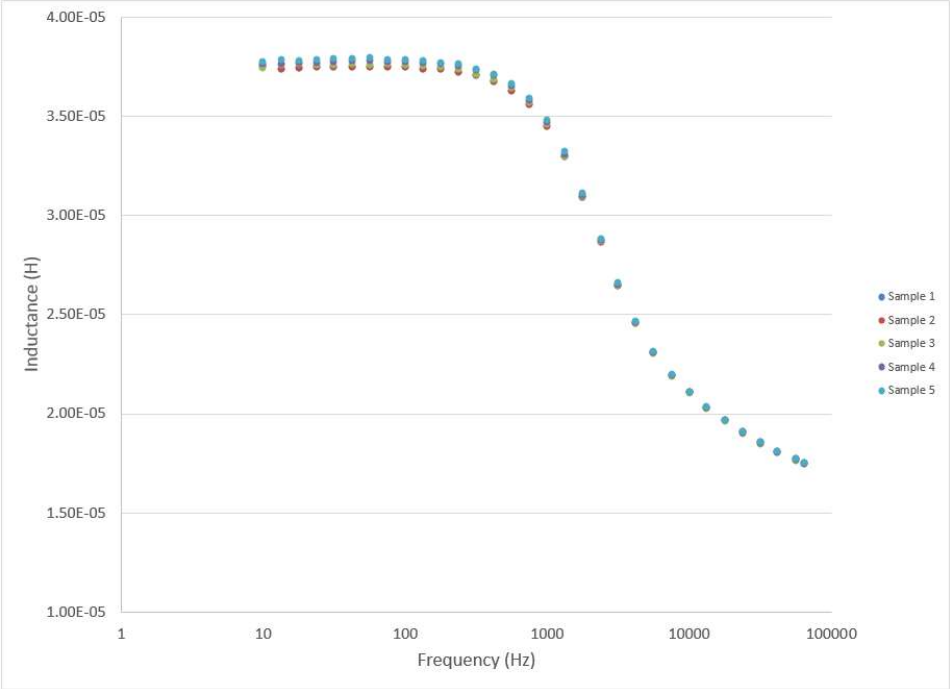

Figure 55: Multi-frequency data recorded for 5 different samples of IF steel within the high temperature cylindrical sensor.

7.7.2. U-Type Sensor Experimental Procedure

The same U-type EM sensor was used for all experiments and results reported in sections 8.1 and 8.3 with the exception of the texture measurements, section 8.2.

U-type EM sensor measurements at a single position used the following procedure:

1. EM sensor measurement positions were marked in the centre of the test sample. All IF steel test samples were prepared to the same dimensions
2. EM sensor was positioned and weighted down using a plastic block which had a mass of 120g. The weight was used to ensure a consistent contact between the test material and the sensor.
3. Multi-frequency reading was taken
4. EM sensor was lifted from surface and repositioned in the same orientation (to avoid any magnetic anisotropy effects)
5. Multi-frequency reading was taken
6. EM sensor was lifted from surface and repositioned in the same orientation

7. Multi-frequency reading was taken
8. Data was downloaded and plotted in Excel for reporting, an average of the three results was used for presented data curves.

Error margins were calculated for U shape EM sensor measurements and are presented as error bars on the data charts. The measurement equipment itself is very accurate, EM sensor measurements presented in this thesis have been controlled through a Solartron 1260A frequency analyser. The Solartron 1260A has a measurement tolerance of +/- 0.1% on any measured value [140]. Further variability errors can be caused by material variability during repeated measurements, it is impossible to place the sensor in exactly the same place each time for each measurement, leading to measurements being taken on slightly different microstructures each time. Therefore, there will be a difference between each measurement recorded for each sample, the error band for this variability can be as high as +/- 1%. Errors presented in this work for U shaped EM sensor measurements are a combination of the Solartron and repeatability errors.

7.7.3.Room Temperature Cylindrical Sensor Multi-Frequency Experiments

Room temperature multi-frequency measurements were taken using the following procedure:

1. EM sensor placed on solid flat non-magnetic, non-electrically conducting surface
2. Sample inserted into the sensor until it touched the silica end plug and could not be inserted further
3. Multi-frequency measurement was taken
4. Data was downloaded and presented in Excel for reporting

Error margins for room temperature multi-frequency measurements were calculated using multiple samples of the same size in the same heat treatment condition.

The Solartron 1260A measurement error is +/- 0.1%. Sample variability

7.7.4. High Temperature Cylindrical Sensor EM Sensor In-Situ Single Frequency Recrystallisation Experiments

Measurements were completed at high temperatures to record inductance changes in samples as they were annealed. These experiments will be referred to as "in-situ". In-situ measurements were recorded using a single frequency of 100Hz. Single frequency measurements were chosen to allow readings to be taken quickly, multi-frequency readings are time consuming and may not have allowed the time resolution to follow the recovery and recrystallisation processes. The following procedure was followed to use the high temperature cylindrical EM sensor for single frequency in-situ measurements.

The high temperature EM sensor and thermocouple were placed into the furnace at room temperature. The thermocouple was located next to the sensor, touching the sensors outer surface and held in place using ceramic blocks. The thermocouple was not attached to the sample as it would have made sample insertion into the EM sensor at high temperature impractical. The cables for the thermocouple and high temperature sensor were trailed through the furnace door. Henceforth all temperatures referring to this experiment refer to sensor temperature and not sample temperature. It is appreciated that due to the differing conductive and convective heat transfer conditions, a sample within the sensor compared to a sample placed conventionally in a furnace different sample heating rates can occur.

Once all of the equipment was placed into the furnace the furnace door was closed and the temperature set using the furnace controls. Monitoring of the furnace and sample temperature was completed using the thermocouple. The furnace's temperature control system was found to be an inaccurate method for controlling sample and sensor temperature due to a temperature gradient across the furnace chamber. The effects of the temperature gradient were negated by ensuring that the sensor, thermocouple and samples were always placed into the furnace in the same central position within the furnaces uniform hot zone. The thermocouple touched the outer surface of the sensor and was within 10mm of the sample giving confidence that the temperature of the sensor and sample at the measuring point were the same.

The furnace was allowed to heat up to the required temperature and then held at temperature for 30 minutes. The 30 minute hold period allowed the furnace chamber and EM sensor temperatures to

stabilise. At the end of the 30 minute stabilisation period the furnace door was opened and the sample was placed into the sensor, the sample was inserted into the sensor until it touched the silica end plug at the back of the sensor. As soon as the sample was located correctly in the sensor the furnace door was closed and inductance measurements were started. Insertion of the sample into the sensor typically took less than 60s and was completed as quickly as possible to minimise any drop in furnace temperature. Observation of the thermocouple showed no significant drop in temperature of the sensor while the furnace door was open. Samples with thermocouples attached were inserted into a pre-heated furnace to establish the time taken for the sample to reach the same temperature as the sensor and furnace, the time taken for a sample to achieve furnace temperature was recorded at approximately 120s.

7.7.5. Interrupted In-Situ Recrystallisation Experiments

Data analysis of the results from the high temperature in-situ experiments identified changes in inductance at specific annealing times at different temperatures where more detailed assessment of microstructural changes was required. Identification of the time periods is discussed on more detail in section 8. These experiments are known as interrupted in-situ measurements. The following procedure was followed to complete interrupted in-situ measurements.

The high temperature EM sensor and thermocouple were placed into the furnace at room temperature. Temperature control and furnace chamber / sensor temperature stabilisation was carried out in the same way as it was for the high temperature in-situ experiments discussed in section7.7.4. When the furnace and sensor were at the correct temperature the sample was inserted into the sensor until it touched the silica end plug. No inductance readings were taken during the heat treatment period; samples were heat treated inside the high temperature EM sensor for experimental consistency.

Once the sample had been heat treated for the required amount of time it was removed from the sensor and water quenched. The quenched sample was sectioned and prepared for optical metallography as discussed in section 7.1

7.7.6.Inductance Change with Increasing Temperature Experiments

To establish the effects of increasing temperature on inductance values for IF and ferritic stainless steel samples the following procedure was used.

Samples measuring 110mm x 19mm x sheet depth (1mm for IF sheet and 2mm for 430 grade ferritic stainless steel) from the annealed IF and as-received 430 grade ferritic stainless steel were prepared; these conditions were chosen as they are microstructurally stable during heating to 800^{o}C for annealed IF steel [1] and 700^{o}C for 430 grade ferritic stainless steel [144]. K type thermocouples were spot welded to the surface of the sample at the centre line of the sample length. The thermocouple wires were connected to a thermocouple data logger to record the temperature profile as the experiment progressed. Insertion of samples into the sensor with thermocouples attached was practical during this type of experiment as the experiment began at room temperature unlike the in-situ high temperature experiments where insertion of samples with attached thermocouples into a hot sensor was practically difficult and would also have been time consuming, causing excessive cooling of the furnace and sensor arrangement.

The high temperature cylindrical sensor was placed into a muffle furnace, the sensor was connected to a Solartron 1260 frequency analyser with a laptop computer used for data collection. The sample was placed into the high temperature EM sensor with thermocouple wires attached. Room temperature multi-frequency tests were completed to ensure that the thermocouple wires did not affect the measured inductance. The thermocouple wires were found to cause an insignificant effect on the measured inductance at low frequencies causing a change of 8.1 x 10^{-7} H (0.02% of the total signal) for frequencies from 10Hz to 150Hz.

Once the sample and sensor were in place in the furnace the furnace door was closed. Inductance measurement and sample temperature data recording was started. The sample was heated in the furnace at a rate of 6.5^{o}C min^{-1} until 780^{o}C, the experiment was stopped when inductance values decreased to a minimum as this indicated that the sample had gone past the materials Curie temperature (T_c). The

furnace was switched off, the sensor and sample were removed from the furnace and allowed to air cool.

7.7.7. Inductance Change with Applied Stress Experiments

To establish the effects of applied stress on inductance for IF steel the following procedure was followed.

IF samples were cut by guillotine from as received sheet. The sample dimensions were 200mm x 25mm x sheet thickness (1mm). Samples were cut from the rolling direction only. Samples were prepared in the as received and annealed conditions. Samples were annealed at 700°C for 3 hours, this annealing time and temperature was chosen to cause full recrystallisation, based in the data gathered in in-situ experiments (section 0). Samples were wrapped in stainless steel foil during the annealing heat treatment to minimise the effects of oxidation and any loose oxide was removed after annealing.

Single axis linear strain gauges with a 0.3mm grid were applied to one side of each sample and were aligned with the centreline of the sample (in line with the applied load). The strain gauge position was chosen to ensure that it was not in the way of the EM sensor mounting position and so that the strain gauge would not interfere with the sensors applied field or inductance measurement while at the same time be representative of the applied load. The sample layout is shown in Figure 56. The trailing wires from the strain gauge were connected to an Intertechnology P-3500 multi-channel strain gauge bridge. The output from the strain gauge bridge was microstrain.

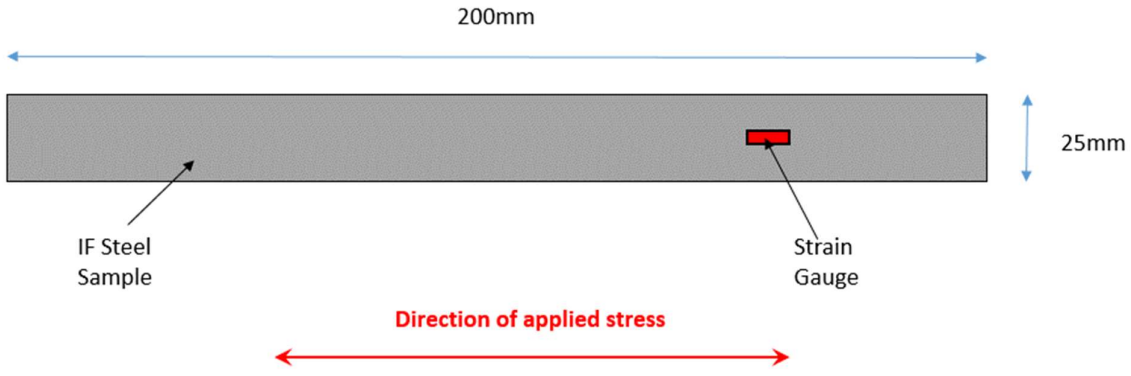

Figure 56: Diagram of the layout of the IF steel sample used for inductance change with applied stress.

To apply stress to the samples they were mounted longitudinally into a 250kN Instron hydraulic tensile test machine. The samples were mounted between friction grips, sample alignment was checked to make sure that the load was only applied along the longitudinal axis of the samples.

A U-shaped EM sensor was mounted close to the surface of the sample after the sample had been installed into the test machine. The sensor was held in place using a retort stand. EM sensor cables were fastened to the test rig frame to make sure that they were not damaged during the experiment and to ensure that the weight of the cables did not move the sensor during the experiment. The EM sensor was aligned such that the applied field from the sensor was in line with the applied load. The EM sensor was connected to a Solartron 1260 frequency analyser which was controlled using a laptop with Solartron SMART software. Figure 57 shows the sample mounted into the test rig before an experiment.

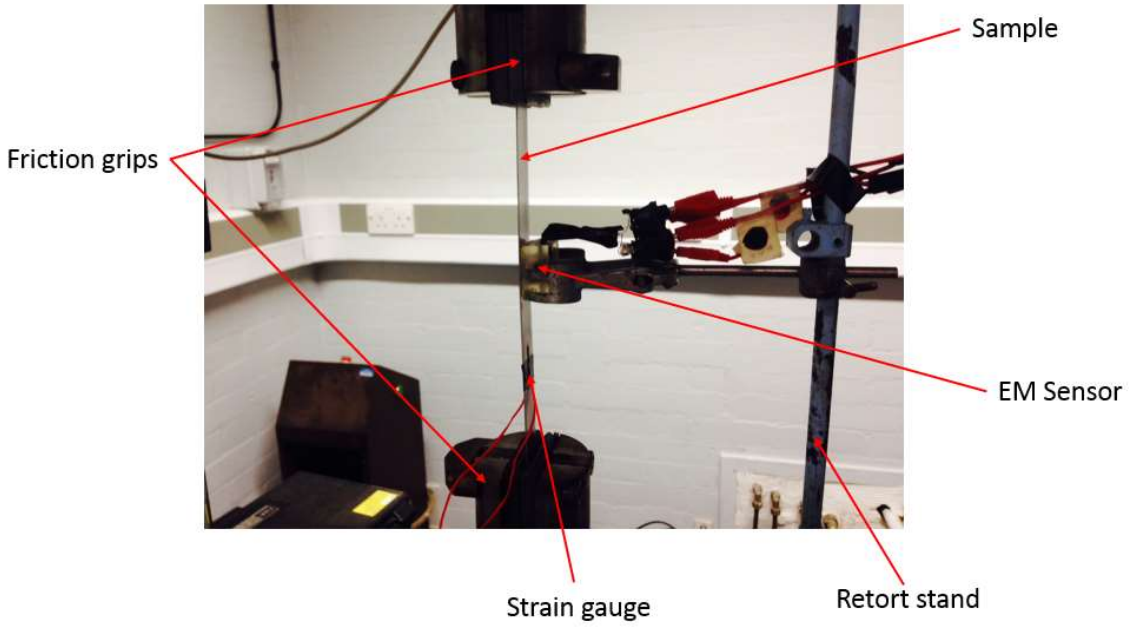

Figure 57: Experimental set up for inductance change with applied stress.

After the samples had been mounted the strain gauge factor was checked and inputted into the strain gauge bridge. The output of the strain gauge bridge was balanced to ensure that the output was 0 microstrain before the start of an experiment.

Load was applied incrementally using the Instron test rig until a set load was achieved within the elastic stress range, the sample was then unloaded incrementally until the sample was fully unloaded. At each increment microstrain was recorded (and converted to a stress value) as well as an inductance value.

8. Results and Discussion

8.1. Cold Rolled IF Steel U-Type Sensor – Edge Effect and Lift Off Effect Measurements

Measurements were completed using a U-type EM sensor to establish the effects that proximity of the EM sensor to the edges of an IF steel sample would have on the magnitude of the inductance measured. These experiments were conducted to establish the sensitivity of the EM sensor to edge effects and lift off for IF steel. Figure 58 shows the orientations of the sensor used for the edge effect measurements when viewed from directly above, looking down onto the sample.

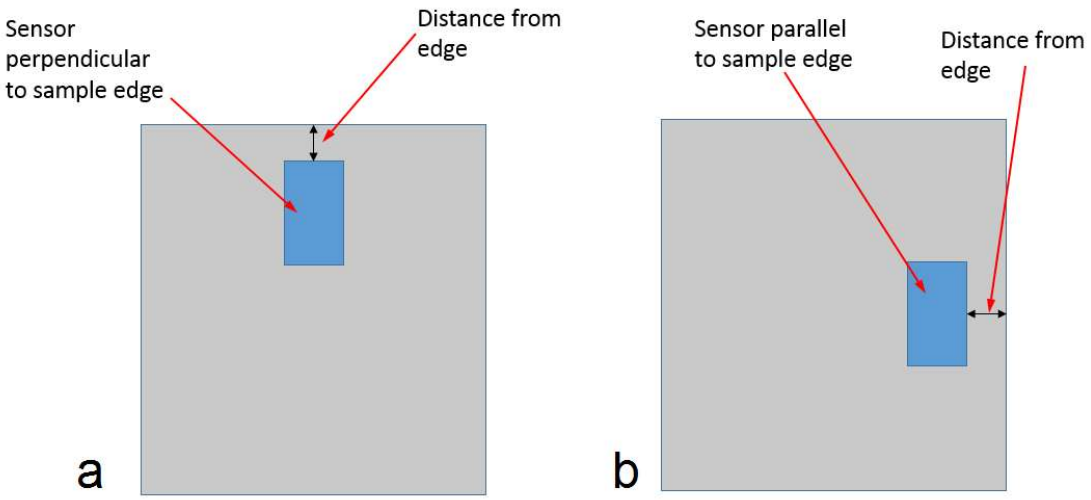

Figure 58: Schematic diagram of U type sensor orientation during edge effect measurements; (a) sensor perpendicular to sample edge and (b) sensor parallel to sample edge.

Figure 59 shows inductance values recorded at increasing distance from the edge of an as-received cold rolled IF steel sample for sensor orientations perpendicular and parallel to the plate edge, measurements were taken at 10Hz. The data shows a significant increase in inductance as the distance away from the edge of the sample increases for both sensor orientations. Inductance values stabilise at a distance of 4mm from the edge of the sample for the parallel orientation and 6mm for the perpendicular orientation. Measured inductance at the plate edge is lower when the sensor is parallel to the plate edge (3.66×10^{-6} H) than when the sensor is perpendicular to the plate edge (3.89×10^{-6} H). The difference in inductance

readings at the plate edge is due to the amount of exciting field contained within the sample, this is greater for the sensor when it is perpendicular to the plate edge than when it is parallel to the plate edge. It is expected that the magnitude of the measured inductance will decrease towards the edge of a sample as the ability of the induced field to spread out around the sensor is decreased. Similar effects on inductance magnitude using this type of sensor have been reported for different carbon steels [145].

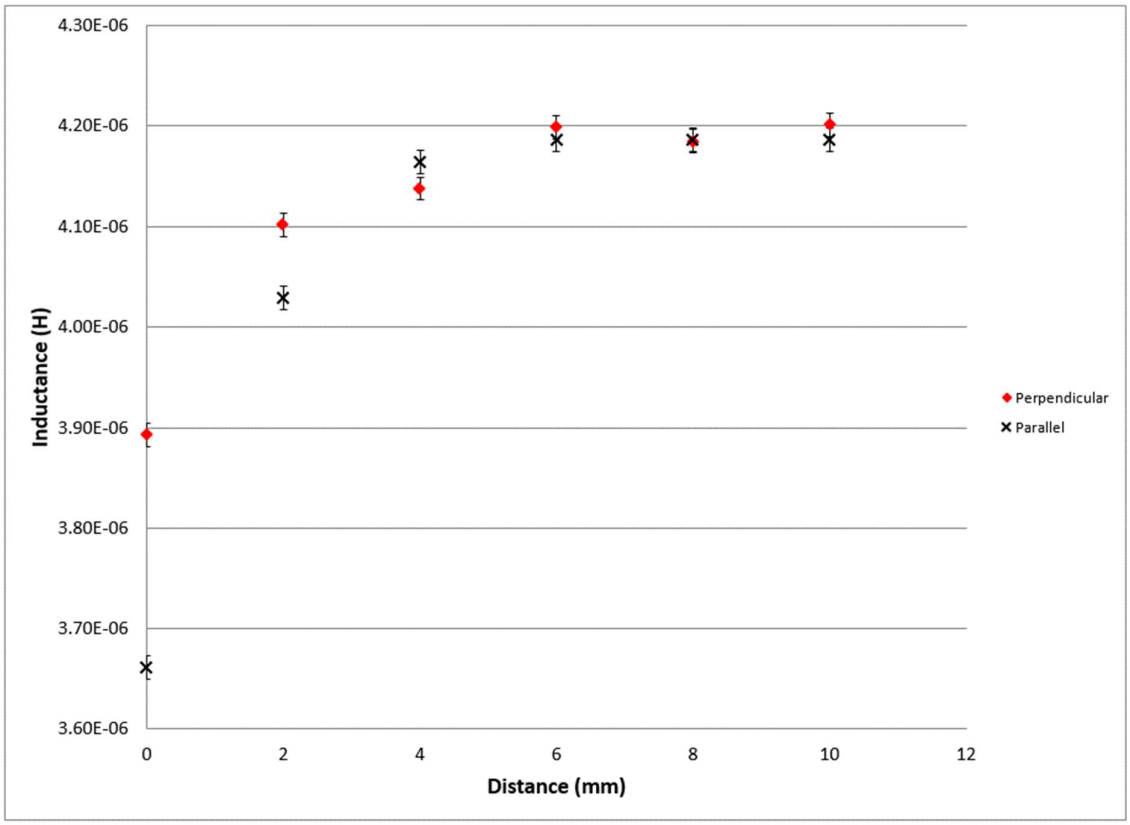

Figure 59: The effects of proximity to sample edge on measured inductance values using a U-type EM sensor on an as received cold rolled sample. All measurements taken at 10Hz. Parallel and perpendicular sensor orientations are shown.

The majority of the magnetic field induced by the sensor into the test specimen is contained between the legs of the sensor, however a significant portion of the field fringes out from the sides of the legs into the wider sample. Figure 60 shows a COMSOL model representation of a U-type EM sensor and its induced magnetic field, the model shows a representation for field line distribution only as the dimensions of the ferrite core are different to that of the U-type sensor used for the experimental work in this thesis [146].

The distribution of the field lines shows that the majority of the induced field is close to the sensor's ferrite core with some of the field fringing out across the sample. The spread of field lines shows that it is important to control sensor position accurately during experimentation as edge effects always have an effect (albeit very small) on the measured output from surface type EM sensors, movement of the sensor closer to or further from a sample edge will affect reproducibility of the results. These effects can be controlled by using the same sample dimensions and relative sensor position or through the use of a ferromagnetic shield around the sensor which would contain the fringing field and prevent it from spreading further into the sample. For industrial applications sensor position relative to the measurement material is critical with relation to both lift-off and edge effects and must be fully controlled.

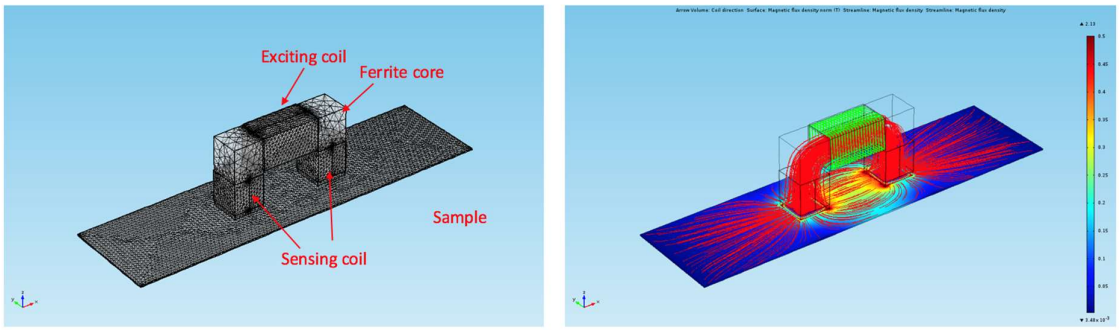

Figure 60: COMSOL model showing the spread of induced magnetic field into a test sample [146].

Figure 61 shows the effects of increasing lift off on the magnitude of measured inductance. The inductance values decrease in magnitude as the list off distance increases, the decrease in inductance value is not linear with distance. The inductance decrease over the initial 1.25mm from the surface of the sample represents 82% of the total decrease in inductance due to lift off. Similar trends have been reported for EMAT systems where the relationship between the lift off and the inductance was found to be $1/(d_0+d_x)^2$ was found during an in-depth study into the effects of lift-off [147]. Where d_0 was the lift off and d_x the nominal increase in lift off. Sensitivity to lift of effects can be reduced by introducing a small permanent lift off between the sensor and measurement surface, this reduces the sensitivity of the sensor to the large measurement changes caused by small increases in lift off immediately at the measurement surface.

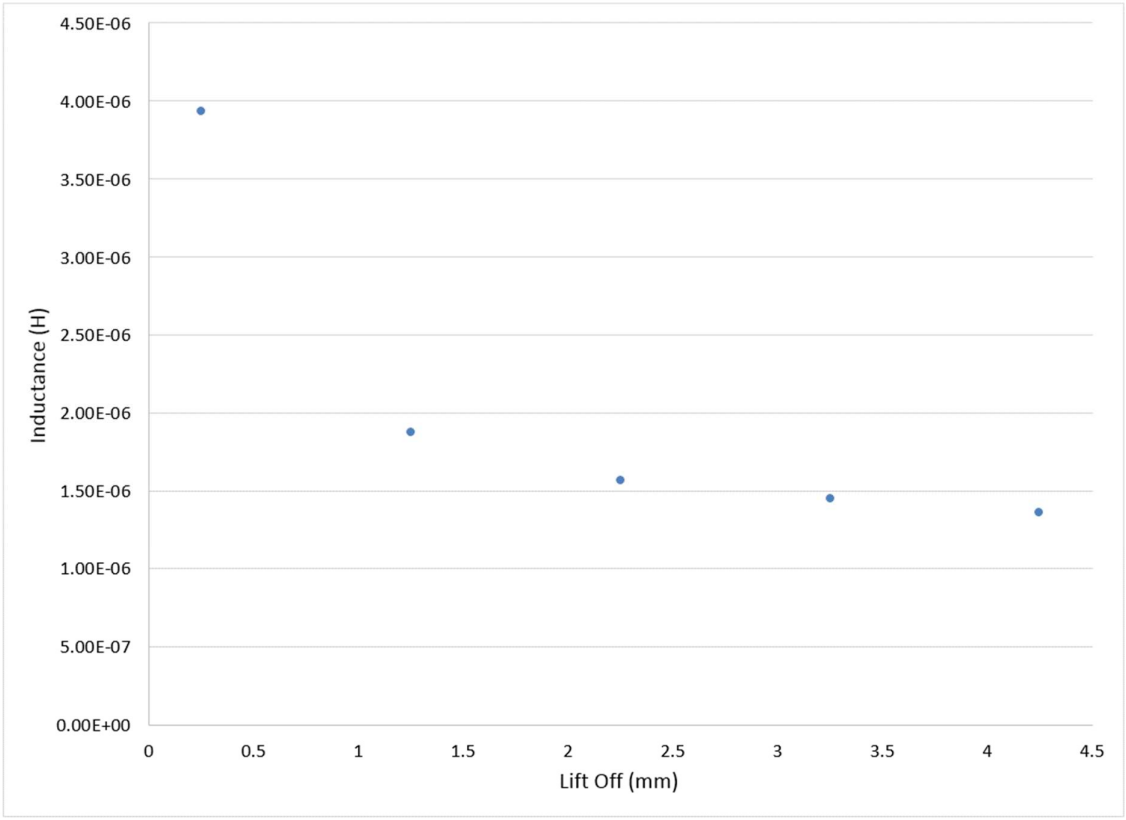

Figure 61: The effect of lift off distance on measured inductance for a U-Type EM sensor used on cold rolled as received IF steel, Lift off values do not start at 0 due to built in lift off in the sensor construction.

Close proximity to the edge of a test sample and very slight lift offs have significant effects on the inductance values measured by a U-type EM sensor. The results from the edge effect and lift-off trial were used to guide sample size, sensor positioning and experimental methods for subsequent tests. All measurements were taken with the sensor at a distance greater than 25mm from the sample edge in any direction. The effects of lift off on measured inductance are particularly important when considering heat treatment of samples as oxide layers may formation caused by annealing may form a nonmagnetic layer between the sensor and the tested material, reducing the measured inductance [145]. The loose oxide was cleaned from the heat treated test samples in subsequent experiments to ensure as small a lift off as possible occurred. A series of tests were conducted on samples that had been heat treated at 650^{o}C for 75 and 120 minutes. Measurements were taken with the adherent oxide layer present and subsequently with the oxide layer had been lightly ground away to reveal clean metal. The measured

inductance difference was typically 0.01 x 10^{-6} H, 2% of the measured inductance signal for as received IF steel recorded with a U shaped EM sensor.

8.2. Texture Effects on EM Sensor Measurements

Texture has an effect on the relative permeability of ferromagnetic materials, and is a cause of magnetic anisotropy (reference section 4.4.4). Texture of cold rolled strip steels change as they are annealed and recrystallisation takes place, generating recrystallisation texture from a deformation texture. Recrystallisation texture is very important for IF steel as correct texture gives high formability and r-values [49].

Investigation of the effects of texture was completed using a U-Type EM sensor and the high temperature cylindrical sensor (described in 7.6.1). Inductance values were measured in different directions related to the sheet RD using both sensors for samples taken from both IF and GO silicon steel sheet. Grain size must also be mentioned as an experimental factor, typical IF steel grain diameters after recrystallisation are 10 - 15μm, whereas grain diameters for GO silicon steel are as large as 30mm. It was possible to make U-type EM sensor measurements primarily within a single grain of GO silicon steel, the sensor could be placed within a single grain and moved within it. The majority of the induced field from the sensor is contained between the sensor feet and therefore will sample the single grain, although some field will spread out into neighbouring grains. This approach is as close as possible to ensuring that only one crystallographic orientation was assessed, whereas inductance measurements for IF steel crossed multiple grains and hence crystallographic orientations in a single measurement.

Figure 62 shows results of U-type sensor measurements made within a single grain of GO silicon steel in RD, 54° to RD and TD. Literature data reports that the easiest magnetic direction for annealed GO silicon steel is the RD, with the TD the next easiest and 54° to RD the lowest. Permeability values reported with an applied field of 796 A/m are 1580 in RD, 1440 in TD and 1320 at 54° to RD (16% lower than the permeability in the RD) [148]. The higher permeabilities in RD and TD are due to the [001] and [110] cube directions being parallel, respectively, to the RD and TD. Whereas at 54° to RD it is the [111] cube direction that is parallel to the orientation [27, 148]. Measured inductance (at 10Hz) in the RD was 4.81×10^{-6} H, at 54° to RD the measured inductance was 4.56×10^{-6} H and 4.68×10^{-6} H in the TD. The inductance measurements for the GO silicon steel agree with the magnetically hard and

easy directions suggested in Table 4 and the data reported in the literature. The difference between the highest and lowest inductance values in Figure 62 is 0.25 x 10^{-6} H, 5% lower at 54° to the RD than parallel to RD.

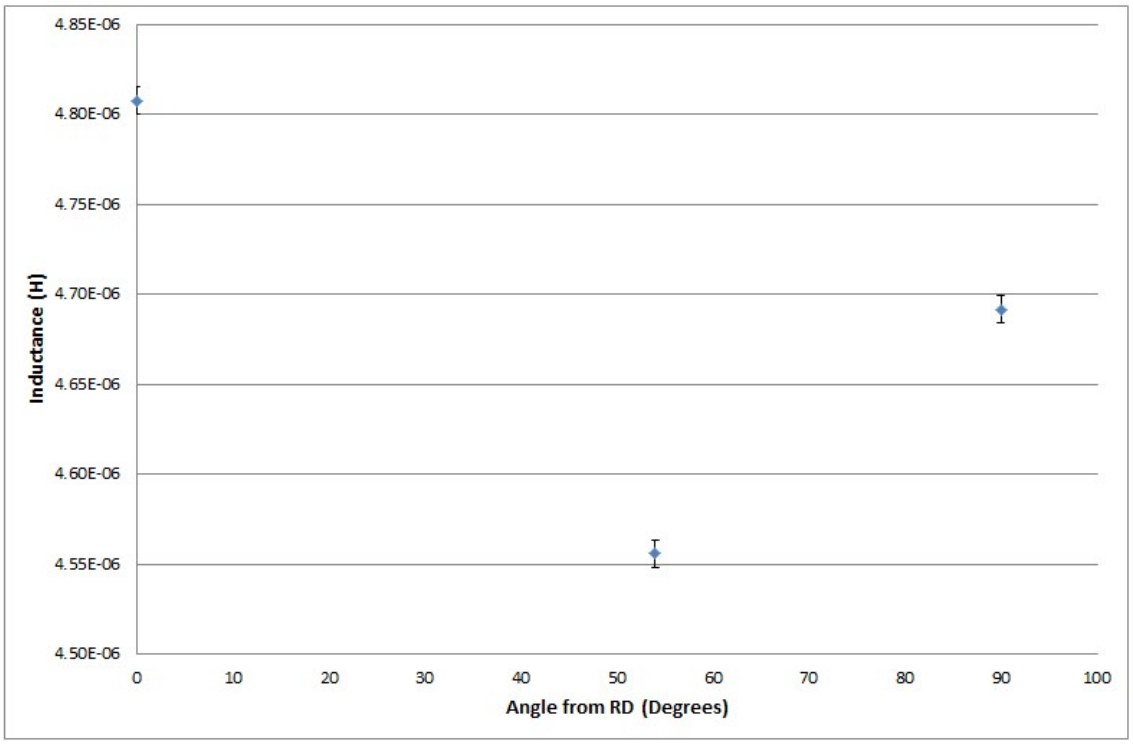

Figure 62: U-type EM sensor inductance measurements within a single grain of 3% Si Steel for RD (0 degrees), 54° to RD and TD (90° to RD).

Figure 63 shows BH loops measured for 3% Si steel samples at 4 different orientations; RD, 45° to RD, 54° to RD and TD. The samples were measured at the University of Manchester using their bespoke BH system. The system comprises of a magnetisation yoke, hall sensor and induction measurement coil, the system is controlled and interpreted using Labview. The system is developed to investigate BH parameters and MBN for strip or bar samples of steel, samples are magnetised using the magnetisation yoke which is driven at very low excitation frequencies (low enough that flux density control is not required) and employing a constant change of voltage [149].

The BH loops show that for the same applied field higher flux densities were recorded in RD, 45° to RD and TD, the highest flux density recorded in RD. The sample measured with orientation 54° to RD had the lowest flux density for the same applied field. The data presented is consistent with the U shape EM sensor testing and literature data [27, 148] and shows that RD is the most easily magnetised direction and 54° to RD is the hardest direction to magnetise. Figure 64 shows the coercivity and remanence data for the same 3% Si steel samples used for BH loop measurement in Figure 63. Coercivity is highest for the sample with orientation of 54° to RD (46 A/m) and lowest in RD (22 A/m), a difference of 53%. The trend for coercivity is the inverse of that for the remanence where RD has the highest value (1.16 T) and 54° to RD has the lowest value (0.29 T), there is a 75% difference between the remanence measurement in RD compared to 54° to RD.

The BH loop, coercivity and remanence data presented shows good sensitivity to the direction measured, and therefore texture, for 3% Si steel. The EM sensor measurements presented for 3% Si steel does not show as big an effect for sample orientation as the BH loop, coercivity and remanence measurements. This suggests that EM sensor measurements are not as sensitive to differences in texture as BH loop measurements, but can be used to indicate the effect of texture.

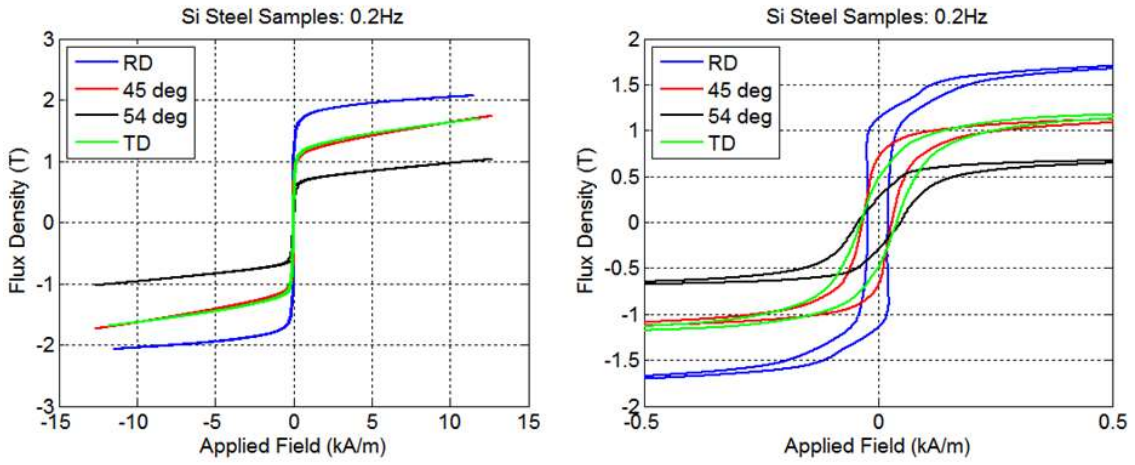

Figure 63: Magnetic hysteresis loops recorded for 3%Si Steel samples which have orientations in RD, 45° to RD, 54° to RD and TD. Chart on the left shows the full loop from -13 to 13 kA/m and the chart on the right shows a magnified view of the same BH loops from -0.5 to 0.5 kA/m.

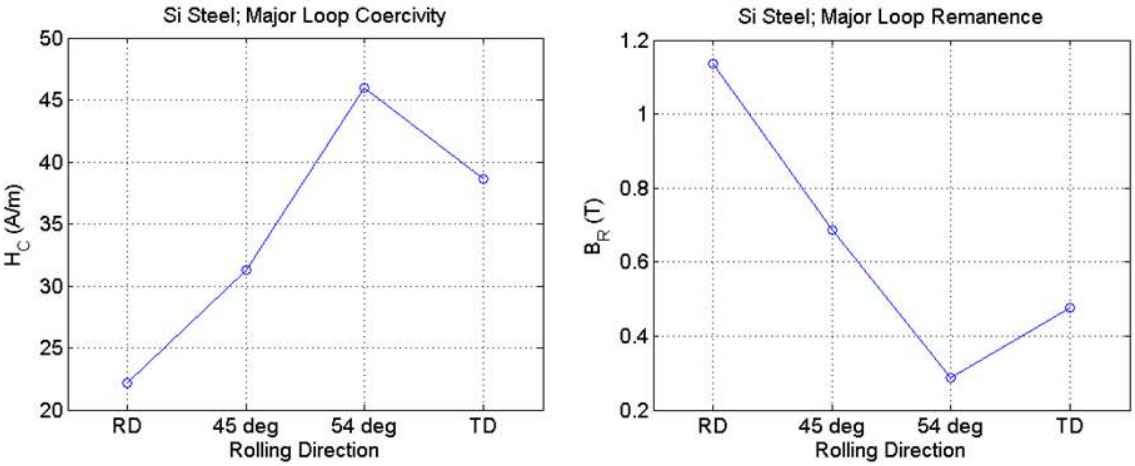

Figure 64: Coercivity and remanence data recorded for 3% Si Steel samples which have orientations in RD, 45° to RD, 54° to RD and TD.

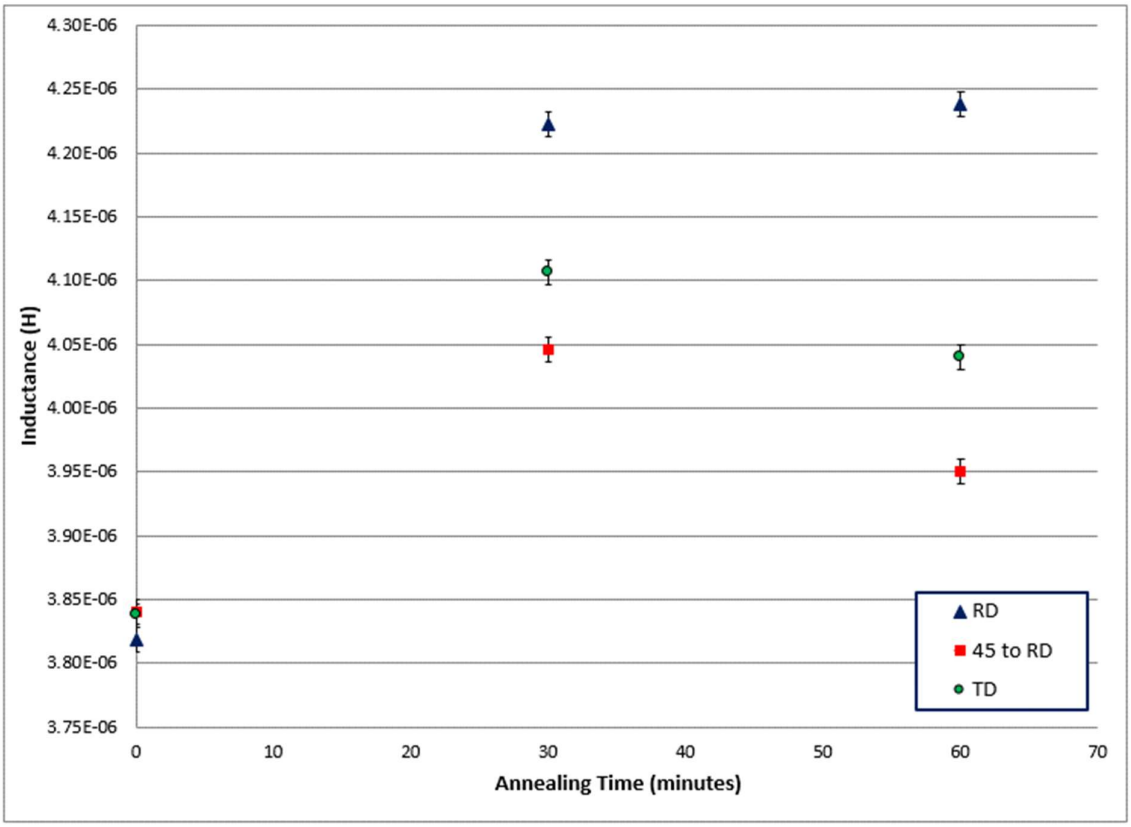

Figure 65: U-type EM sensor measurements recorded at 100Hz in RD, 45º to RD and TD orientations for IF steel samples in the as received (0 minute) condition and annealed for 30 and 60 minutes at 650ºC.

Figure 65 shows inductance data taken from three IF steel samples in three different conditions: the first (0 minutes annealing time) in the as received condition, the second annealed for 30 minutes at 650°C and the third annealed for 60 minutes at 650°C. Table 9 shows the inductance values at 100 Hz for each data set in Figure 65. The U-type sensor used for this work was different to the sensor used for the edge effect experiments and the interrupted recrystallisation experiments, it was the same sensor as that used for the 3% Si steel measurements. A different sensor was used as the original sensor was damaged and a new one had to be constructed. The sensor was of a similar configuration to the original sensor with the same dimensions. Due to the slightly different winding configuration (this comes from being hand wound) the magnitude of the measured inductance is different but the overall trends measured are the same.

The data in Figure 65 and Table 9 shows that the inductance measurements recorded in the RD have the greatest differential between the as received and the annealed for 60 minutes condition and that in the RD measured inductance increases with annealing time, discussed further in sections 8.3 and 0. Inductance measured for the 0 minute (as-received condition) data set shows little variation between the measurements in the different sensor orientations. The 30 and 60 minute data sets show significant differences between the RD, 45° to RD and TD directions, indicating that magnetic anisotropy changes during annealing.

Texture is expected to have a greater effect on inductance (permeability) anisotropy with respect to measurement orientation as recovery and recrystallisation take place. In the as-received condition the very high dislocation density will act as the dominant domain wall pinning factor, preventing the domain walls from moving in association with other factors that affect their freedom, resulting in lower permeability and therefore inductance values. As the dislocation density decreases during recovery other factors that impact upon domain wall motion will become more significant and the effect that texture has on magnetic properties will become more significant. Typical deformation textures for IF steels are {112}<110>, {001}<110>, {111}<110>, {111}<123> and {111}<112> [65, 150]. In the as-received condition (0 minutes, Figure 65) there is no significant difference between the inductance measurements in the different orientations, it is thought that the effects of the heavy dislocation density in the as-received condition is dominant over any effects on magnetic anisotropy caused by texture.

The microstructural conditions for the samples used are shown in Figure 66. The microstructures shown in Figure 68 indicate that whilst a significant amount of recrystallisation is complete after 30 minutes, the presence of elongated grains shows that recrystallisation is not fully complete. The hardness value for the sample heat treated for 30 minutes at 650°C was 97 HV. The micrograph for the sample heat treated for 60 minutes at 650°C shows a similar amount of recrystallisation to the 30 minute sample but has a lower hardness value of 84 HV, indicating that further recrystallisation has taken place. Hardness values are known to stabilise once recrystallisation is complete (assuming no grain growth has taken place) [1].

Literature data for IF steels reports that textures evolve during recovery and recrystallisation (detailed in section 3.2.6), as the amount of recrystallisation has increased between the 30 and 60 minute samples it is reasonable to expect some differences in texture.

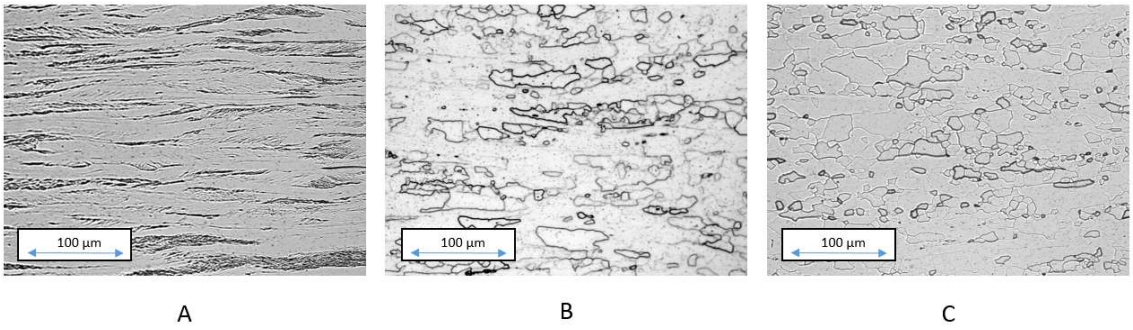

Figure 66: Micrographs for samples heat treated at 650°C and used for U shaped sensor inductance measurements, rolling direction is left to right. (A) as received condition; (B) annealed for 30 minutes at 650°C, the hardness value was HV 97; (C) annealed for 60 minutes at 650°C, the hardness value was HV 84.

Inductance measurements in the 45° to RD and transverse directions show an increase in inductance between the as received and annealed for 30 minute conditions and then a decrease in inductance between the annealed for 30 minute and 60 minute samples. After annealing for 30 minutes the measured inductance is lowest at 45° to RD and highest in RD, the same trend is seen after annealing for 60 minutes. The differences in inductance values for the 45° to RD and TD samples may be due to texture evolution during annealing. It is not immediately obvious from the recrystallisation textures reported in literature for IF steels (section 4.4.4, Table 3) that there is a dominant set of textures which align the magnetically easy directions ([100], [010] and [001]) in such a way that magnetic anisotropy due to crystallographic orientation occurs.

The sensor orientation that aligns the applied field closest to the greatest proportion of magnetically easy directions ([100], [010] and [001]) after recrystallisation should record the highest inductance values. This would be consistent with the results measured for the 3% Si steel, where the highest inductance values were recorded in the RD as the applied field was aligned with the [100] direction. Using the data in Table 3 it is possible to work out the relative contributions of the magnetically easy

directions for each texture and sensor orientation (calculated using vectors related to each sensor orientation in the RD plane).

The contributions can then be compared to the measured inductance values shown in Figure 65. Table 9 shows the relative contributions of the different orientations compared to the measured inductance values for each sensor orientation.

Table 9: Relative contributions of magnetically easy directions ([100], [010] and [001]) compared to measured inductance values for each sensor orientation for IF samples in the as-received (deformed condition) and 60 minutes annealing at 650°C conditions.

Sensor Orientation	Deformed		Recrystallised	
	Directional contribution (%)	Measured inductance (H)	Directional contribution (%)	Measured inductance (H)
RD	22.3	3.82 x 10-6	22.9	4.24×10^{-6}
45 degrees	26.0	3.84 x 10-6	24.9	3.95×10^{-6}
TD	21.5	3.84 x 10-6	19.6	4.04×10^{-6}

Table 9 indicates that when the sensor is oriented at 45° to RD the applied field will be aligned the most closely with the greatest proportional amount of magnetically easy directions, the next close orientation is RD and when the sensor is oriented with TD the applied field is aligned with the lowest proportion of magnetically easy directions. Consideration of the orientations of the magnetically easy directions alone suggests when the sensor is oriented at 45° to RD it should record the highest inductance value and when compared to the actual measured inductance values it is clear that this is not the case as the inductance measurement in the RD returns the highest inductance value (4.24×10^{-6} H), the inductance measurement with the sensor oriented to TD is the next highest (4.04×10^{-6} H) and the measured inductance when the sensor is oriented at 45° to RD is the lowest (3.95 x 10-6 H).

The explanation for the discrepancies are unclear although there are a number of possible reasons why the inductance values recorded using the U-shaped EM sensor are not consistent with the relative directions of the magnetically easy cube directions. The analysis of the magnetically easy direction contributions assumes an even spread of the different recrystallisation textures. It is unlikely that this

will be the case and it is reported that in recrystallised IF steels there will also be a significant amount of other textures that will affect magnetic measurements [65].

The exact textures present in this sample may not match those reported in literature, this cannot be seen without completing texture measurements on the samples used for this study. Texture was not measured for the experimental samples as it was considered that literature data would be sufficient and that it was not part of the primary objective of this research, the effect of texture was assessed to determine the significance of any anisotropy to determine if measurements in a consistent orientation would be essential for in-situ measurement of recrystallisation. However, if development of a relationship between these EM sensor measurements and texture in IF steels was a desired objective then texture measurement would be essential. Experimentally there are difficulties with taking inductance measurements using U shaped EM sensors as there can be an effect of sample geometry (if the samples are not flat) which causes different degrees of lift off in each different sensor orientation. The samples used are slightly curved in the RD due to the coiling / uncoiling process, this causes different lift-offs when the sensor is re-oriented for measurements in different directions and the inductance measurement differences shown in the 45° to RD and TD may be a combined effect of sensor lift-off as well as texture evolution.

Magnetic hysteresis loop measurements completed on IF steel samples in the RD, 30° to RD, 45° to RD, 60° to RD and transverse directions in the as received, annealed for 30 minutes at 650°C and 60 minutes at 650°C conditions are shown in Figure 67, with corresponding coercivity and remanance measurements shown in Figure 68. The magnetic hysteresis loops, coercivity and remanance data was measured by Dr John Wilson at Manchester University [149]. The hysteresis loops for the 0 minute data set show a significant amount of variation for the different orientation samples, this is most easily seen in the coercivity and remanance data where the variation is more obvious. The remanence variation for the 0 minute sample is 0.9 T (RD) to 1.05 T (TD), with measurement errors of +/- 0.04 T. The difference in remanence between RD and TD are significant (outside the error margin), whereas the differences in remanence between the other orientations (30°, 45° and 60° to RD) are not significantly different as they are inside the error margin. The remanence and coercivity values for the annealed

samples (30 minutes and 60 minutes) are similar in all orientations and it cannot be said that these orientations return different enough values to be significant.

The data presented shows that there is a significant difference in measured inductance related to texture with a U type EM sensor for 3% Si steel and a lesser effect measured using a high temperature cylindrical EM sensor at room temperature. Measurements of IF steels in different orientations for samples which have undergone annealing at 650^{o}C for different times show possible effects of texture evolution when measurements in different orientations are considered, but it is not possible to clearly demonstrate with the data presented that texture is the main cause of the differences in the inductance values measured for the different orientations. Literature data reports that the amounts of different texture changes during the annealing process as recovery and recrystallisation take place, texture must therefore play a part in any magnetic measurements. It is however clear from other experiments completed and literature data that texture is only one factor that affects permeability through the recovery and recrystallisation processes. Comparison of the relative contributions of the magnetically easy crystal axes between the deformed and recrystallised conditions (Table 9) shows similar values suggesting that the effect of texture on electromagnetic measurement for IF steels is relatively small. In subsequent experiments all inductance measurements were recorded using the RD only to ensure that any effects of texture evolution would be consistent.

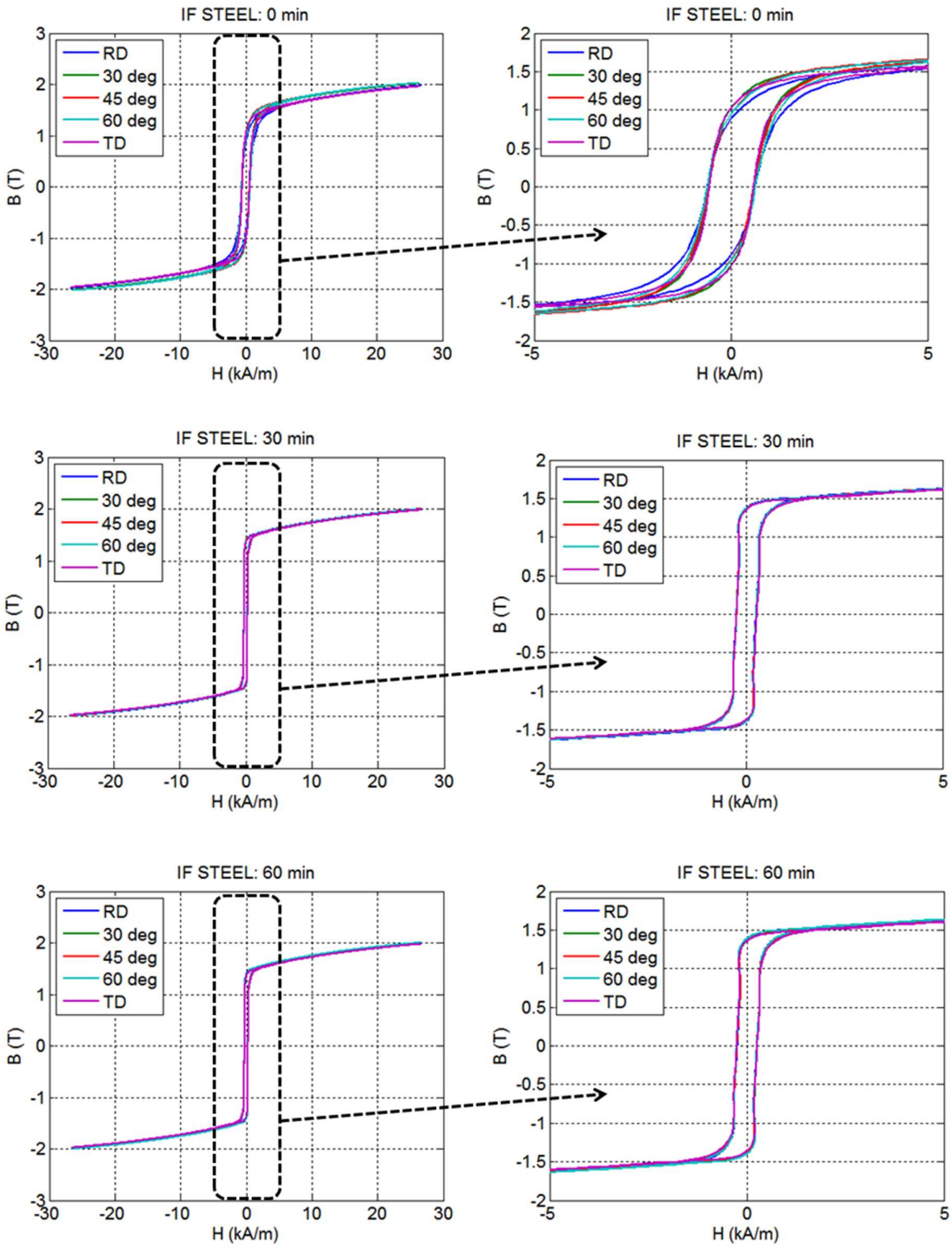

Figure 67: Magnetic hysteresis loops for IF steel samples in the RD, 30° to RD, 45° to RD, 60° to RD and transverse directions in the as received, annealed for 30 minutes at 650°C and 60 minutes at 650°C conditions.

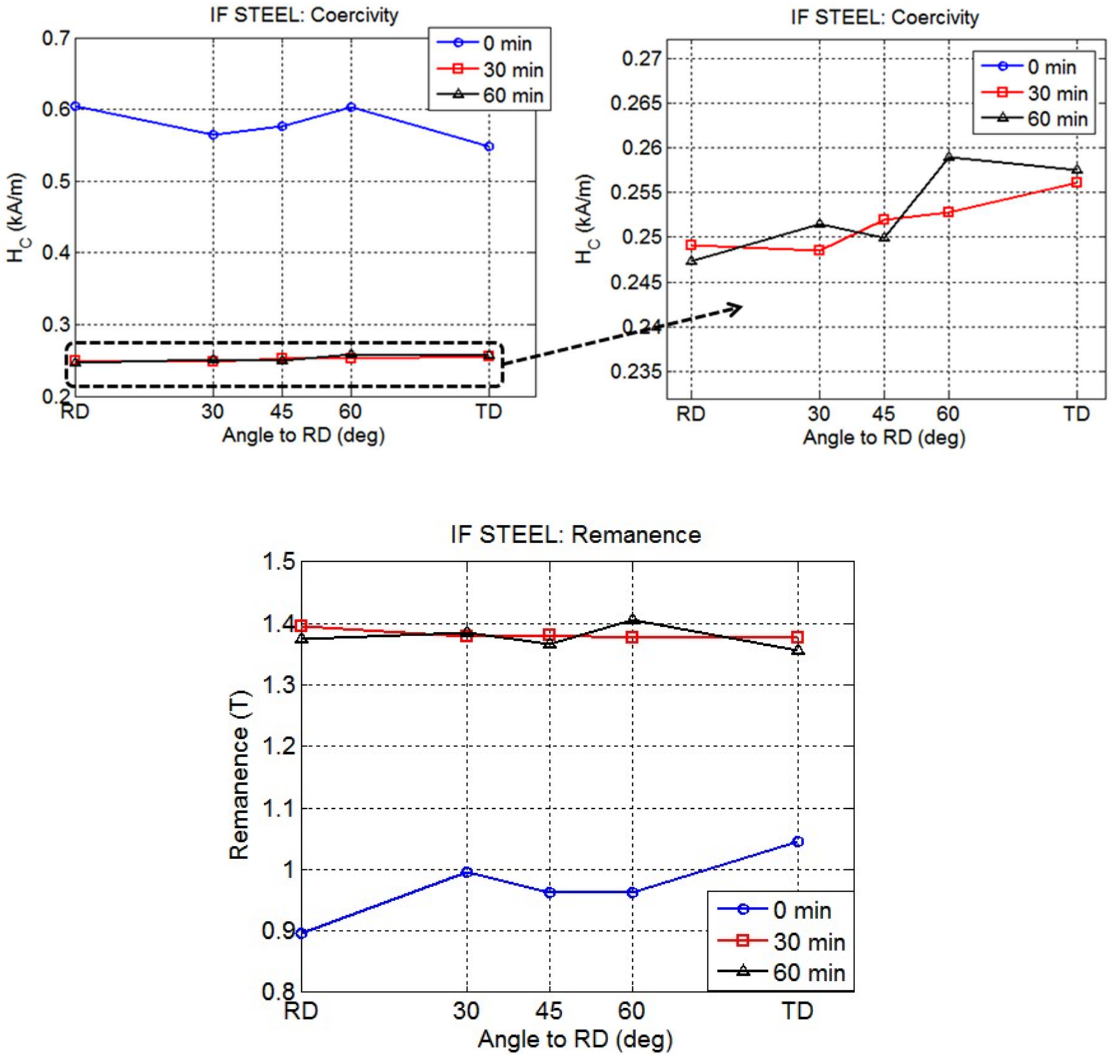

Figure 68: Coercivity and remanance charts for IF steel samples in the RD, 30º to RD, 45º to RD, 60º to RD and transverse directions in the as received, annealed for 30 minutes at 650ºC and 60 minutes at 650ºC conditions. Data extracted from magnetic hysteresis loops shown in Figure 67.

8.3. Interrupted Recrystallisation Experiments – U-Type Sensor

The purpose of these experiments was to establish whether EM sensor measurements at room temperature and in laboratory conditions were sensitive to microstructural changes caused by recovery and recrystallisation. If these tests proved successful then further development of the technique for in-situ, high temperature measurements would be completed. The heat treatments were designed to generate different amounts of recrystallisation and used a U-type EM sensor to record inductance changes.

Figure 69 shows the inductance measured against annealing times at 650°C and 620°C in the rolling direction only. The data shows an increase in inductance values for annealing time at both temperatures. Inductance values stop increasing at around 30 minutes for both samples. Inductance increases at the first-time points (7.5 minutes for 650°C and 10 minutes for 620°C) are comparatively larger than for longer time periods, the inductance increases by 46% after 7.5 minutes at 650°C and 43% at 10 minutes at 620°C (percentages calculated from the total inductance change for each temperature). Observation of the microstructure for the samples heat treated at 7.5 minutes for 650°C and 10 minutes at 620°C do not demonstrate visibly that any recrystallisation has taken place when compared to the heavily deformed microstructure for the as received condition (Figure 70).

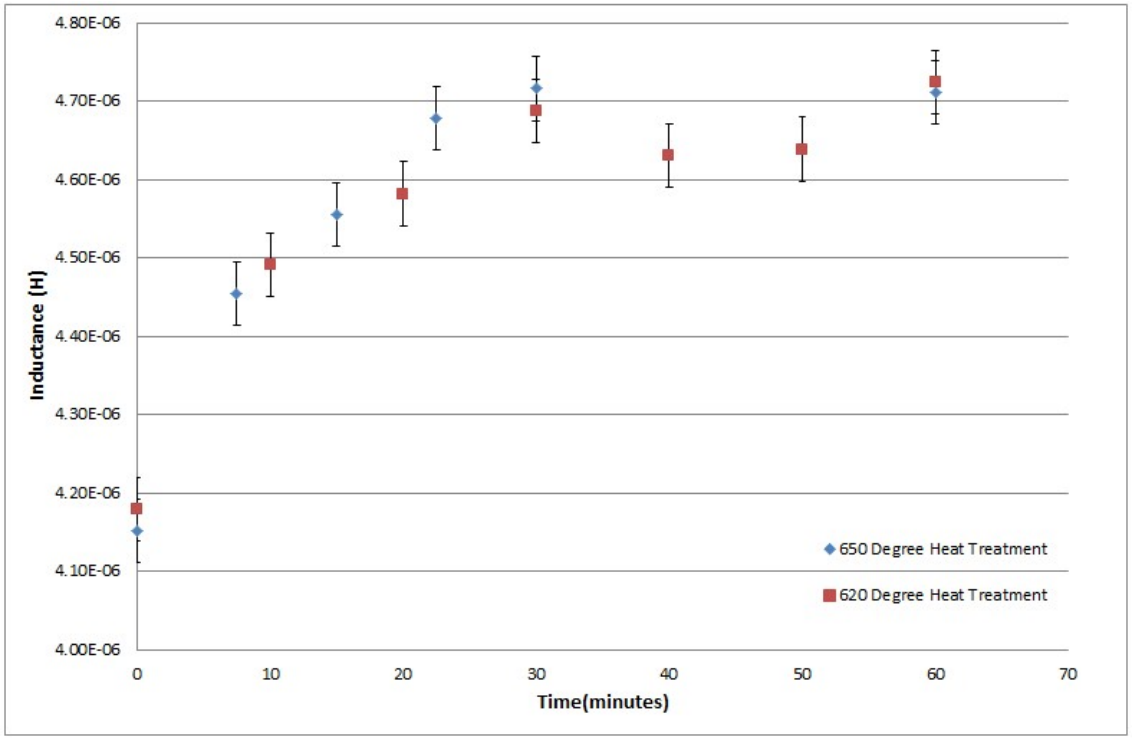

Figure 69: Inductance measured for different annealing times at 650ºC and 620ºC

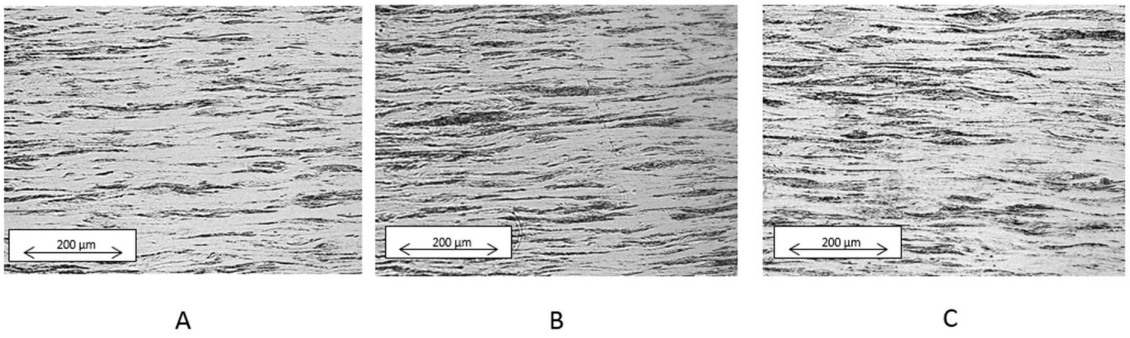

Figure 70: IF steel micrographs, rolling direction is left to right; (A) as received cold rolled condition; (B) after 10 minutes at 620ºC; (C) 7.5 minutes at 650ºC

After 30 minutes the increase in inductance is similar for both 650ºC and 620ºC samples (5.6 x 10^{-7} H and 5.1 x 10^{-7} H respectively), there is then no significant further increase in inductance as annealing time increases up to 60 minutes where the inductance values are 4.7 x 10^{-6} H for samples heat treated at both temperatures (increases in inductance of 5.5 x 10^{-7} for 620ºC and 5.6 x 10^{-7} for 650ºC).

Figure 71 shows micrographs taken at 30 minutes for both temperatures indicating significant recrystallisation for both temperatures, with large well defined recrystallised grains evident in the 650ºC

micrograph, an indication that a greater degree of recrystallisation has been completed at 650°C after 30 minutes than at 620°C after 30 minutes. There is evidence of some remaining elongated deformed grains in the rolling direction for both of the samples, with a greater area fraction of elongated grains shown in the 620°C sample, this sort of structure indicates that recrystallisation has taken place but is not complete. Figure 72 shows micrographs taken from samples heat treated for 60 minutes at both 620°C and 650°C, both samples show evidence of greater recrystallisation than the samples heat treated at the same temperatures for 30 minutes. The sample heat treated at 620°C for 60 minutes still shows some elongated grain structure and internal etching showing that recrystallisation is advanced but not complete. The sample heat treated at 650°C for 60 minutes shows few elongated grains and a larger amount of equiaxed grains, showing that recrystallisation is more advanced than it is in the sample heat treated at 620°C for 60 minutes.

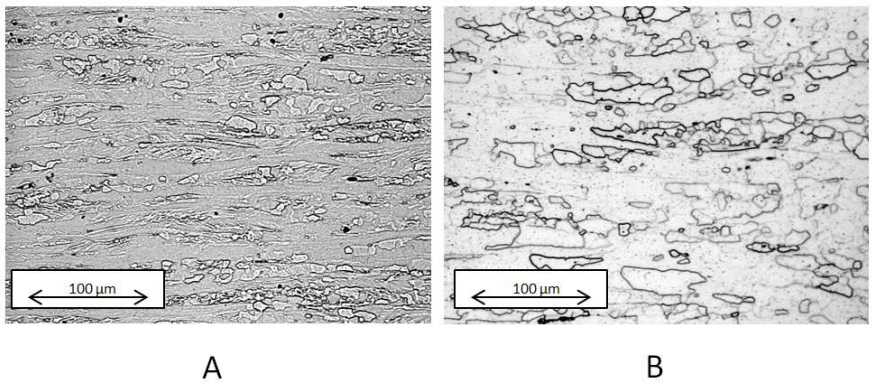

Figure 71: IF steel micrographs, rolling direction is left to right; (A) 30 minutes at 620°C; (B) 30 minutes at 650°C

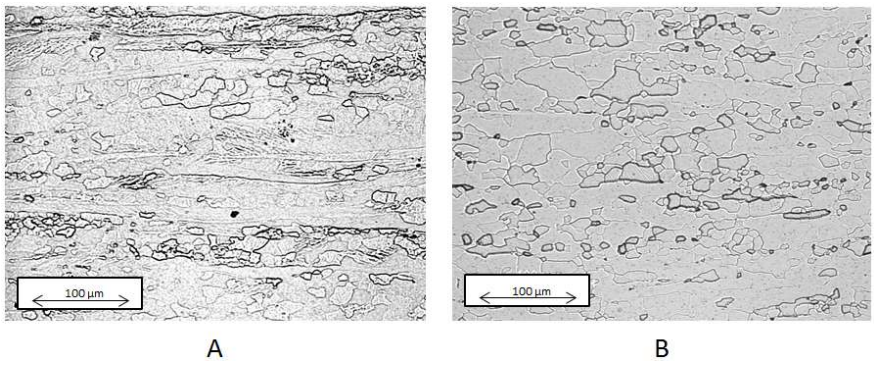

Figure 72: IF steel micrographs, rolling direction is left to right; (A) 60 minutes at 620°C; (B) 60 minutes at 650°C

Hardness values were recorded for the samples heat treated at 620°C and 650°C, Figure 73 shows a decrease in hardness with annealing time which is consistent with recovery and recrystallisation taking place. A small decrease in hardness is observed for both samples after 10 minutes at 620°C and 7.5 minutes at 650°C, observation of the micrographs at this stage indicates that no observable recrystallisation has taken place. Hardness decreases for both samples, decreases of 22 HV for 10 minutes at 620°C and 36 HV for 7.5 minutes at 650°C. Literature data reports decreases of between 10 and 20 HV for recovery only [91, 151], with larger decreases associated with recovery and recrystallisation. Comparison of literature data and the results recorded indicate that only recovery took place for the sample heat treated for 10 minutes at 620°C. The larger hardness decrease (36 HV) for the sample heat treated at 650°C for 7.5 minutes is indicative of recovery having taken place and also that some recrystallisation may have begun, although this was not observed on the optical images. The percentage hardness changes after 10 minutes at 620°C is 24% of the total hardness change for the samples heat treated at 620°C and 28% after 7.5 minutes at 650°C. The recovery process has been reported to cause large changes in permeability in steels, and the large inductance changes at the 10 minute for 620°C and 7.5 minute for 650°C data points are consistent with this [84].

Hardness values for samples heat treated at both temperatures decreased continuously until 30 minutes, the percentage hardness change at 30 minutes for the 620°C sample is 88% and the percentage hardness change for the 650°C sample is 86%. This, in association with the micrograph data, indicates that a significant amount of recrystallisation has taken place by 30 minutes of annealing. After 30 minutes the proportional decrease in hardness with annealing time is smaller, the micrographs show that a significant amount of recrystallisation has taken place at 30 minutes and that some recrystallisation is still occurring but to a lesser extent for subsequent heat treatment time.

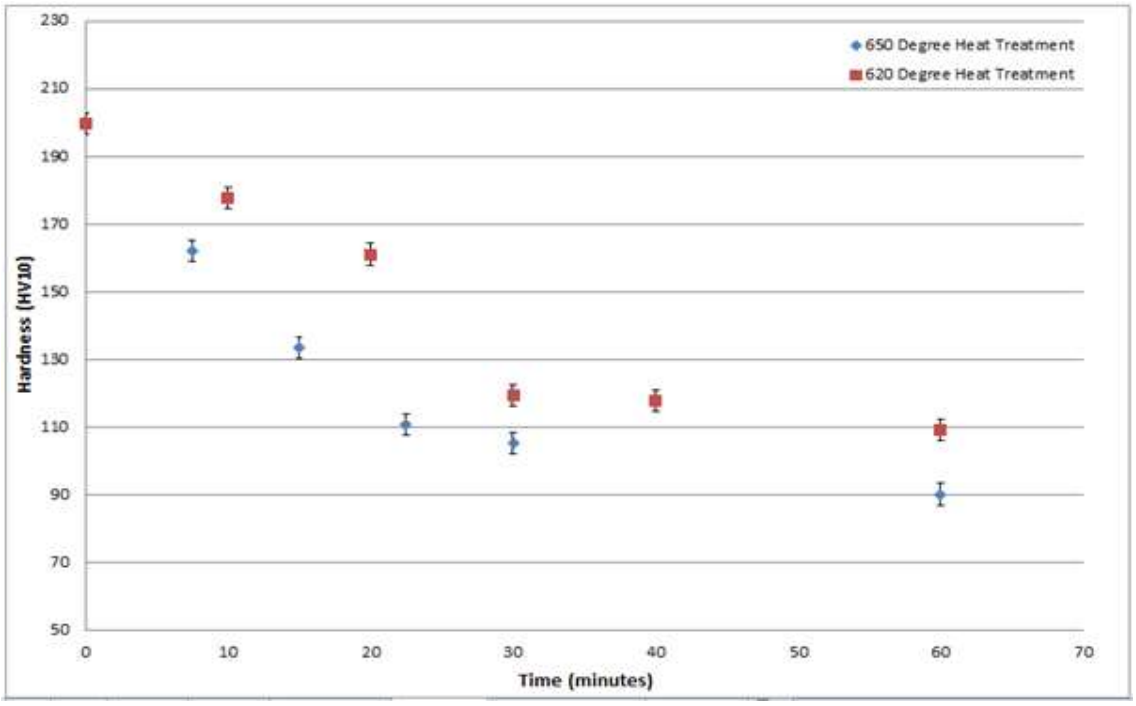

Figure 73: Hardness values plotted against annealing time for IF steel samples heat treated at 620°C and 650°C for different times

Figure 74 shows measured inductance values against recorded hardness values for all of the samples heat treated at 620°C and 650°C. The data shows linear trends for the samples annealed at both temperatures, inductance increases as hardness decreases. The increase of inductance is consistent with reported increases in permeability caused by recrystallisation for cold-rolled low carbon steels [84] and IF steels that have been measured using magnetic hysteresis loops [37]. The inductance values for the samples annealed at 650°C for 30 and 60 minutes are the same (allowing for error, 4.72×10^{-6} H and 4.71×10^{-6} H) at the lowest hardness values (97 and 84 HV). Hardness values would cease to decrease if recrystallisation was complete and inductance values would no longer increase since there would be no further changes to the microstructure or stored energy state of the material (unless grain growth occurred, in which case there would be an increase in inductance value and a decrease in hardness [138]).

Figure 74 indicates that recrystallisation is incomplete for the samples heat treated at 620°C because inductance is still increasing and hardness decreasing, but is complete (or near complete) for the samples heat treated at 650°C. The micrograph taken at 60 minutes for the sample heat treated at 620°C shows

a large number of elongated grains still present, with some equi-axed grains present amongst them, representative of a significant amount of recrystallisation having taken place but not complete recrystallisation. The micrograph taken for the sample heat treated at 650°C after 60 minutes has some elongated grains still present and a large quantity of equi-axed grains, indicative of almost complete recrystallisation. In both cases recrystallisation is not complete, and this may be because there was insufficient driving force in this time frame and at these temperatures for full recrystallisation, particularly for the samples heat treated at 620°C [152].

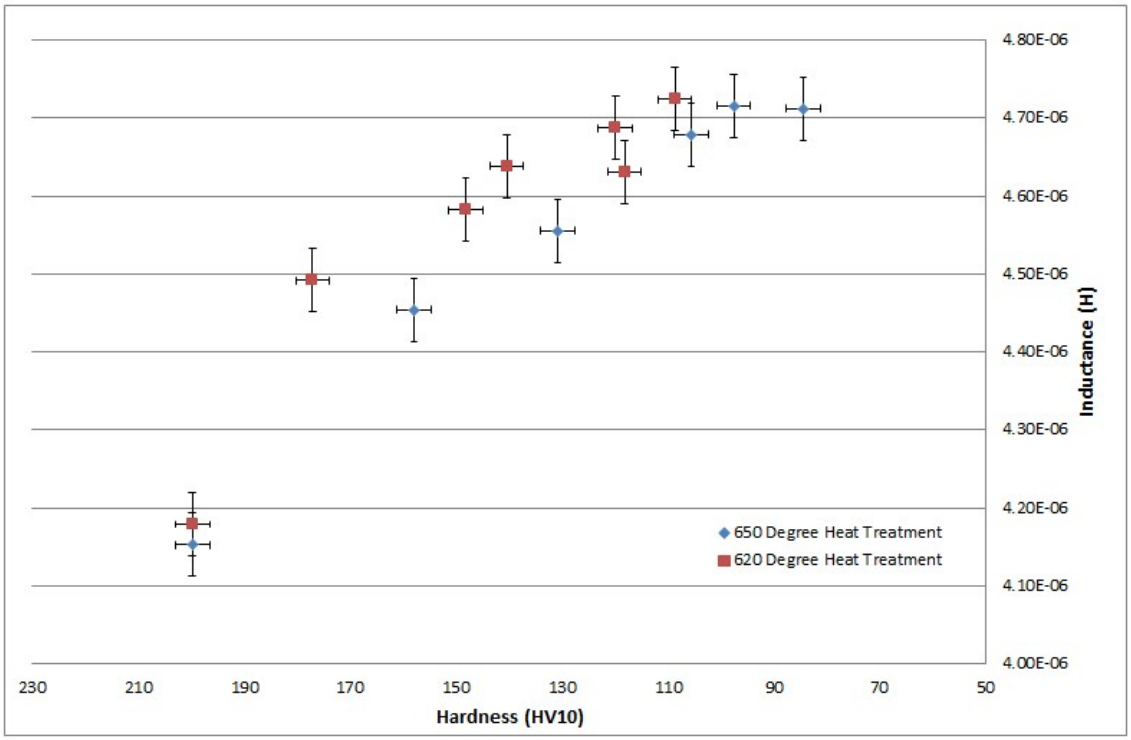

Figure 74: Inductance values plotted against hardness for IF steel samples annealed at 620°C and 650°C for different periods of time.

The data presented shows that EM sensors are capable of monitoring the progression of recovery and recrystallisation off line and that it should therefore be possible to trace the progress of recovery and recrystallisation in-situ during the annealing process.

8.4. High Temperature EM Sensor Heating

An experiment was completed to establish that there was no effect of heating on the high temperature sensor that would then affect the values recorded for in-situ measurements of recovery and recrystallisation or for inductance change with increasing temperature. The high temperature sensor was placed empty into a furnace and heated to 760°C; inductance was measured during the sensor heating. The measured inductance was then compared to a typical data plot from an in-situ recovery and recrystallisation measurement. Figure 75 shows the inductance data recorded during heating of the empty sensor from room temperature to 760°C, the lowest inductance value recorded during sensor heating was 1.53 x 10^{-5} H and the highest inductance value was 1.64 x 10^{-5} H, with a mean inductance value of 1.59 x 10^{-9} H. The data shows a small variation in inductance as the sensor increased in temperature, with increasing signal noise as the temperature increases.

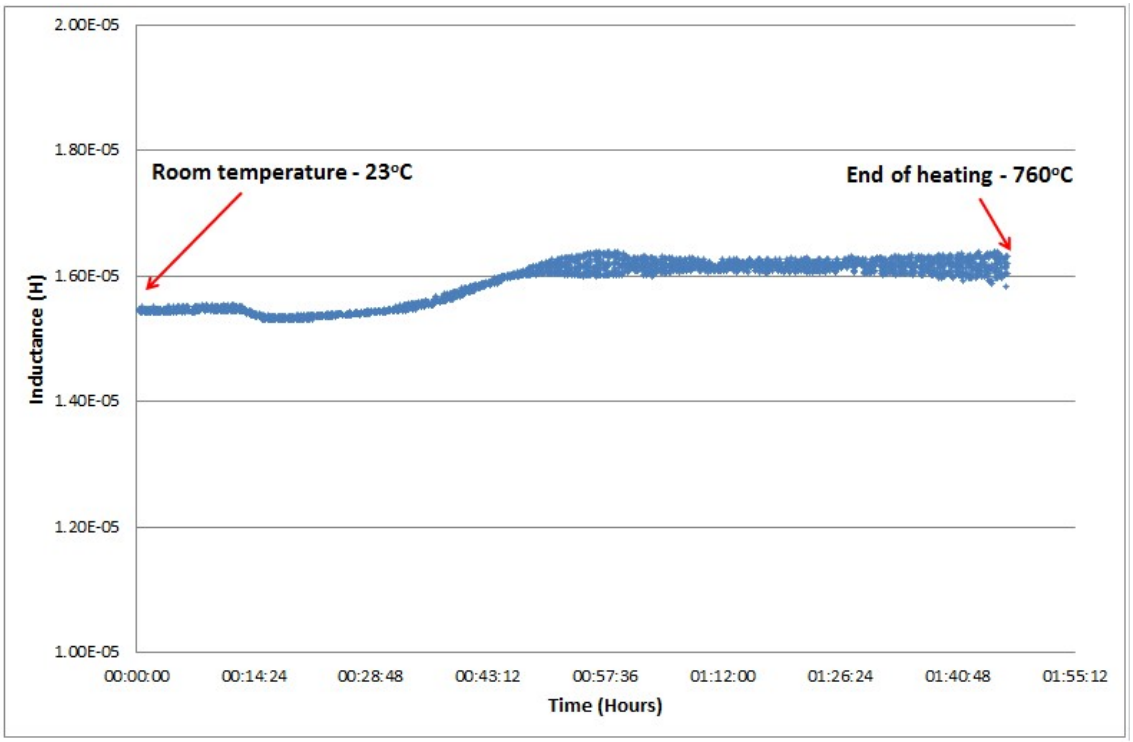

Figure 75: Inductance measured for empty high temperature in-situ sensor during heating from room temperature to 760°C

Figure 76 compares the measured inductance during heating for the empty high temperature EM sensor and a typical inductance measurement recorded for an as-received IF steel sample annealed at 650ºC for 4 hours, where the signal change due to heating of the sample and due to recovery and recrystallisation is shown (discussion on these changes is given later in section 8.6). The lowest inductance value recorded during annealing of the IF steel sample was 4.46 x 10^{-5} H and the highest value recorded was 8.23 x 10^{-5} H, the difference between highest and lowest values being 3.80 x 10^{-5} H. The maximum noise recorded during heating of the empty high temperature EM sensor (difference between highest and lowest values) was 1.1 x 10^{-6} H, 2.8% of the difference between the highest and lowest values of inductance values recorded during in-situ annealing for the IF steel annealed at 650ºC. As the effect of temperature on sensor heating was very small compared to the effects of temperature on inductance of IF samples it was judged to be insignificant in terms of its effects on the in-situ measurement of recovery and recrystallisation and that there was no need to correct measured inductance data recorded during in-situ tests for effects of temperature on the sensor.

The noise and small signal change observed for the empty high temperature sensor heating is thought to have been caused by the effect of the resistance heating process within the furnace on the sensor. The furnaces use a resistance heating method to generate heat [153], this in turn generates an electromagnetic field around the heating elements within the furnace which may have an effect on the magnetic field generated/received by the sensor. Magnetic fields generated by equipment around any magnetic sensor are a concern as they can affect the quality of the data collected. Continuous Annealing Lines (CALs) have many sources of electromagnetic fields, these include electrical motor units used to drive the rollers which move the strip and furnace heating elements. Any sensor deployed onto a CAL must take sources of electromagnetic noise into consideration using either sensor shielding or appropriate sensor placement. Another source of signal variation with heating may be small dimensional changes caused by sensor heating, different parts of the sensor will expand and contract at different rates as the sensor both heats up and cools down. The effect will be slight variations in the strength of the magnetic fields generated and received by the sensor. The changes will be minimal and very difficult to measure while the sensor is at high temperatures.

The expansion and contraction of the sensor with increasing temperature may also change the tension within the wires used to form the coils in the sensor, any change will be very small but could cause further slight changes to the magnetic fields that are generated and received. Any sensor that is deployed into a CAL would need to consider thermal expansion effects on the senor windings. Mechanically this effect may cause fatigue in the sensor windings causing a sensor failure as well as causing electromagnetic variation in measured signal.

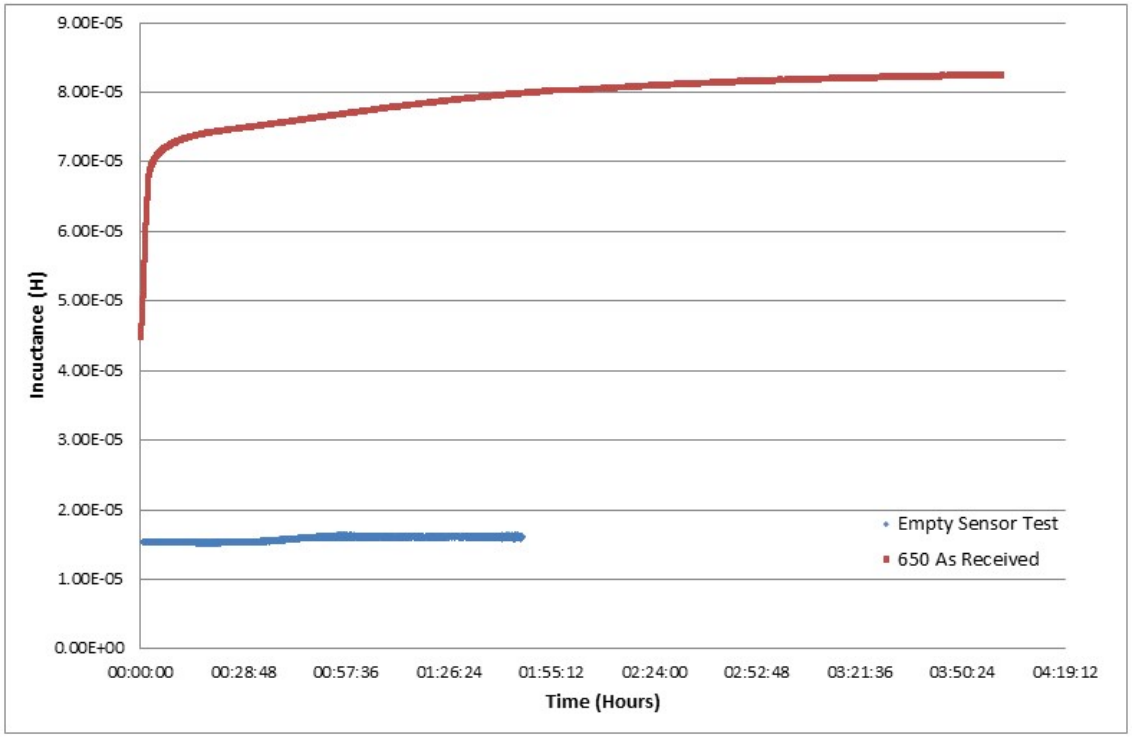

Figure 76: Inductance values recorded for empty high temperature EM sensor and for in-situ measurement completed during annealing of IS steel sample at 650°C.

8.5. In-Situ Inductance Change with Temperature

An IF steel sample which had already been annealed at 700°C for 3 hours and was fully recrystallised was used to investigate how much the inductance changed due to the increase in temperature of the material. An already annealed sample was used to ensure that recovery and recrystallisation would not affect the results of any inductance change recorded. The EM sensors used in this work generate very weak electromagnetic fields (calculated to be 45 A/m by 2D asymmetric COMSOL finite element multiphysics model using exact sensor geometry and experimental setup, completed by Dr L. Zhou [154]), the inductance / temperature response trend recorded was expected to be similar to the low field permeability / temperature trend shown in Figure 19 (and reproduced as an inset in Figure 77). It should be noted that the high temperature sensor used for high temperature measurements was air cored unlike the U shape sensors used for the interrupted recovery and recrystallisation measurements shown in section 8.3, and so there is no effect of the Curie temperature for a sensor core.

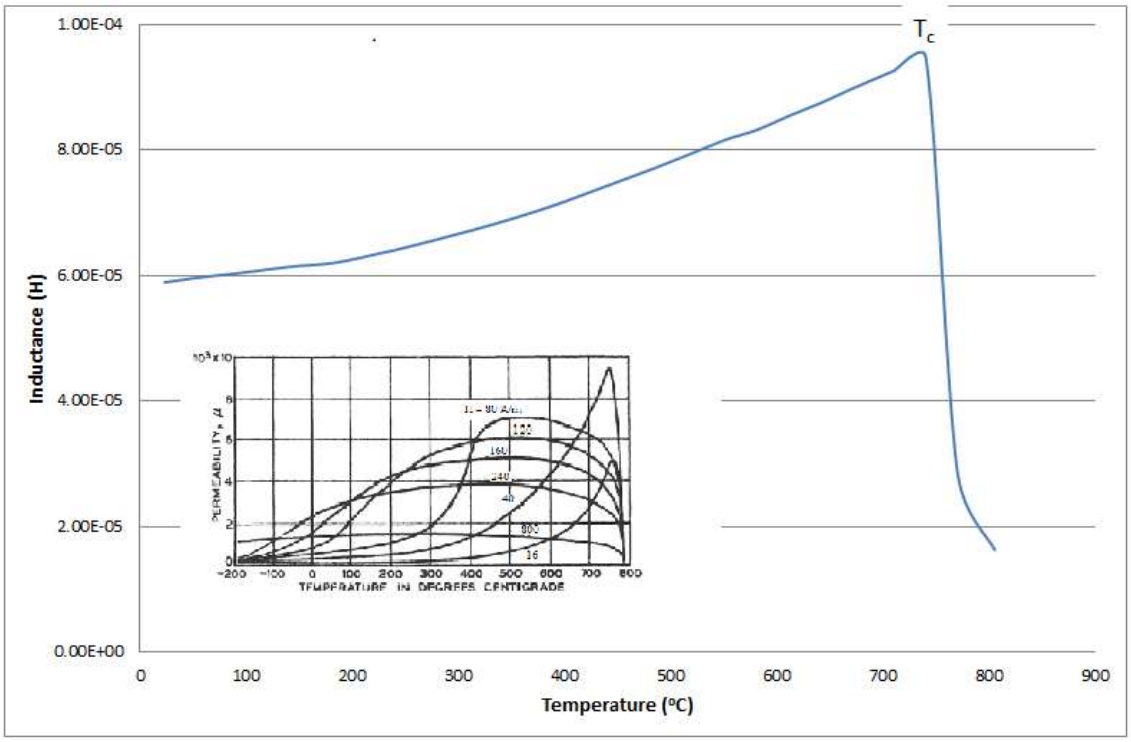

Figure 77: Measured inductance change with increasing temperature for annealed IF steel, inset chart shows permeability change with increasing temperature for iron [27]. T_c marks the Curie point for IF steel. Measurements recorded at 100 Hz.

Figure 77 shows the measured change in inductance against temperature for annealed IF steel measured at 100 Hz, the heating rate was 6.5°C min^{-1}. The inductance / temperature trend shown is similar to the permeability / temperature curve for iron at low fields (16 and 40 A/m). The low frequency inductance, which is related to permeability, increases with temperature until it reaches T_c, after which there is a sudden drop in inductance caused by a change in the magnetic behaviour of the material from ferromagnetic to paramagnetic [27]. The inductance measurements may include some effects of resistivity on the measured inductance values, it is known that the effects of resistivity on inductance increase with temperature [155, 156].

T_c for IF steel measured using the EM sensor is approximately 740°C and for iron T_c is estimated to be 770°C [27]. IF steel possesses small amounts of alloying elements which will reduce T_c, literature reports that T_c for ferromagnetic materials changes depending upon the chemical composition of the material [27]; ferritic stainless steels have been reported to have T_c which varies from 670°C to 750°C depending on composition with the more highly alloyed steels having Curie points lower than less alloyed steels [54, 157]. Establishing true T_c is difficult as the change between the ferromagnetic and paramagnetic state is not perfectly sharp (this is evident in the rounded peaks shown in Figure 19 and Figure 77). Measuring T_c values also varies depending on the applied field strength, Figure 19 shows that for iron at the lowest field strengths (16 and 40 A/m) the Curie point behaviour is observed at a lower temperature (760°C) when the 40 A/m field is used compared to the 16 A/m applied field (770°C) [27]. The high temperature cylindrical EM sensor has a field strength of approximately 45 A/m, the effect of this would be measure a slightly lower T_c than with a 16 or 40 A/m field.

An already annealed 430 grade ferritic stainless steel sample (430SS) was also tested to establish the reliability of the test and to establish that the sensor recorded different behaviours for ferromagnetic steels of different compositions. Figure 78 shows two different responses, one for annealed IF steel and one for annealed 430SS. From the graph different room temperature inductance values are observed, 5.9×10^{-5} H for the IF steel and 4.6×10^{-5} H for the 430SS. Lower inductance values at all temperatures are expected for the stainless steel as it has a lower μ_r than the IF steel as it has a higher content of non-magnetic alloying elements [27] (reference section 6 for chemical compositions).

T_c for the 430SS sample tested, 660°C, is similar to the T_c for the 430FMo stainless steel produced by the Lucefin Group (671°C) [158]. The composition for the 430FMo stainless steel is shown in Table 10.

Table 10: Chemical composition for 430FMo stainless steel [129]

Element	C	Si	Mn	P	S	Cr	Ni	Mo
% by weight	0.08	0.3	0.4	0.04	0.2	16.0	1	1.1

Table 10 shows that there are differences between the chemical compositions of the 430SS grade and the 430FMo stainless steel grades. They share a similar Cr content (16 %wt) but the 430FMo has a higher C content (0.08 %wt compared to 0.035 %wt for 430SS), a higher S content (0.2 %wt compared to 0.001 %wt for 430SS) and a higher Ni content (1.0 %wt compared to 0.18 %wt for 430SS), with all other elements being similar. As the Cr content is similar between the two grades (Cr being the primary alloying element) it is reasonable to assume that they should share similar T_c values.

The closeness of the T_c values for the ferritic stainless steel samples gives confidence that the high temperature EM sensor is responding correctly to permeability changes caused by temperature. The inductance values of the stainless steel approach those of the IF steel at the highest temperatures but do not match them. This is because inductance change with temperature is not linearly proportional to permeability change with temperature, inductance is also affected by the effects of both permeability increase with temperature and also resistivity increase with temperature [159].

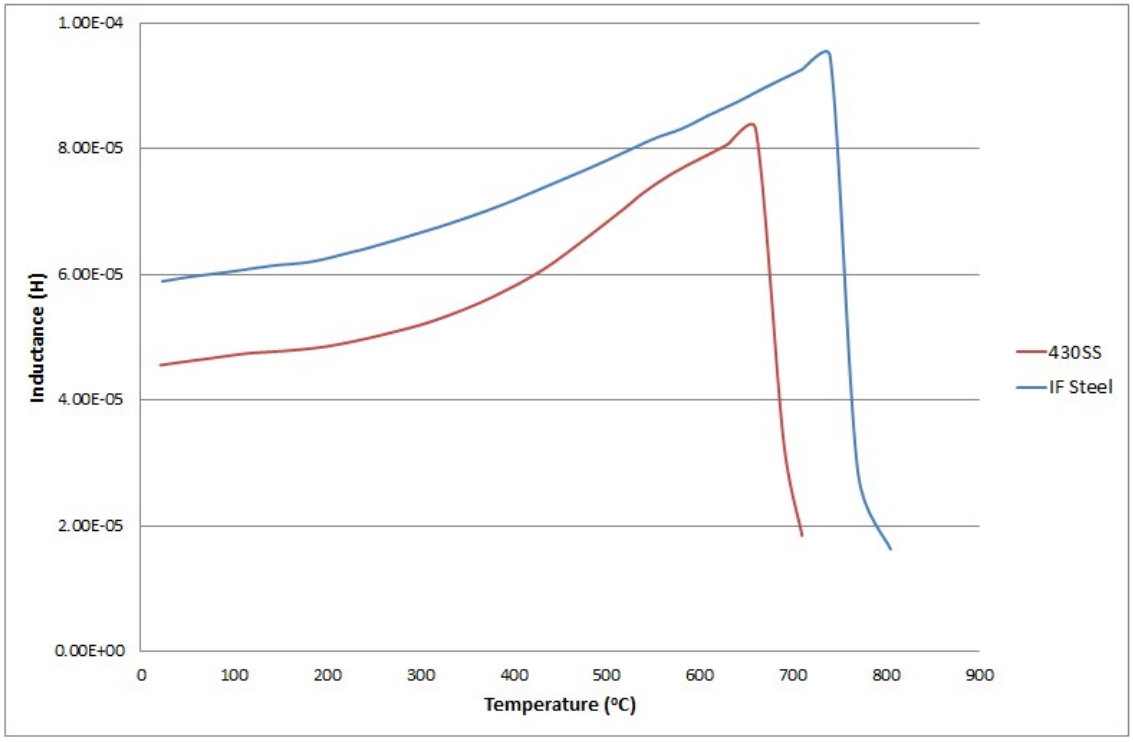

Figure 78: Inductance change with increasing temperature for IF and 430SS. Measurements recorded at 100 Hz.

Figure 79 shows optical micrographs taken before and after the inductance measurements for both the IF and stainless steel. The micrographs were taken to observe if there had been any change in microstructure during the in-situ inductance change with temperature experiments. The micrographs do not show any major changes in microstructure from before and after the inductance change with temperature experiments. Average grain diameters for the IF sample before the in-situ inductance heating experiment was 25.7µm and 24.7µm after the experiment (standard error of 2.2µm), revealing no significant change in grain diameter. The average grain diameter for the 430SS sample before the in-situ inductance change with temperature experiments was 8.3µm and 9.0µm after the experiment, revealing no significant change in grain diameter. Hardness data was also recorded for the IF and 430SS samples. For the IF steel the hardness before the in-situ inductance change with temperature experiment was HV 84 and after the experiment was HV 86 (standard error for hardness values is HV 4), showing no significant difference between the hardness before and after the experiment. For the 430SS samples the hardness values before and after the in-situ inductance change with temperature experiment were

HV 212 and HV 210 respectively, showing no significant change in hardness that would indicate a microstructural change caused by the experimental heating process.

The results from the in-situ inductance change with temperature experiments show that EM sensors are sensitive to changes in inductance caused by temperature change. This is important for the research presented in this thesis as sample heating occurs at the beginning of in-situ experiments to monitor recovery and recrystallisation for IF steel. An EM sensor deployed in a CAL would need to have its inductance output corrected for any temperature changes that occurred in the furnaces. It is likely that a series of sensors would need to be deployed at different points in a CAL, taking readings from before, during and after the annealing process. The steel being analysed by the sensors will be at different temperatures. Sensor outputs would need to be corrected to ensure that the output measured reflected microstructural changes in the steel and not temperature difference. This could be done using correction factors based upon induction changes for increasing temperature for different steel grades. Pyrometers are already present in CALs (used for temperature monitoring and to provide data for existing models), the same or similar pyrometers could be used to measure the temperature of the strip as it passed the EM sensors.

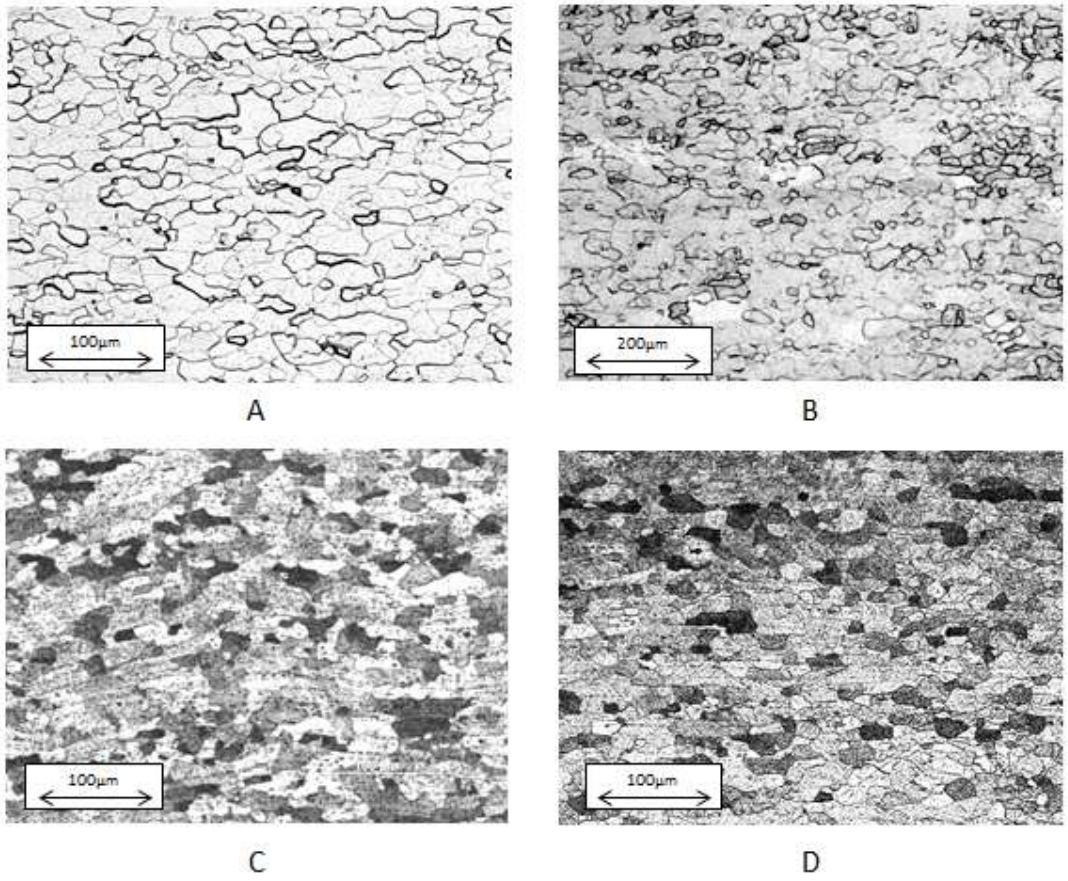

Figure 79: Optical micrographs taken before and after inductance change for increasing temperature experiments. Rolling direction is left to right. (A) IF steel annealed at 700°C for 160 minutes; (B) IF steel after inductance / temperature experiment; (C) recrystallised 430SS steel in as-received condition; (D) 430SS after inductance / temperature experiment.

8.6. In-Situ Measurement of Recovery and Recrystallisation

As-received condition IF steel samples were annealed at different temperatures and times, during the annealing process inductance changes were measured using a high temperature cylindrical EM sensor which was taking readings at 100Hz. Readings were taken every 2 seconds for the length of the experiments. All temperatures referred to in this section are sensor temperatures and not sample temperatures, a description of this can be seen in section 7.7.4.

Figure 80 shows in-situ inductance measurements for a single sample, annealed at 700°C for four hours, in two different conditions. The blue line shows the inductance recorded for the sample when it was annealed from the as received (cold rolled) condition and the red line shows the inductance values recorded for the sample in the already annealed condition (the sample was taken out of the sensor after the first test, cooled and then put back into the sensor to repeat the experiment when it was annealed). In both cases the inductance measurements began with the sample at room temperature being inserted into the EM sensor which was at furnace temperature. The data shows different initial inductance values, which is expected as the microstructures at the start of each annealing sequence are different, heavily deformed in the as received condition and fully recrystallised in the annealed condition (confirmed by optical microscopy).

As explained in section 4.4.1 and shown in section 8.5, permeability and hence inductance increases with temperature, therefore inductance measurements shown in Figure 80 are affected by increases in temperature up until the point in time where the sample reaches the stable furnace temperature. Sample heating trials, using thermocouples attached to a sample and the sample being placed into the sensor already at temperature, showed the IF samples reached furnace temperature after approximately two minutes. The inductance increase rate during sample heating is different for the as received and annealed tests; this is due to different starting microstructures. Recovery is initiated during sample heating for the heavily deformed as received microstructure, whereas during the annealed test the microstructure is already recrystallised and the inductance increase is only affected by permeability change due to increasing temperature and resistivity.

Once sample heating is complete the as received and annealed tests show different trends, the measured inductance of the as received test reaches a stable value at around 10 minutes and there is a significant increase in inductance after sample heating up until the 10 minute point of 7.5 x 10^{-5} H to 8.7 x 10^{-5} H. The annealed sample shows no significant increase in inductance with time after sample heating suggesting that no major changes in microstructure are taking place. There is a small increase, 8.5 x 10^{-5} H to 8.7 x 10^{-5} H, which will be discussed later.

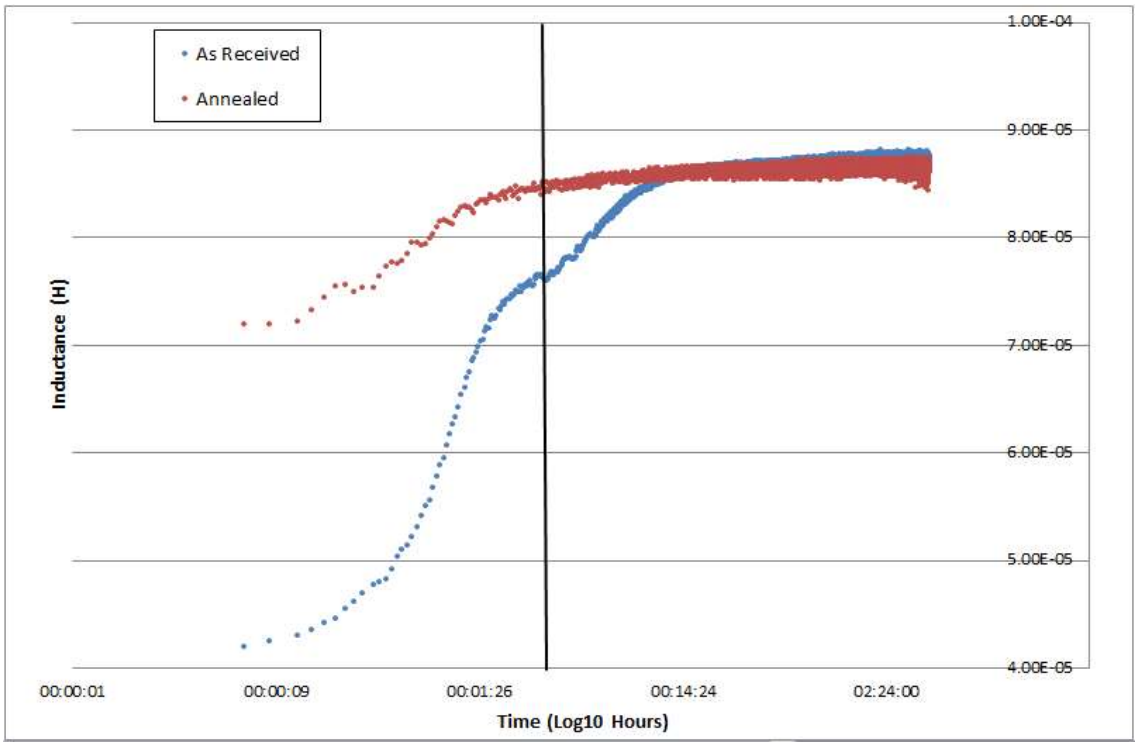

Figure 80: Annealed and as received sample in-situ inductance measurements recorded at 700ºC, time taken for the sample to reach furnace temperature is shown by a vertical line at 2 minutes.

Figure 81 shows in-situ inductance measurements for an as received IF sample and a second inductance measurement for a sample annealed at 420°C. The end of the sample heating is marked by a vertical line at 2 minutes. Annealing at 420ºC was expected to cause recovery only as it has been reported that recrystallisation is not expected at annealing temperatures of less than 500ºC for IF steels [151]. The initial inductance value for the as received sample is less than that of the annealed sample, consistent behaviour with the in-situ experiment conducted at 700ºC, and expected as recovery should have taken place during the first heat treatment sequence at 420ºC.

After the sample heating period the inductance change for the sample initially in the as received condition shows a continuous increase until the end of the annealing time. The inductance for the sample when annealed for the second time at 420°C shows no significant increase in inductance after the sample heating period, this is consistent with recovery having taken place and no further microstructural changes occurring. The rates of change for inductance against time until the end of the sample heating period are different for the as received and annealed conditions, which is accounted for by recovery taking during heating for the as received sample and less or no recovery taking place during heating when the sample is in the annealed condition.

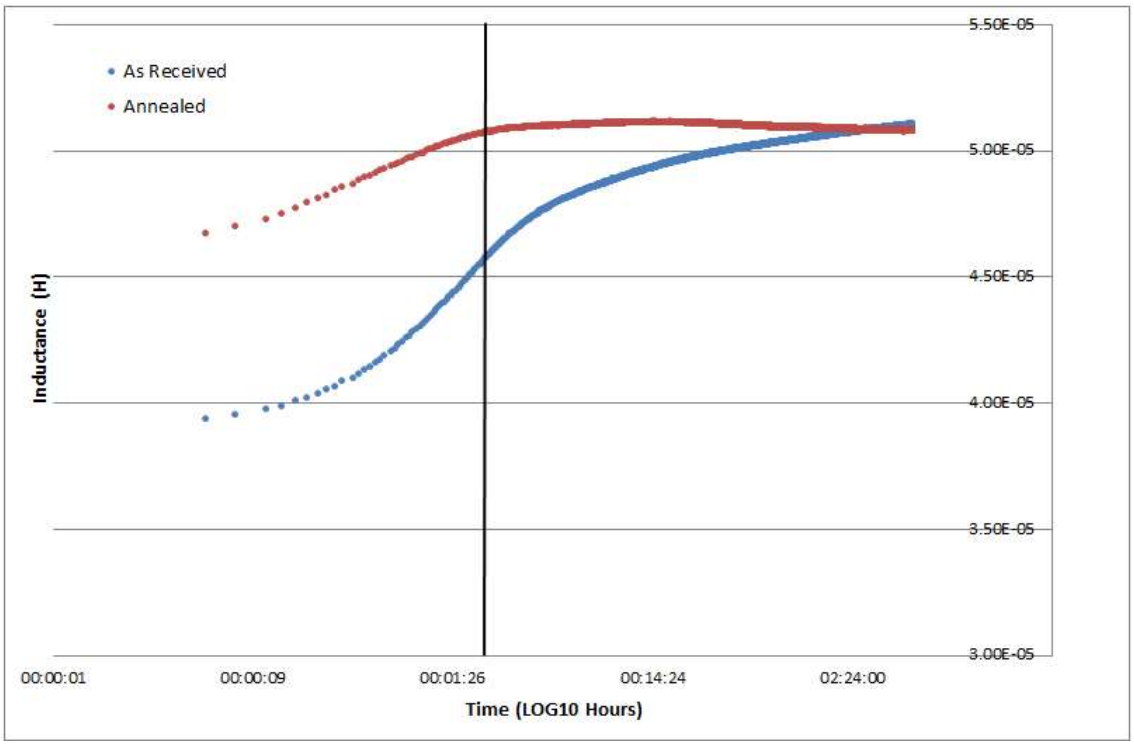

Figure 81: Annealed and as received sample in-situ inductance measurements recorded at 420°C, time taken for the sample to reach furnace temperature is shown by a vertical line at 2 minutes.

In-situ experiments were conducted at four different temperatures of 365°C, 420°C, 650°C and 700°C. The lower temperature in-situ experiments (365°C and 420°C) were to investigate recovery only and the higher temperature in-situ experiments (650°C and 700°C) were to investigate changes in inductance caused by both recovery and recrystallisation. Figure 82 shows the measured inductance data from in-situ trials at 365°C, 420°C, 650°C and 700°C.

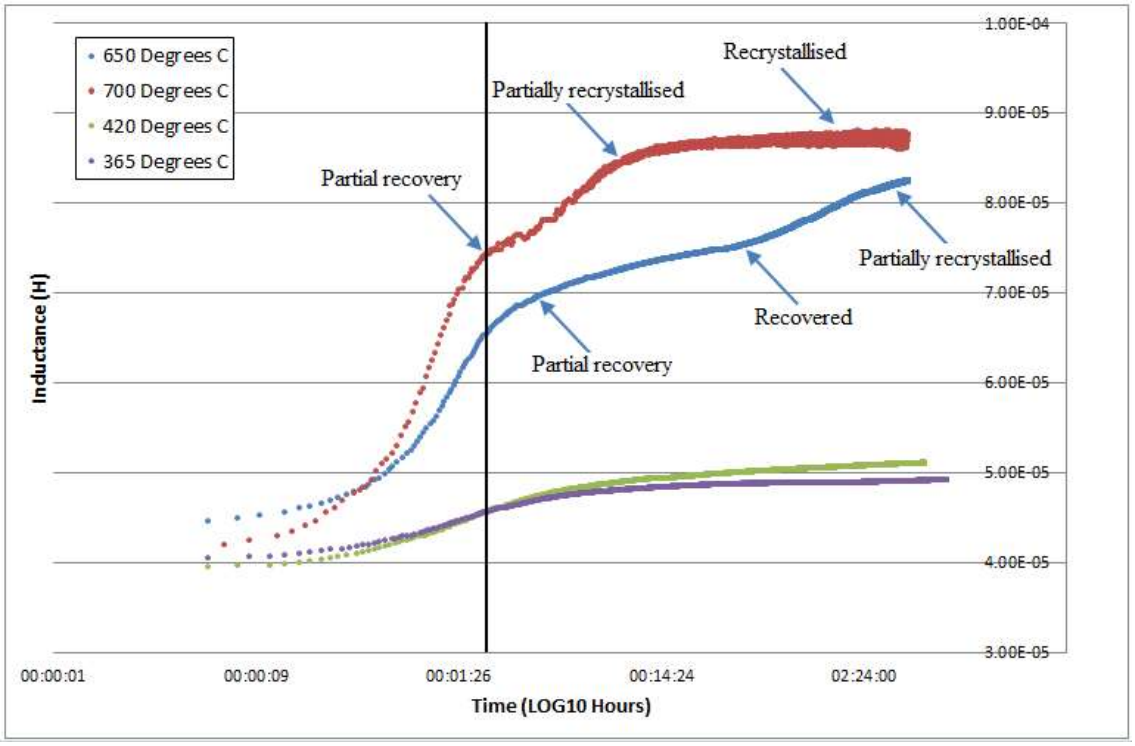

Figure 82: In-situ inductance measurement data for 365°C, 420°C, 650°C and 700°C. End of sample heating period is marked by a vertical line at 2 minutes. Arrows on the chart mark points of key gradient change where different aspects of recovery and recrystallisation are considered to have occurred.

Different rates of change of inductance with time are observed in Figure 82, the two higher temperatures (650°C and 700°C) showing similar trends to each other and different trends to the lower temperature tests (420°C and 365°C). Micrographs taken from the lower temperature in-situ measurements (Figure 83) show no obvious signs of recrystallisation and hardness values for the samples annealed at 420°C and 365°C reveal only small decreases in hardness, 192 HV for 420°C and 191 for 365°C. The as received condition hardness value is 200 HV. Small decreases in hardness are consistent with recovery but not recrystallisation [91, 160]. The observed increase in inductance value with recovery is consistent with reported changes in magnetic measurements (magnetic coercivity and permeability) for samples that have undergone recovery when measured at room temperature [37, 161], they are also consistent with the increases in inductance measured during the interrupted recrystallisation measurements completed using the U-type EM sensor (section 8.3).

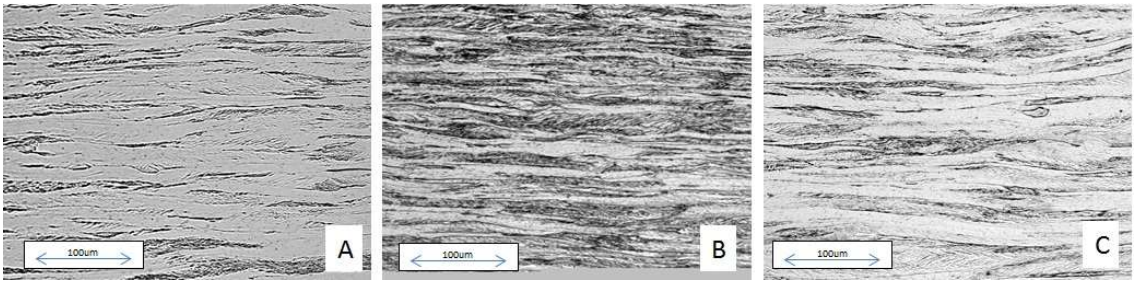

Figure 83: Optical micrographs taken from in-situ recovery experiments. (A) as received condition; (B) 365°C after 360 minutes and (C) 420°C after 300 minutes. At the end of each annealing sequence the samples were water quenched. Rolling direction is left to right across the page.

The higher temperature (650°C and 700°C) in-situ experiments show different trends of inductance against time compared to the lower temperature in-situ experiments (365°C and 420°C). There are several changes in inductance against time gradients for the temperature measurements, whereas the lower temperatures show more shallow and constant changes in inductance with time.

It was considered that the changes in slope shown for the responses at higher temperatures may be similar to those observed in Avrami recrystallisation curves during isothermal heating [129], where gradient changes in recrystallisation fraction against time can be used to mark different points of the recrystallisation process and the gradient of the curve is related to the rate of recrystallisation. Figure 84 shows example Avrami recrystallisation curves produced for cold deformed 304 stainless steel during annealing at different isothermal temperatures (950°C, 1050°C and 1150°C) [56], initial gradient changes are observed at initiation of recrystallisation and a second change of gradient is observed at the end of the recrystallisation process as grain impingement occurs and recrystallisation ends. The overall gradient of the curves is steeper at higher temperatures as recrystallisation occurs at a faster rate.

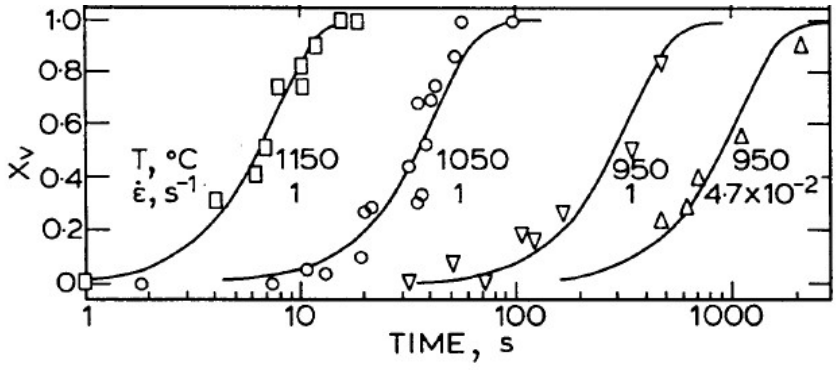

Figure 84: Example Avrami curves showing different trends for recrystallisation at different temperatures (950°C, 1050°C and 1150°C) and two strain rates at 950°C for 304 stainless steel (recrystallisation fraction (X_V) is shown on the y axis) [56].

In order to establish whether the measured inductance curves shown for the higher temperatures in Figure 82 fit the same behaviour as that seen in Avrami recrystallisation curves interrupted in-situ experiments were completed at key time points identified from the gradient changes (highlighted by arrows in Figure 82). Samples were heat treated for 3 minutes, 40 minutes and 240 minutes at 650°C and for 2 minutes, 10 minutes and 150 minutes at 700°C.

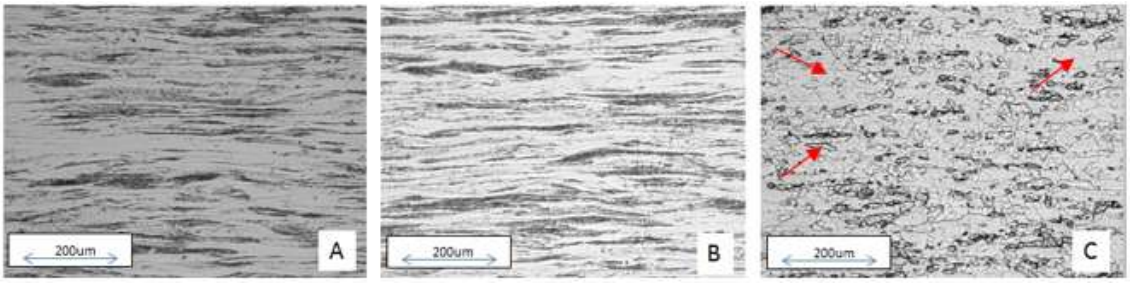

Figure 85: Optical micrographs for 650°C interrupted in-situ tests. A: 3 minutes, B: 40 minutes and C: 240 minutes. The sample heat treated for 240 minutes shows some areas where the grains are still elongated, indicating that recrystallisation is not fully complete (marked with arrows).

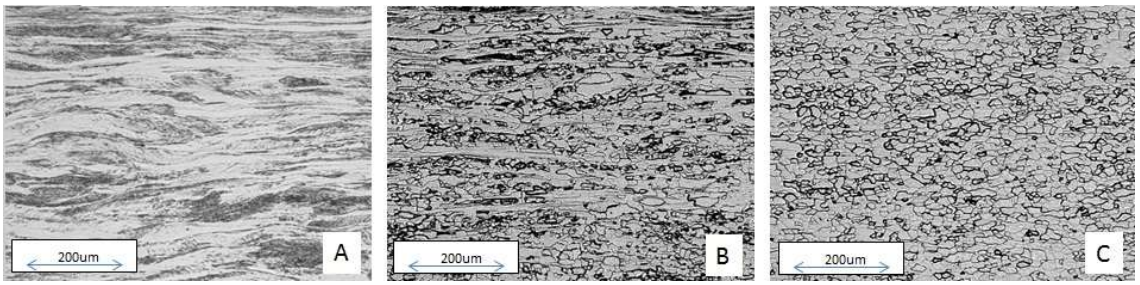

Figure 86: Optical micrographs for 700°C interrupted in-situ tests. A: 2 minutes, B: 10 minutes and C: 150 minutes.

Figure 85 and Figure 86 show the optical micrographs taken at the different time points identified for the 650°C and 700°C interrupted in-situ tests. During annealing at 650°C there is very little difference in observed microstructure between the 3 minute and 40 minute samples, both samples still showing the heavily deformed microstructure seen in the as-received condition. The optical micrograph taken for the sample heat treated at 650°C for 240 minutes shows significant recrystallisation, with little evidence of deformed grains still present. The optical micrographs taken for the interrupted tests at 700°C annealing temperature shows a heavily deformed microstructure at 2 minutes, significant recrystallisation at 10 minutes and complete recrystallisation at 150 minutes.

Table 11 shows inductance values measured at room temperature after heat treatments at 650°C and 700°C, in-situ inductance measurements taken from continuous in-situ experiments and corresponding hardness values. Initial values for inductance at the start of the in-situ experiments are not included as they cannot be compared with each other due to the inductance readings starting at slightly different times (related to the time taken to insert the sample into the sensor in the furnace) and sample heating affecting the initial inductance value.

Table 11: Inductance and hardness data for interrupted in-situ tests performed at 650°C and 700°C

Temperature	**650°C**			
Time (minutes)	0	3	40	240
Microstructure	As-rolled	Partial recovery	Recovered	Partially recrystallised
Room temperature Inductance (H)	3.8×10^{-5}	4.7×10^{-5}	4.9×10^{-5}	5.2×10^{-5}
In-situ inductance value (H)	-	6.9×10^{-5}	7.6×10^{-5}	8.3×10^{-5}
Hardness (HV5)*	200	181	168	84

Temperature	**700°C**			
Time (minutes)	0	2	10	150
Microstructure	As-rolled	Partial recovery	Partially recrystallised	Recrystallised
Room temperature Inductance value (H)	3.8×10^{-5}	4.7×10^{-5}	5.5×10^{-5}	5.8×10^{-5}
In-situ inductance value (H)	-	7.4×10^{-5}	8.5×10^{-5}	8.7×10^{-5}
Hardness (HV5)*	200	181	90	82

*Repeatability error for hardness is +/- HV 2.4.

After heat treatments of 2 minutes at 700°C and 3 minutes at 650°C the hardness values are the same (HV 181), giving a small drop in hardness from the as-rolled hardness value of 200. Small drops in hardness combined with no obvious change in observed microstructure is indicative of recovery only having taken place [160]. After heat treatment for 10 minutes at 700°C sample hardness has decreased by 110 to a value of 90, the corresponding micrograph shows a partially recrystallised microstructure with some evidence of deformed grains and equiaxed grains present. After 40 minutes of annealing at 650°C the hardness value is 168 and the corresponding micrograph exhibits no obvious signs of recrystallisation, indicating that recrystallisation had not yet started and that recovery is still taking place. After 240 minutes at 650°C and 150 minutes at 700°C the hardness values have dropped to 84 and 82 respectively, the low hardness values and corresponding observed microstructures indicating that recrystallisation has taken place at both temperatures.

The largest changes in inductance take place during recovery, the changes in inductance at room temperature being 1.1 x 10^{-5} H after 40 minutes of annealing at 650°C and 0.9 x 10^{-5} H after 10 minutes of annealing at 700°C. Changes in inductance during recrystallisation are comparatively smaller, 0.3 x 10-5 H for 650°C heat treatment (40 minutes to 240 minutes) and 0.3 x 10^{-5} H for 700°C (10 minutes to 150 minutes). The in-situ inductance changes for the same time periods are 0.7 x 10^{-5} H at 650°C and 0.2 x 10^{-5} H at 700°C.

Final inductance values, after the longest time periods (240 minutes at 650°C and 150 minutes at 700°C) are the largest for both the in-situ and room temperature measurements. The in-situ inductance measurements are higher than the room temperature inductance measurements; this is due to the measurements being taken at high temperatures. The in-situ inductance value taken after 150 minutes at 700°C (8.7 x 10^{-5} H) is higher than the reading taken after 240 minutes at 650°C (8.3 x 10^{-5} H), the higher value at the end of the 700°C experiment is consistent with a higher permeability caused by the reading being taken at a higher temperature. These are comparable with the data recorded in the inductance change with temperature experiments (Figure 78) where an inductance value of 9.0 x 10^{-5} H was recorded at 700°C and an inductance value of 8.6 x 10^{-5} H was recorded at 650°C. The difference in inductance reading between the experiments at 650°C and 700°C is 0.3 x 10^{-5} H. The difference between the readings may be due to differences in sample size, the samples were not exactly the same size, and position within the sensor as it was easier to place samples into a cold sensor than it was to place the samples into a hot sensor for the in-situ inductance change with recrystallisation experiments.

The room temperature inductance readings are 5.2 x 10^{-5} H after a heat treatment of 240 minutes at 650°C and 5.8 x 10^{-5} H after 150 minutes at 700°C, the readings were taken at the same temperature, the difference in inductance values between the two readings is due to a combination of grain size difference, differing degrees of recrystallisation and some small differences in sample size. The average grain diameter for the sample annealed at 650°C for 240 minutes is 11 μm and the average grain diameter for the sample annealed at 700°C for 150 minutes is 14 μm (standard deviation for grain diameter measurements is 1.3 μm).

It is known that measured inductance increases with grain size [138] however the grain size difference alone is not enough to explain the differences in inductance values. It is also possible that there are some small areas within the 650°C sample where recrystallisation is not fully complete, the micrograph for the sample heat treated at 650°C for 240 minutes (Figure 85) shows some areas where the grains still appear to be elongated (example areas identified in Figure 85 by arrows) with the rolling direction and not fully equiaxed like the microstructure for the sample annealed for 150 minutes at 700°C (Figure 86). The hardness values are only slightly different at the end of both heat treatment processes, the sample heat treated at 650°C for 240 minutes has a hardness value of HV 84 and the sample heat treated at 700°C for 150 minutes has a hardness value of HV 82. The repeatability error (standard deviation) for the hardness measurements is HV 3.5. The rate of change of hardness decreases as full recrystallisation is approached, as the sample heat treated at 650°C is almost fully recrystallised so it is not unreasonable that the hardness values are similar [1].

After 2 minutes at 650°C and 3 minutes at 700°C both samples show a drop in hardness from 200 HV to 181 HV, with corresponding increases in inductance at room temperature of 0.9×10^{-5} H. Room temperature inductance differences for the interrupted measurements from 3 minutes to 240 minutes at 650°C and from 2 minutes to 150 minutes at 700°C are 0.7×10^{-5} H is 1.0×10^{-5} H respectively. The inductance differences for the in-situ high temperature measurements, with samples stabilised at furnace temperature, for the same time periods are 1.4×10^{-5} H for 650°C and 1.3×10^{-5} H for 700°C, showing that the inductance responses recorded during in-situ measurements are more sensitive to recrystallisation than inductance responses caused by recrystallisation recorded at room temperature. The difference in the readings is caused by the increased permeability at high temperatures, the material responds to applied fields more easily and therefore changes in microstructure will have a greater effect on measured permeability, and therefore inductance values. This sensitivity would be particularly appropriate for sensors operating in a continuous annealing line where both sensor and steel strip are at high temperature.

8.7. EM Sensor Response to Stress and Strain

Changes in stress and strain have effects on the electromagnetic properties of ferromagnetic materials [27, 46, 60, 145]. Strip moving through a continuous annealing line between pulleys is under tension, not in an equilibrium strain condition and the amounts of strain applied to a strip varies throughout an annealing line. Strip tension is a factor that can affect the quality of the end product [162] and must be monitored to ensure the annealing line is operating in a stable and controlled manner [64]. Tensile forces applied in CALs are reported to be around 1750N to 2000N (10 to 12 MPa for the reported cross sectional area) with fluctuations in line tension of up to 350N (2 MPa) [26].

Measured inductance changes as a result of changes in material microstructure, temperature and stress. It has already been established that both changes in temperature and microstructure have significant effects on measured inductance, therefore experiments were completed to establish whether an EM sensor could monitor response to the effects of changes in tensile stress and if so what the comparative significance of the change in inductance was when compared to the changes caused by microstructure and temperature changes. Experimental procedures are outlined in section 7.7.7.

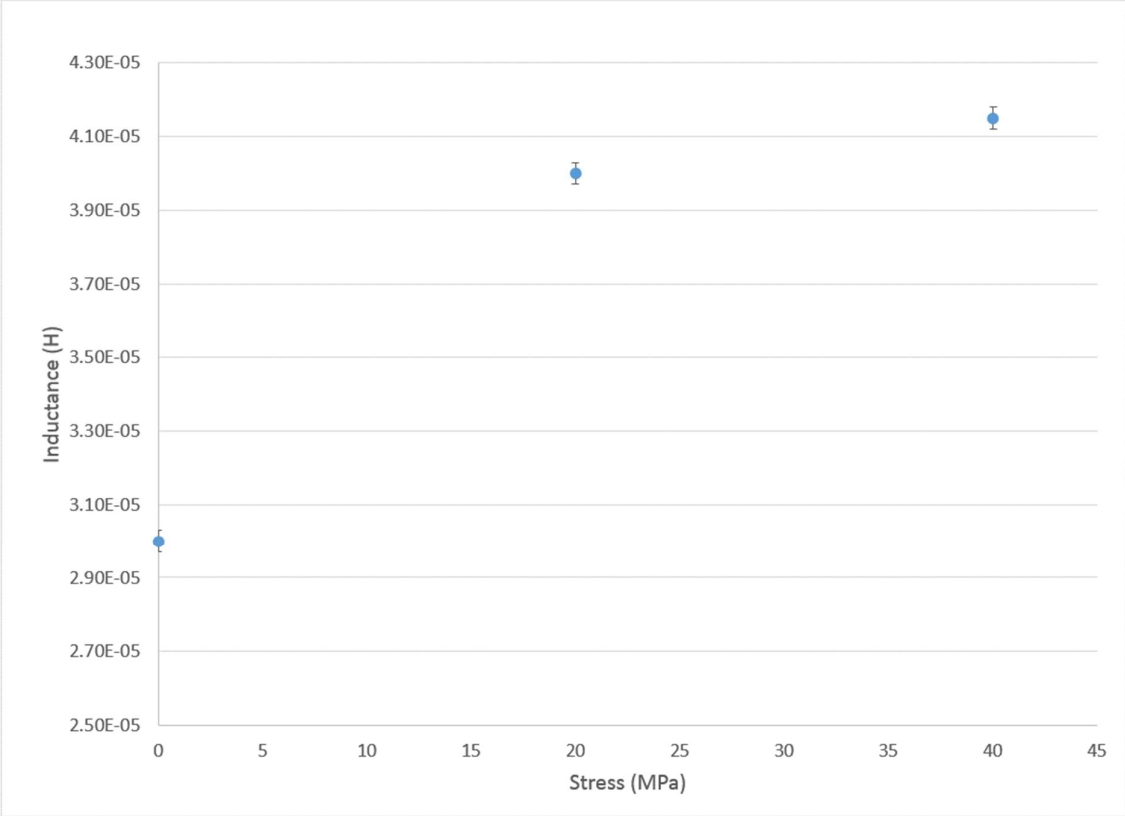

Figure 87: Inductance against stress for tensile stresses of 0, 20 and 40 MPa, recorded for an as received IF steel sample. Measurements were recorded at 10Hz.

Figure 87 shows inductance measurements recorded using an as received IF steel sample with increasing tensile stress levels applied, from unloaded to a stress of 40 MPa. The purpose of the experiment was to establish that an EM sensor aligned with the applied stress was responsive to changes in applied stress. The stresses in Figure 87 are significantly larger than those measured for a strip passing through a CAL, which vary from 10 MPa to 12 MPa [26], information received from the Tata Steel CAL at Port Talbot reports strip tensions of 3.5 MPa to 8 MPa [163]. Each line in Figure 87 represents an average taken from three measurements at the defined stress level, the same sample was used for each measurement. The measurements were completed using a U-shaped EM sensor. The measurements show that measured inductance increases with applied tensile stress. At the lowest measured frequency, 10 Hz, the measured inductance is 3.7 x 10^{-5} H when unloaded (0 MPa), 4.0 x 10^{-5} H with an applied stress of 20 MPa and 4.15 x 10-5 H with an applied stress of 40 MPa. The data is consistent with an expected increase in permeability and therefore inductance, for measurements where

the applied stress is aligned with the applied magnetic field [27, 46]. The difference in the measured inductance from 0 MPa to 20 MPa is 0.3 x 10^{-5} H and from 20 MPa to 40 MPa is 0.15 x 10^{-5} H. The different relative increases in inductance for the same applied stress level (20 MPa) may be associated with experimental error at low loads, as tensile force is applied to the sample the distance to the EM sensor (which was held still in a retort stand) changes slightly, decreasing the lift off between the sample and the sensor. It is known that decreasing lift off will increase the measured inductance (shown by experiment in section 8.1) [145]. The data shows that the EM sensor is sensitive to small changes in tensile stress.

The total measured inductance recorded is 0.45 x 10^{-5} H when a 40 MPa stress is applied. This equates to a change of 0.011 x 10^{-5} H for 1 MPa (assuming a linear relationship, consistent with literature data for elastic stresses in iron [27]). The total change in measured inductance for recovery and recrystallisation was 2 x 10^{-5} H (interrupted measurements at room temperature, Table 11). Reported stress values in CALs can be as high as 12 MPa [26, 163] which equates to an inductance change of 0.13 x 10^{-5} H, 6% of the inductance change recorded during the interrupted in-situ measurements. Direct comparison of the inductance changes between the interrupted in-situ measurements at room temperature and those carried out for stress and strain is difficult as different sensors (due to sensor damage new sensors had to be constructed during the research programme) and sample sizes were used. However the data does show that there is a change in inductance caused by applied stress and that the change is indicated to be smaller, for the stresses seen in the CAL, than that caused by recovery and recrystallisation. However, the inductance change caused by line tension in a CAL will affect the signal and should not be ignored for an EM sensor deployed into a CAL, although if a constant line tension is used this will manifest itself in an offset in the base line inductance value which can be accounted for.

8.8. Summary Discussion

Interrupted and in-situ measurements both show increases in inductance for recovery and recrystallisation. Interrupted tests show smaller increases in inductance for recrystallisation compared to relatively large increases for recovery. Temperature also causes an increase in measured inductance; for example an increase of 3.6×10^{-5} H for a temperature increase of 745°C from room temperature (Figure 77) for measurements recorded using a high temperature cylindrical EM sensor using an annealed IF steel sample, equivalent to a 37% change in total measured inductance compared to the initial value (annealed IF steel sample) for that sensor and temperature increase. Changes in measured inductance recorded using the high temperature cylindrical EM sensor at room temperature for samples that have been heat treated from an initial cold worked condition to a fully recrystallised state show a change in inductance of 2.0×10^{-5} H (Table 11), equivalent to a 35% change in measured inductance due to recovery and recrystallisation, compared to the initial value (as-received cold worked IF steel sample).

Investigation of the effects of stress on measured inductance using a U-shaped EM sensor aligned to the applied stress direction at room temperature show an increase in measured inductance of 0.45×10^{-5} H for an applied stress of 40 MPa, equivalent to an increase of 10% in the measured signal (Figure 87) compared to the initial value (as received IF steel sample).

Comparison of the percentage changes of measured inductance for each of those experiments gives an indication of the relative significance of each variable, although it isn't an ideal comparison as the output from different sensors are used and the relationship between permeability and inductance is not linear. The percentage changes in inductance caused by temperature and the recovery / recrystallisation process are similar. Temperature in a CAL will vary from room temperature to above T_c so the overall inductance change shown is relevant (in practice sensors would only be positioned at individual points on a CAL and would not see the entire temperature range). Line stress in a CAL will not vary as much as 40 MPa, reported values for line tension in a CAL are only as high as 12 MPa. Therefore the effects

of applied stress on any inductance value measured in a CAL will not be as significant as the effects of recovery, recrystallisation and temperature on inductance.

The results indicate that if EM sensors were to be placed into a continuous annealing line (such as Tata Steel's CAPL line based at Port Talbot, Wales) then the progress of recovery and recrystallisation could be monitored. Figure 88 shows a typical layout for a CAL with potential positions for deployment of EM sensors indicated. The positions where the sensors are deployed will be critical in terms of the useful feedback that they can provide as well as the factors that affect their measurements of recovery and recrystallisation. The first factor that must be considered when choosing a position for sensors is temperature. It has been shown that there is a temperature ceiling (T_c) for IF and 430SS grade steels, sensors deployed into a CAL would need to be in locations where the strip temperature is low enough for reliable EM sensor readings to be recorded.

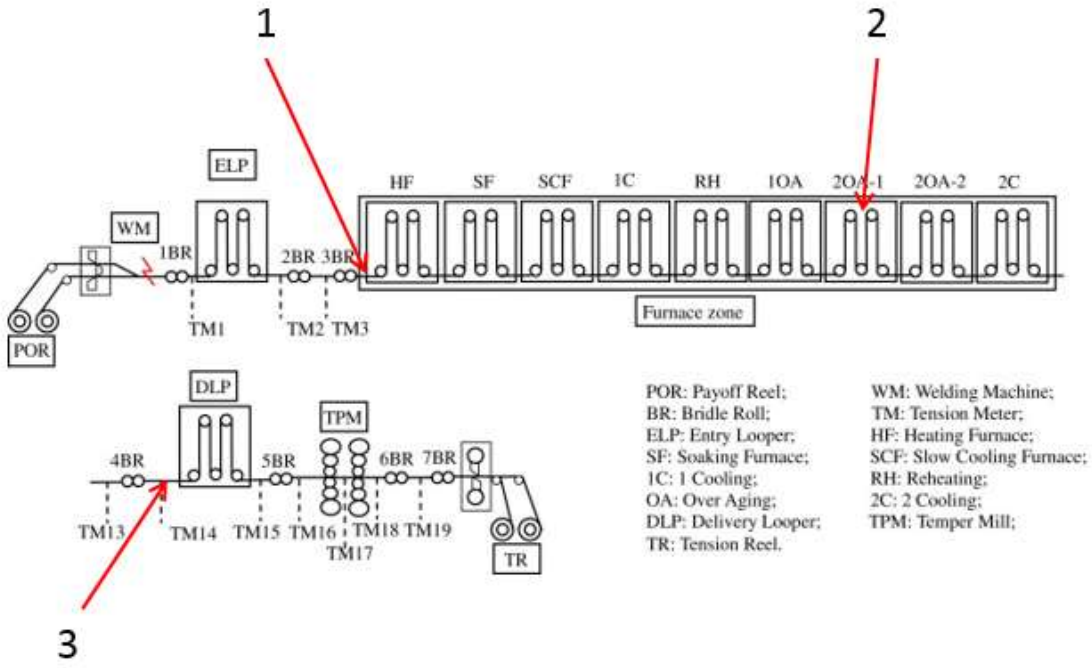

Figure 88: Typical layout of a CAL [17]. The arrows indicate positions where EM sensors could be deployed to monitor material properties.

The potential EM sensor positions shown in Figure 88 are positions where the strip would be below T_c. Position 1, at the entry to the heating furnace could be used to provide a base line inductance

measurement for the material in the cold rolled state before annealing has begun. Position 1 is a position where the strip temperature will be known (close to room temperature), or could be measured easily and also a position where the strip will not have undergone any recovery or recrystallisation (which occurs towards the centre of the heating furnace). If the sensor was positioned later in the heating furnace, which operates at 800°C then the strip may be too hot for EM measurement [25]. The furnace temperature at position 2 is around 500°C, below T_c and is a position after the maximum furnace temperature and hence when recovery / recrystallisation should have occurred. EM measurements for recovery and recrystallisation would need to be corrected for temperature at this point as it is a different temperature than position 1, a measurement at position 2 would indicate whether (full) recovery and recrystallisation had taken place. For accurate determination of recovery and recrystallisation a temperature sensor would be required to correctly measure the strip temperature. If recovery and recrystallisation had not been completed then there are still furnace banks available after the sensor which would be able to further heat the strip. A sensor at position 3 would act as a confirmation that the annealing process in the CAL had been successful and that full recovery and recrystallisation had been achieved.

It has been shown that line stress causes a change in measured inductance, and therefore permeability, it is important therefore that line tension is taken into account when positions for EM sensors in a CAL are chosen. Line tension at sensor positions 1 and 3 in Figure 88 are aligned to strip tension meters where line tension is recorded and can easily be accounted for. Line tension at position 2 would need to be inferred or assumed using the layout of the CAL shown in Figure 88 so that applied stress was considered, although the effects of line stress at position 2 would be much smaller than the effect of line temperature and may be insignificant in comparison.

It is possible to relate the measured inductance values to the relative permeability (μ_r) values at the different sensor points marked in Figure 88. This is important to consider as μ_r values are a material parameter and directly related to the material condition. The effects of stress, temperature, recovery and recrystallisation would need to combined to give values for μ_r at a measurement position in a CAL,

equation 7 shows a simple approach on how they can be combined to give an overall change in μ_r for the different parameters.

$$\mu_r = \Delta\mu_{stress} + \Delta\mu_{temp} + \Delta\mu_{recovery} + \Delta\mu_{recrystallisation} \quad (7)$$

Where μ_r is the relative permeability, $\Delta\mu_{stress}$ is the change in permeability associated with the applied stress, $\Delta\mu_{temp}$ is the change in permeability associated with temperature, $\Delta\mu_{recovery}$ is the change in permeability associated with recovery and $\Delta\mu_{recrystallisation}$ is the change in permeability associated with recrystallisation.

Using the inductance values presented in results sections 8.4 to 8.7, estimates of the variation in μ_r for the different measurement positions can be calculated by using a rearranged form of equation 6:

$$\mu_r = \frac{Ll}{N_1 N_2 \mu_o A} \quad (8)$$

Using the experimental inductance data to estimate μ_r values for the different CAL positions requires several assumptions to be made:

- There is no inter-relation between the different variables described in equation 7. This is to say that the effects of stress on μ_r are discrete and are not affected by changes in other measured variables.
- The relationship between inductance and μ_r is linear as temperature increases, whilst it is known that the relationship is non-linear [27], Figure 19, this has been used as a first approximation and reflects the relationship at lower temperatures (< 600 °C).
- That equation 8 is a reasonable descriptor of the response between inductance and permeability for the high temperature laboratory sensor and can be used to indicate the response for a sensor that would be deployed in a CAL. Whilst the absolute values of inductance will be different as the geometry, scale and position relative to the measured media will be different to the laboratory samples the relative changes can be inferred.

Approximate conditions for the IF steel strip for the different sensor positions shown in Figure 88 are shown in Table 12.

Table 12: Assumed conditions for EM sensors in CAL

	Position 1	Position 2	Position 3	Condition
Strip Tension (MPa)	12	12	12	Strip tension is constant
Temperature (°C)	25	500	25	Increased temperature at position 2
Recovery (%)	0	100	100	Recovery is complete at positions 2 and 3
Recrystallisation (%)	0	100	100	Recrystallisation is complete at positions 2 and 3

Using the conditions from Table 12 it is possible to estimate the changes in inductance that would be measured using a high temperature EM sensor like that used for this project work. The inductance values for the different conditions at the different measurement conditions are shown in Table 13. The figures shown have been calculated using recovery and recrystallisation values derived from Table 11, inductance values for temperature from Figure 78 for IF steel and strip tension values estimated from Figure 87.

Table 13: Inductance values for the different sensor measurement conditions shown in Table 13. All values for inductance are in Henrys (H)

Inductance Change	Position 1	Position 2	Position 3	Condition
Baseline values	3.8×10^{-5}	3.8×10^{-5}	3.8×10^{-5}	Cold rolled material only
Predicted inductance increase for tension	0.3×10^{-5}	0.3×10^{-5}	0.3×10^{-5}	Predicted increase for applied stress (12 MPa)
Predicted inductance increase for temperature	0	1.8×10^{-5}	0	Predicted increase for applied temperature (500°C)
Predicted inductance increase for recovery and recrystallisation	0	2.0×10^{-5}	2.0×10^{-5}	Assumes 100% recovery at positions 2 and 3
Predicted measured inductance value	4.10×10^{-5}	7.90×10^{-5}	6.10×10^{-5}	

μ_r values can then be calculated from the baseline cold rolled condition for the strip for each of the measurement positions using equation 8.

Table 14: µr values for the different sensor measurement conditions shown in Table 14.

μ_r Change	Position 1	Position 2	Position 3	Condition
Baseline values	123	123	123	Cold rolled material only
Predicted inductance increase for tension	10	10	10	Predicted increase for applied stress (12 MPa)
Predicted inductance increase for temperature	0	58	0	Predicted increase for applied temperature (500°C)
Predicted inductance increase for recovery and recrystallisation	0	65	65	Assumes 100% recovery at positions 2 and 3
Measured permeability value	133	256	198	

Figure 89 shows the cumulative estimated μ_r values from table 15 for the different measurement positions identified in Figure 88.

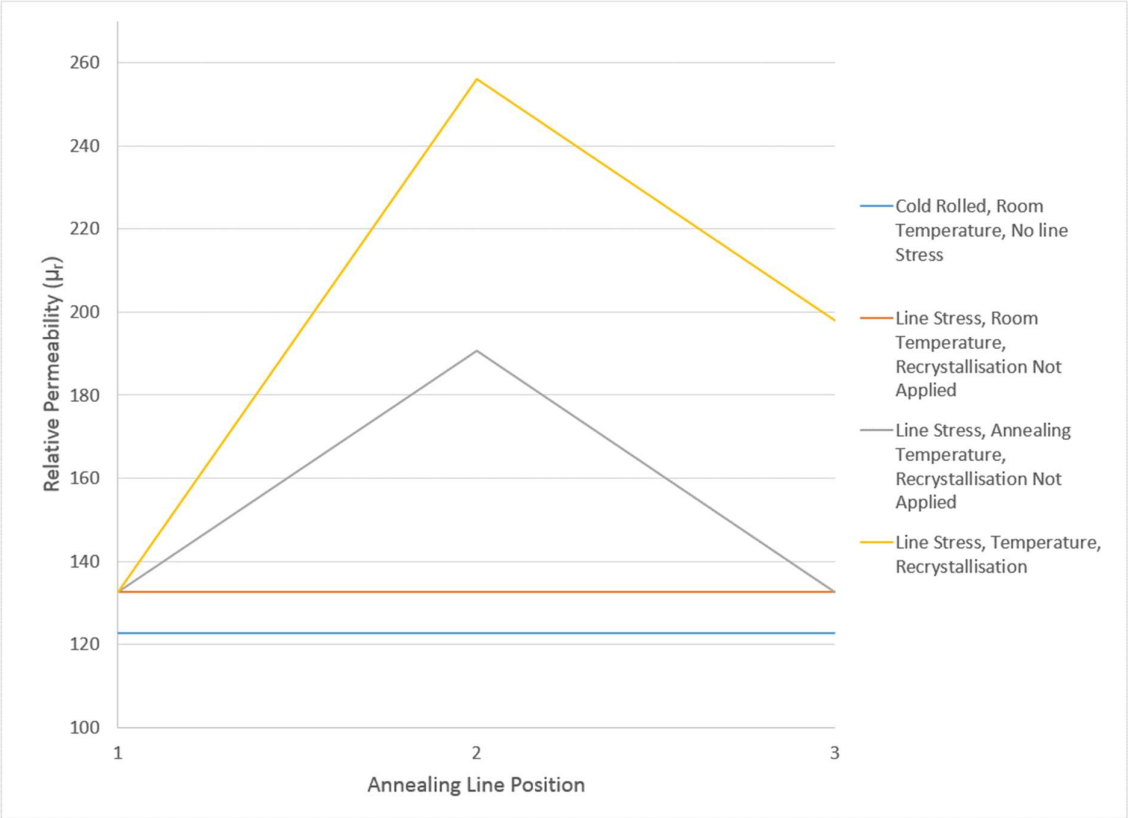

Figure 89: μ_r estimations for the EM sensor positons shown in Figure 88 for combined factors (line stress, temperature, recovery and recrystallisation) affecting the measurement values.

Figure 89 shows that if the strip passing through the CAL was not annealed, did not have applied stress or an applied temperature there would be a baseline value of μ_r which would remain unchanged throughout the length of the CAL (blue line, $\mu_r = 123$). With a line stress (tension) applied to the strip the μ_r values for the strip increase, and if no recovery or recrystallisation and no temperature changes occur the μ_r values at the measurement points remain constant (orange line, $\mu_r = 133$). The effects of temperature combined with line tension on μ_r values are shown by the grey line in Figure 89, it can be seen that μ_r increases with temperature at measurement point 2 and then decreases back to a room temperature value at measurement point 3.

The yellow line in Figure 89 shows the combined effects of all factors that can affect μ_r values through the CAL. At measurement point 1 no recovery or recrystallisation has taken place and the strip is at room temperature, the only factor affecting the μ_r value is line stress. At measurement point 2 the strip is at high temperature (~500°C), but since it has experienced the high temperature (≈ 800°C) soak it is reasonable to assume that recovery has taken place and that recrystallisation has also taken place, therefore the μ_r values are at the highest estimated value ($\mu_r = 256$). At measurement point 3 recovery and recrystallisation is complete, the strip has returned to room temperature but still has tension applied to it, so μ_r values decrease from the peak value at measurement point 2 but remain higher than the initial μ_r value estimated at measurement point 1. The increase in μ_r would show that recovery and recrystallisation had taken place.

The relationship presented between inductance and μ_r is very simplistic, it is used to show that it is possible to estimate μ_r values from measured inductance values. A significant amount of further work would be required to make the model relationship more accurate, this would need to consider the non-linear relationship between temperature and μ_r for IF steel and which includes resistivity (for full inductance-frequency relationship) as well as sensor – sample geometry (as a side note this work has already begun at the University of Warwick in association with Tata Steel Ltd and Primetals Technology Limited). Further work would also be needed to relate the sample size and position to the measurement coil for the sort of sensor that would be used in the CAL.

9. Conclusions

The main aim of this project was to show that EM sensors are responsive to the effects of recovery and recrystallisation in IF steels at high temperatures similar to those used for annealing in a Continuous Annealing Line (CAL). It was important that other factors which could affect changes in inductance measured by the EM sensor were also taken in account and that the effects of recovery and recrystallisation were distinguishable from those factors, giving confidence that an EM sensing system could be used to monitor recovery and recrystallisation successfully in-situ in an annealing environment.

Laboratory based EM sensors have been used to measure changes in microstructural state caused by recovery and recrystallisation at room temperature in IF steels; the effect that temperature has on magnetic properties (measured inductance, inferring relative permeability) in annealed IF steel and annealed 430 grade ferritic stainless steel; to monitor the progress of recovery in in-situ experiments at two different temperatures of 360°C and 420°C; to monitor the progress of recovery and recrystallisation during in-situ experiments at 650°C and 700°C; and to establish whether there is an inductance change caused by variations in tensile stress in IF steel. From the evidence presented, the main conclusions that can be made are:

- EM sensors are sensitive to changes in the microstructural state in IF steels. Samples of interstitial free steel were annealed to take them through the recovery and recrystallisation process, changing their microstructure from a cold rolled, heavily deformed microstructure with highly elongated grains and high hardness (200 HV) to a fully recrystallised, equi-axed microstructure with low hardness (82 HV). A corresponding increase in measured room temperature inductance is observed using two different kinds of EM sensor (cylindrical and U-shaped) throughout this process.

- Inductance values are affected by temperature. As the temperature of a ferromagnetic material increases so does its relative permeability and resistivity. This means that inductance values recorded at different temperatures cannot be directly related to a microstructural condition without taking into account the effect of temperature. Hence, inductance values recorded at different temperatures would need to be corrected to reflect the temperature at which they were recorded. However inductance values measured at a set temperature can be used to monitor changes in microstructural state caused by recovery and recrystallisation. It was seen that EM sensor measurements become more sensitive to changes in permeability caused by changes in material properties at higher temperatures.
- An EM sensor has been used to monitor changes in recovery and recrystallization in-situ during furnace heat treatments. Different rates of recovery were observed at two different temperatures (360°C and 420°C). Different rates of both recovery and recrystallisation were observed at two different temperatures (650°C and 700°C). Verification of the link between measured inductance and recovery and recrystallisation was completed by using optical microscopy and hardness values. It was seen that recovery causes a comparatively larger change in inductance than recrystallisation.
- Inductance values are affected by changes in the stress state of IF steel. It has been shown that as tensile stress increases there is an increase in measured inductance, this has been corroborated using strain gauges. The change in measured inductance recorded for applied stress indicates that the effects of line stress in a CAL would be significant and cannot be ignored for EM sensors deployed into a CAL.

- The effects of crystallographic texture in IF steels through the recovery and recrystallisation process were considered and compared to the effects of texture in a 3% Si steel. EM sensors were used for the measurements as well as B-H loop measurements for coercivity and remanence. For the 3% Si steel samples it was shown that texture has a clear effect on both EM sensor and B-H loop measurements for samples measured in RD, 54° to RD and TD, with higher inductance values being recorded when the magnetic easy directions are more closely aligned with the magnetic field direction, in agreement with expectations from the literature. Measurements on IF steel samples in the cold rolled condition for different orientations (RD, 45° to RD and TD) were similar with no discernible difference caused by texture. Subsequent measurements on samples using the same measurement orientations which had been annealed for 30 minutes and 60 minutes at 650°C showed an increase in measured inductance at 30 minutes for all orientations (as expected from the effect of recovery and recrystallisation on the overall inductance value) and then relative decreases in measured inductance for the 45° to RD and TD directions on further annealing to 60 minutes. B-H loop measurements for the IF samples annealed at 650°C for different times showed no significant difference in coercivity or remanence caused by measurement orientation that could be related to texture. The measurements were affected by the geometry of the IF samples used (curved or bowed samples) with different amounts of curvature being seen for the samples in different orientations. Therefore the results were inconclusive about the magnitude of the effect of texture in IF steels on the magnetic properties.

10.Future Work

The work presented in this project shows that the EM sensors are sensitive to changes in microstructure caused by recovery and recrystallisation, temperature variation and applied stress within IF steels.

CALs are used to process different types of steel, not just IF steels, therefore for an EM sensing system to be effective in a CAL environment experimental work would need to be repeated for different steel grades. The inductance change during the recovery and recrystallisation process will be different for each steel grade as each steel grade will have a different permeability – microstructure relationship because of the different microstructures. For IF steels, which are purely ferrite the inductance change from the cold rolled condition during annealing can be attributed to recovery and recrystallisation alone, for steels with more complex chemistry, which also have different phases present, the inductance response through the annealing process may not be attributed to recovery and recrystallisation alone but also due to in-situ phase change – some steels pass through the CAL in order to develop specific microstructures (e.g. dual phase steels) and there is potential for this to be monitored in-situ using high temperature EM sensors. The principle for this approach has been established by the EMSpec^{TM} system installed in the Tata Steel IJmuiden works, where the sensor is operated at room temperature but the steel is hot undergoing transformation [127, 128]. Extension of this approach to the CAL based on the work done in this project for high temperature sensors is therefore appropriate.

Analysis of the inductance response with changing temperature for different steel grades will need to be completed. The data shown in section 8.5 shows that different steel grades (IF and 430SS) have different measured inductance responses with increasing temperature. Generation of inductance change with increasing temperature curves will need to be developed so that measured inductance change (and therefore permeability) can be taken into account for sensors in different places within a CAL. For steels with different phases the inductance change measured as temperature increases will not be due to temperature alone, but also due to phase changes that occur at high temperatures. This work has begun at the University of Warwick in association with Tata Steel UK. To complete this activity then modelling of the EM sensor to allow the material properties (i.e. permeability) to be determined will be required, as the inductance value is sensor geometry dependant. FE models for EM sensors are being developed [164].

To deploy an EM sensor into a real CAL a significant amount of development work would be required. The high temperature sensor used for this project work is designed for laboratory trials and does not have a suitable configuration for deployment into a CAL. The sensor is not designed for long term use therefore a more robust construction would need to be considered. In a CAL it would not be possible to have a sensor which surrounds the strip, strip within a CAL can be up to 1.8m in width [163]. Trials with different sensor configurations at a larger scale will need to be completed to ensure that the characteristics of the inductance measurements for IF steels are similar to those presented in this project. This work has already begun at the University of Manchester in conjunction with Tata Steel Europe's research and development team. A sensor with a helical design is being considered that can fit into a housing which can withstand the harsh environment of a CAL. The different sensor designs will require optimisation, the frequency at which inductance measurements are recorded will be different than those used in this project work. In order to compare one sensor with another inductance data recorded will need to be converted to permeability for steel grade being measured. For this to be completed at different frequencies knowledge of how resistivity changes with temperature will need to be understood and combined with the understanding of the inductance changes with recovery, recrystallisation and temperature.

The experimental work presented for the effects of applied stress is limited and should be expanded to include greater stress ranges and to provide a better resolution of inductance change with applied stress in comparison to the effects on measured inductance caused by recovery, recrystallisation and temperature. It would also be useful to consider the combined effect of stress and temperature on measured inductance at annealing temperatures. This is important as it will show whether the effects of stress at annealing temperatures become more or less significant.

Further work relating measured inductance values to crystallographic texture would be required to fully quantify the effects of texture on inductance values for different grades of steel as they pass through a CAL. Electron backscatter diffraction (EBSD) can be used to measure the bulk texture in the steel samples so that it is known before inductance measurements are recorded, providing a link between the primary textures of the steel samples and measured inductance.

11 References

1. CALLISTER, W., *Materials Science and Engineering - An Introduction*. 7th Edition ed. 2007: John Wiley and Sons. 721.
2. GURRUCHAGA, K., et al., *Magnetic Barkhausen Noise for Characterization of Recovery and Recrystallization.* IEEE Transactions on Magnetics, 2010. **46**(2): p. 513-516.
3. OYARZABAL, M., et al., *Sensitivity of Conventional and Non-destructive Characterization Techniques to Recovery and Recrystallization.* ISIJ INTERNATIONAL, 2007. **47**(10): p. 1458-1464.
4. UNIVERSITY, S. *Steel Manufacturing Process*. [.jpeg] 2015 [cited 2015 24/03/2015]; Overview of Steel Manufacturing Process]. Available from: http://steeluniversity.lms.crossknowledge.com/data/content/Final/1284/222D9A74-6437-DDE4-3B95-F0C89DC9DC28/index.html#gotoExercise=1332.
5. SARNA, S.K. *Interstitial Free Steels*. 2014 13/06/2014 [cited 2016 30/03/2016]; Available from: www.ispatguru.com/interstitial-free-steels/.
6. LENARD, J., *4 - Flat Rolling – A General Discussion*, in *Primer on Flat Rolling (Second Edition)*, J.G. Lenard, Editor. 2014, Elsevier: Oxford. p. 39-55.
7. BOLJANOVIC, V., *Metal Shaping Processes*. 2009. 129 - 136.
8. EVANS, *Process Parameters Influencing Tertiary Scale Formation at a Hot Strip Mill Using a Multinomial Logit Model.* Journal of Manufacturing Science and Engineering, 2013. **135**: p. 13.
9. BIBBY, J.B.M., *Principles of Metal Manufacturing Processes*. 1999, Great Britain: Arnold. 326.
10. ASENSIO, J., et al., *Ferrtic Steels Optimisation of Hot-Rolled Textures Through Cold Rolling and Annealing.* Materials Characterization, 2001. **47**: p. 119-127.
11. SMITH, W. and J. HASHAMI, *Foundations of Material Science and Engineering*. 2011: McGrawHill. 1072.
12. LLOYD, D., *Fundamentals of Roll Cooling and Control of Flatness at Primary Cold Reduction*. 2010, Lechler Ltd.: www.lechler.de. p. 14.
13. BUSCHOW, K., et al., *Encyclopedia of Materials - Science and Technology, Volumes 1-11*. Elsevier. p. 5500 - 5506.
14. HOILE, S., *Processing and Properties of Mild Insterstitial Free Steels.* Materials Science and Technology, 2000. **16**: p. 1079 - 1093.
15. DOHERTY, R., et al., *Current Issues in Recrystallisation: A Review.* Materials Science and Engineering, 1997. **A238**: p. 219-274.
16. ARCELORMITTAL. *High Strength IF Steels*. 2015; Available from: http://automotive.arcelormittal.com/europe/products/HYTSS/IF/EN.
17. LIU, Q., T. CHAI, and S. JOEQIN, *Fault diagnosis of continuous annealing processes using a reconstruction-based method.* Control Engineering Practice, 2012. **20**(5): p. 511-518.
18. AG, S., *SIROLL MSM - microstructure monitor for hot rolling mills*. 2010, Siemens AG: Siemens Website.
19. ANDORFER, J., *Properties of Hot Rolled Strip Obtained by Calculcation or Testing - A Critical Comparison.* ECNDT, 2006: p. 15.
20. YOSHITANI, N. and A. HASEGAWA, *Model-Based Control of Strip Temperature ot the Heating Furnace in Continuous Annealing.* IEEE Transcations on Control Systems Technology, 1998. **6**(2): p. 146-156.
21. YAHIRO, K., et al. *Development of Strip Temperature Control System for a Continuous Annealing Line*. in *IECON 1993*. 1993.
22. YOSHITANI, N., *Modelling and Parameter Estimation for Strip Temperature Control in Continuous Annealing Processes*, in *IECON 1993*. 1993. p. 469-474.
23. KELLY, C., D. WATANAPONGSE, and K. GASKEY, *Application of Modern Control to a Continuous Anneal Line*, in *1987 American Control Conference*. 1988: Minneapolis.

24. SONG, S.-H. and S.-K. SUL, *A New Tension Controller for Continuous Strip Processing Line.* IEEE TRANSACTIONS ON INDUSTRY APPLICATIONS, 2000. **36**(2): p. 633-639.
25. WOO LEE, C. and K. HYUN SHIN, *Strip tension control considering the temperature change in Multi-Span systems.* Journal of Mechanical Science and Technology, 2005. **19**(4): p. 958-967.
26. QIANG, L., et al. *Modeling and gain scheduling adaptive control of tension control system for continuous annealing process*. in *Decision and Control, 2009 held jointly with the 2009 28th Chinese Control Conference. CDC/CCC 2009. Proceedings of the 48th IEEE Conference on*. 2009.
27. BOZORTH, R., *Ferromagnetism*. 1951: John Wiley and Sons Inc. 959.
28. HUMPHREYS, F. and M. HATHERLY, *Recrystallisation and Related Annealing Phenomena*. 2 ed. 2004: Elsevlier Ltd. 628.
29. LUKINA, Y., et al., *Structure of IF Steel in Continuous Annealing.* Steel in Translation, 2012. **42**(4): p. 365-367.
30. SAMAJDAR, I., et al., *Recrystallisation kinetics in IF-steel: A study on the sluggish recrystallisation behaviour.* Scripta Materialia, 1997. **37**(6): p. 869-874.
31. YE, W., R.L. GALL, and G. SAINDRENAN, *A study of the recrystallization of an IF steel by kinetics models.* Materials Science and Engineering: A, 2002. **332**(1–2): p. 41-46.
32. DŽUBINSKÝ, M., Z. HUSAIN, and W.M. VAN HAAFTEN, *Comparison of recrystallisation kinetics determined by stress relaxation, double hit, optical metallography and EBSD approaches.* Materials Characterization, 2004. **52**(2): p. 93-102.
33. PERTTULA, J. and L. KARJALAINEN, *Recrystallisation rates in austenite measured by double compression and stress relaxation methods.* Materials Science and Technology, 1998. **14**(7): p. 626-630.
34. LISSEL, L., *Modeling the microstructural evolution during hot working of C-Mn and Nb microalloyed steels using a physically based model*, in *School of Industrial Engineering and Management*. 2006, Dalarna University. p. 42.
35. LANDGRAF, G., et al., *Effect of grain size, deformation, aging and anisotropy on hysteresis loss of electrical steels.* Journal of Magnetism and Magnetic Materials, 2000. **215–216**(0): p. 97-99.
36. SONG, X.L., et al. *Effect of Micro-Alloying Elements of Ti, Nb and B on Recrystallization Behavior of Cold-Rolled Interstitial-Free Steel Sheets*. in *Materials Science Forum*. 2013. Trans Tech Publ.
37. KIZKITZA GURRUCHAGA, ANE MARTÍNEZ-DE-GUERENU, and O. ARIZTI, *Monitoring Recovery and Recrystallization in Interstitial Free (IF) Steel by Magnetic Hysteresis*, in *9 th European Conference on NonDestructive Testing (ECNDT)*. 2006: Berlin, Germany. p. 1-8.
38. AKBARI, G.H., C.M. SELLARS, and J.A. WHITEMAN, *Static restoration processes in warm rolled interstitial free steel.* Materials Science and Technology, 2002. **18**(8): p. 885-891.
39. KNOWLES, K. *Crystallographic Texture*. [Teaching and Learning Package, University of Cambridge] 2015 [cited 2016 04/05/2016]; Available from: www.doitpoms.ac.uk/tlplib/crystallogrpahic_texture/printall.php.
40. CASTRUITA ÁVILA, L.G., F. GARCIA PASTOR, and M.D.J. CASTRO ROMÁN, *Evolution of texture and microstructure during thermo-mechanical processingin ultrathin low carbon steels.* Matéria (Rio de Janeiro), 2015. **20**: p. 714-721.
41. ASHCROFT, N. and D. MERMIN, *Solid State Physics*. 1976: Brooks / Cole, Cengage Learning. 826.
42. KHATIRKAR, R. and S. KUMAR, *Comparison of recrystallization textures in interstitial free and interstitial free high strength steels.* Materials Chemistry and Physics, 2011. **127**(1–2): p. 128-136.
43. JINXIA, L., et al., *Evolution of textures in interstitial free steel during multiple cold rolling and annealing.* Journal of Materials Processing Technology, 2005. **167**(1): p. 132-137.
44. ZHOU, L., et al., *Quantification of the Effect of Changes in Steel Microstructural Parameters on EM Sensor Signals*, in *NDESAI 2011*. 2011: Jamshedpur, india. p. 208-215.

45. BURROWS, C.W., *Correlation of the magnetic and mechanical properties of steel*. Bulletin of the Bureau of Standards ;v. 13, no. 2. 1917, Washington, D.C.: U.S. Dept. of Commerce, Bureau of Standards : U.S. Govt. Print. Off. p. 173-210.
46. YAMASAKI, T., S. YAMAMOTO, and M. HIRAO, *Effect of Applied Stresses on Magnetostriction of Low Carbon Steel.* NDT&E International, 1996. **29**(5): p. 263-268.
47. JUNTUNEN, P., et al., *Optimizing continuous annealing of interstitial-free steels for improving deep drawability.* METALLURGICAL AND MATERIALS TRANSACTIONS A, 2001. **32**(8): p. 1989-1995.
48. CAREY, R. and E.D. ISAAC, *Magnetic domains and techniques for their observation*. 1966: Academic Press.
49. BANERJEE, K., *Physical Metallurgy and Drawability of Extra Deep Drawing and Interstitial Free Steels,*. 2012.
50. SHINGAKI, Y. and S. OKABE, *Influence of Crystal Orientation on Magnetic Properties in 3% Silicon Steel With Ultra-High Tension TiN Coating.* IEEE Transactions on Magnetics, 2012. **48**(4): p. 1469-1472.
51. NAVE, R. *Relative Permeability*. 2015; Available from: http://hyperphysics.phy-astr.gsu.edu/hbase/solids/ferro.html.
52. TAKAHASHI, N., et al., *Examination of Magnetic Properties of Magnetic Materials at High Temperature Using a Ring Specimen.* Magnetics, IEEE Transactions on, 2010. **46**(2): p. 548-551.
53. MORISHITA, M., et al., *Examination of Magnetic Properties of Several Magnetic Materials at High Temperature.* PRZEGLĄD ELEKTROTECHNICZNY (Electrical Review), 2011. **87**(9): p. 106-110.
54. ARA, K., *Magnetic Characteristics of Ferromagnetic Stainless Steels.* IEEE Transaction on Magnetics, 1989. **25**(3): p. 2617-2623.
55. THOMPSON, S., *The Magnetic Properties of Plastically Deformed Steels*. 1991, Durham University: Available at Durham E-Thesis Online: http://ethesis.dur.ac.uk/3600/.
56. CHEN, K., F.P. BRENNAN, and W.D. DOVER, *Non-contacting Residual Stress Decay Detecting Using Alternating Current Stress Measurement.* JOURNAL OF STRAIN ANALYSIS FOR ENGINEERING DESIGN, 2000. **35**(4): p. 227-233.
57. CHENNUPATI JAGADISH, LYNANN CLAPHAM, and D. ATHERTON, *Influence of Uniaxial Elastic Stress on Power Spectrum and Pulse Height Distribution of Surface Barkhausen Noise in Pipeline Steel* IEEE Transaction on Magnetics, 1990. **26**(3): p. 1160-1163.
58. STEFANITA, C.G., D.L. ATHERTON, and L. CLAPHAM, *Plastic versus elastic deformation effects on magnetic Barkhausen noise in steel.* Acta Materialia, 2000. **48**(13): p. 3545-3551.
59. THOMAS W. KRAUSE, ANDRAS PATTANTYUS, and D.L. ATHERTON, *Investigation of Strain Dependent Magnetic Barkhausen Noise in Steel.* IEEE Transaction on Magnetics, 1995. **30**(6): p. 3376-3378.
60. KWUN, H. and G.L. BURKHARDT, *Effects of grain size, hardness, and stress on the magnetic hysteresis loops of ferromagnetic steels.* Journal of Applied Physics, 1987. **61**(4): p. 1576-1579.
61. SIPEKY, A. and A. IVANYI, *Magnetic hysteresis under applied stress.* Physica B: Condensed Matter, 2006. **372**(1–2): p. 177-180.
62. WILSON, J.W., G.Y. TIAN, and S. BARRANS, *Residual magnetic field sensing for stress measurement.* Sensors and Actuators A: Physical, 2007. **135**(2): p. 381-387.
63. CALLISTER, W., *Magnetic Properties*, in *Materials Science and Engineering*, K. Santor, Editor. 2007, John Wiley and Sons, Inc.: USA. p. W19 - W56.
64. QIANG, L., et al. *Tension soft sensor of continuous annealing lines using cascade frequency domain observer with combined PCA and neural networks error compensation*. in *Decision and Control (CDC), 2010 49th IEEE Conference on*. 2010.
65. NAKAMICHI, H., F.J. HUMPHREYS, and I. BROUGH, *Recrystallization phenomena in an IF steel observed by in situ EBSD experiments.* Journal of Microscopy, 2008. **230**(3): p. 464-471.

66. JACQUES, N., et al., *Buckling and wrinkling during strip conveying in processing lines.* Journal of Materials Processing Technology, 2007. **190**(1–3): p. 33-40.
67. BADJI, R., et al., *Phase transformation and mechanical behavior in annealed 2205 duplex stainless steel welds.* Materials Characterization, 2008. **59**(4): p. 447-453.
68. PARKER, S., *Personal Communication - IF Steel Textures*, R. Hall, Editor. 2015. p. 1.
69. SIXTUS, K.J., *Magnetic Anisotropy in Silicon Steel.* Journal of Applied Physics, 1935. **6**(3): p. 105-111.
70. *Silicon Steels and Their Applications*. 2010 [cited 2015 28/07/2015]; Available from: http://steel.keytometals.com/articles/art101.htm.
71. EMURA, M., et al., *Angular dependence of magnetic properties of 2% silicon electrical steel.* Journal of Magnetism and Magnetic Materials, 2001. **226–230, Part 2**: p. 1524-1526.
72. HUSAIN, Z., P. MORRIS, and A. HOWE, *The Assessment of Recrystallisation in Low Carbon Alloy Steel Using Alternating Current Potential Drop (ACPD) Measurements.* Materials Science Forum, 1993. **113-115**: p. 667-672.
73. JILES, D.C. and D.L. ATHERTON, *Theory of Ferromagnetic Hysteresis.* Journal of Magnetism and Magnetic Materials, 1986. **61**(1–2): p. 48-60.
74. LIU, J., et al., *Measurement of microstructure changes in 9Cr–1Mo and 2.25Cr–1Mo steels using an electromagnetic sensor.* Scripta Materialia, 2012. **66**(6): p. 367-370.
75. HUI, Y.-J., et al., *Strain-induced Precipitation in Ti Micro-alloyed Interstitial-free Steel.* Journal of Iron and Steel Research, International, 2016. **23**(4): p. 385-392.
76. RAMIREZ-LEDESMA, A.L., et al., *Development of Al-killed/Ti stabilized steels.* Journal of Physics: Conference Series, 2015. **582**(1): p. 1-5.
77. HOU, C.-K., *The effects of grain size on the magnetic properties of fully processed, continuous-annealed low-carbon electrical steels.* IEEE Transactions on Magnetics, 1996. **32**(2): p. 471-477.
78. QIN, J., et al., *Effect of texture and grain size on the magnetic flux density and core loss of cold-rolled high silicon steel sheets.* Journal of Magnetism and Magnetic Materials, 2015. **393**: p. 537-543.
79. GOODENOUGH, J., *A Theory of Domain Creation and Coercive Force in Polycrystalline Ferromagnetics.* Physical Review, 1954. **95**(4): p. 917-932.
80. DE CAMPOS, M.F., J.C. TEIXEIRA, and F.J.G. LANDGRAF, *The optimum grain size for minimizing energy losses in iron.* Journal of Magnetism and Magnetic Materials, 2006. **301**(1): p. 94-99.
81. LANDGRAF, F.J.G., J.R.F. DA SILVEIRA, and D. RODRIGUES-JR, *Determining the effect of grain size and maximum induction upon coercive field of electrical steels.* Journal of Magnetism and Magnetic Materials, 2011. **323**(18–19): p. 2335-2339.
82. SHIN, S., R. SCHÄFER, and B.C.D. COOMAN, *Grain Boundary Penetration by Lancet Domains in Fe-3%Si Grain-Oriented Steel.* IEEE Transaction on Magnetics, 2010. **46**(9): p. 3574 - 3581.
83. LITTMANN, M.F., *Iron and silicon-iron alloys.* Magnetics, IEEE Transactions on, 1971. **7**(1): p. 48-60.
84. GURRUCHAGA, K., A. MARTINEZ-DE-GUERENU, and I. GUTIERREZ, *Sensitiveness of Magnetic Inductive Parameters for the Characterization of Recovery and Recrystallization in Cold-Rolled Low-Carbon Steel.* Metallurgical and Materials Transactions: A, 2010. **41A**: p. 985-993.
85. NDT_RESOURCE_CENTRE. *Basic Principles of Ultrasonic Testing*. 1996; Available from: https://www.nde-ed.org/EducationResources/CommunityCollege/Ultrasonics/Introduction/description.htm.
86. SCRUBY, C. and L. DRAIN, *Laser Ultrasonics*. 1990: Taylor and Francis Ltd.
87. *Basic Principles of Ultrasonic Testing*. 2015; Available from: https://www.nde-ed.org/EducationResources/CommunityCollege/Ultrasonics/Introduction/description.htm.
88. OGI, H., M. HIRAO, and T. HONDA, *Ultrasonic Attenuation and Grain Size Evaluation Using Electromagnetic Acoustic Resonance.* Journal of the Acoustical Society of America, 1995. **98**(1): p. 458-464.

89. A. MORO, C. FARINA, and F. ROSSI, *Measurement of ultrasonic wave velocity in steel for various structures and degrees of cold-working.* NDT International, 1980. **13**(4): p. 169-175.
90. B. HUTCHINSON, E. LINDH-ULMGREN, and L. CARLSON, *Application of Laser Ultrasonics to Studies or Recrystallisation and Grain Growth in Metals*, in *1st International Symposium on Laser Ultrasonics: Science, Technology and Applications*. 2008: Montreal, Canada.
91. PANDEY, J., *Study of Recrystallization in Interstitial Free (IF) Steel by Ultrasonic Techniques.* Materials and Manufacturing Processes, 2011. **26**(1): p. 147-153.
92. KRUGER, S., et al., *In-Situ, Laser-Ultrasonic Monitoring of the Recrystallization of Aluminum Alloys.* Materials Science Forum, 2003. **426-432**: p. 483-488.
93. B. HUTCHINSON, et al., *Online characterisation of steel structures in hot stripmill using laser ultrasonic measurements.* Journal of Ironmaking and Steelmaking, 2002. **29**(1): p. 77 - 80.
94. LAMOUCHE, G., et al. *Laser Ultrasonic Characterization of the Annealing Process of Low-Carbon Steel*. in *Review of Progress in Quantative Nondestructive Evaluation*. 2003. Bellingham, Washington (USA).
95. A. SMITH, et al., *Laser-ultrasonic monitoring of ferrite recovery in ultra low carbon steel.* Materials Science and Engineering: A, 2007. **458**(1–2): p. 391-401.
96. HEDIN, A., et al., *Laser-Ultrasonics for Microstructure Characterisation On-Line in Steel Processing*, in *1st International Symposium on Laser Ultrasonics: Science, Technology and Applications*. 2008: Montreal, Canada.
97. YONGTAO, Z., et al., *Quantitative carbide analysis using the Rietveld method for 2.25Cr–1Mo–0.25V steel.* Materials Characterization, 2009. **60**(9): p. 953-956.
98. BÉNÉTEAU, A., et al., *Tempering of a martensitic stainless steel: Investigation by in situ synchrotron X-ray diffraction.* Acta Materialia, 2014. **81**(0): p. 30-40.
99. DUNN, C.G. and E.F. KOGH, *Comparison of dislocation densities of primary and secondary recrystallization grains of Si-Fe.* Acta Metallurgica, 1957. **5**(10): p. 548-554.
100. CASTELNAUA, O., et al., *Dislocation density in single grains of steel by X-ray scanning microdiffraction.* Nuclear Instruments and Methods in Physics Research A, 2001. **467-468**: p. 1245-1248.
101. SCHINO, A.D., J.M. KENNY, and G.ABBRUZZESE, *Analysis of the recrystallization and grain growth processes in AISI 316 stainless steel.* Journal of Materials Science, 2002. **37**(24): p. 5291-5298.
102. ZHAO, H., et al., *Experimental study of deep drawability of hot rolled IF steel.* Journal of Materials Processing Technology, 2002. **128**(1–3): p. 73-79.
103. WANG, Z.-D., et al., *Effect of Processing Condition on Texture and Drawability of a Ferritic Rolled and Annealed Interstitial-Free Steel.* Journal of Iron and Steel Research, International, 2006. **13**(6): p. 60-65.
104. JANG, D.Y., et al., *Surface residual stresses in machined austenitic stainless steel.* Wear, 1996. **194**(1–2): p. 168-173.
105. SATO, S., et al., *Relationship between dislocations and residual stresses in cold-drawn pearlitic steel analyzed by energy-dispersive X-ray diffraction.* Materials Characterization, 2013. **83**(0): p. 152-160.
106. KOPINECK, H.-J., R. LOFFEL, and H.-B. OTTEN, *Industrial On-line Texture Determination in Rolled Steel Strips.* Journal of Nondestructive Evaluation, 1993. **12**(1).
107. KOPINECK, H.J., *Industrial Application of On-line Texture Measurement*, in *Nondestructive Characterization of Materials*, P. Höller, et al., Editors. 1989, Springer Berlin Heidelberg. p. 740-752.
108. JENSEN, D.J., et al., *X-ray microscopy in four dimensions.* Materials Today, 2006. **9**(1–2): p. 18-25.
109. OFFERMAN, S., et al., *Solid-state phase transformations involving solute partitioning: modeling and measuring on the level of individual grains.* Acta Materialia, 2004. **52**(16): p. 4757-4766.

110. BUNGE, H.J., *On-line determination of texture-dependent materials properties.* Journal of Nondestructive Evaluation, 1993. **12**(1): p. 3-11.
111. YALE. *Environmental Health and Safety - X-Ray Diffraction Safety Information*. 2014 12/12/2014; Available from: http://ehs.yale.edu/training/x-ray-diffraction-safety.
112. DURIN, G. and S. ZAPPERI, *Chapter 3 - The Barkhausen Effect*, in *The Science of Hysteresis*, G.B.D. Mayergoyz, Editor. 2006, Academic Press: Oxford. p. 181-267.
113. O'SULLIVAN, D., et al., *Characterisation of ferritic stainless steel by Barkhausen techniques.* NDT & E International, 2004. **37**(6): p. 489-496.
114. BUTTLE, D.J., V. MOORTHY, and B. SHAW, *Measurement Good Practice Guide No.88 - Determination of Residual Stresses by Magnetic Methods*. 2006, National Physics Laboratory. p. 56.
115. STUPAKOV, O. and Y. MELIKHOV, *Influence of Magnetizing and Filtering Frequencies on Barkhausen Noise Response.* Magnetics, IEEE Transactions on, 2014. **50**(4): p. 1-4.
116. BLAOW, M., J.T. EVANS, and B.A. SHAW, *Magnetic Barkhausen noise: the influence of microstructure and deformation in bending.* Acta Materialia, 2005. **53**(2): p. 279-287.
117. STEFANITA, C.G., *Barkhausen Noise as a Magnetic Nondestructive Testing Technique*, in *From Bulk to Nano: The Many Sides of Magnetism*, C.-G. Stefanita, Editor. 2008, Springer Berlin Heidelberg: Berlin, Heidelberg. p. 19-40.
118. STRESSTECH. *Barkhausen Noise grinding burn and heat treatment defect testing equipment*. [cited 2016 27/01/2016]; Available from: http://www.stresstechgroup.com/content/en/1034/1050/Barkhausen%20Noise%20grinding%20burn%20and%20heat%20treat%20defect%20testing%20equipment.html.
119. WILCOX, M. and T. MYSAK, *An Introduction to Barkhausen Noise and its Applications*. 2004, Insight NDT Equipment Ltd. p. 19.
120. DICKINSON, S.J., et al. *The Development of a Multi-frequency Electromagnetic Instrument for Monitoring the Phase Transformation of Hot Strip Steel*. in *Instrumentation and Measurement Technology Conference, 2005. IMTC 2005. Proceedings of the IEEE*. 2005.
121. ANGLADA-RIVERA, J., L.R. PADOVESE, and J. CAPÓ-SÁNCHEZ, *Magnetic Barkhausen Noise and hysteresis loop in commercial carbon steel: influence of applied tensile stress and grain size.* Journal of Magnetism and Magnetic Materials, 2001. **231**(2–3): p. 299-306.
122. NG, D.H.L., et al., *Study of microstructure, mechanical properties, and magnetization process in low carbon steel bars by Barkhausen emission.* Materials Science and Engineering: A, 2003. **358**(1–2): p. 186-198.
123. AMIR ANSARIPOUR, HOSSEIN MONAJATIZADEH, and J. AMIGHIAN, *Effect of Isothermal Annealing on the Magnetic Properties of Cold-Rolled Low-Carbon Steel with Magnetic Hysteresis Loop Measurements.* Materials and Technology. **48**(3): p. 367-371.
124. YU. LUKIN, et al., *Structure of IF Steel in Continuous Annealing.* Steel in Translation. **42**(4): p. 365-367.
125. DEGAUQUE, J., et al., *Influence of the grain size on the magnetic and magnetomechanical properties of high-purity iron.* Journal of Magnetism and Magnetic Materials, 1982. **26**(1–3): p. 261-263.
126. L. ZHOU, et al., *Magnetic NDT for Steel Microstructure Characterisation – Modelling the Effect of Ferrite Grain Size on Magnetic Properties*, in *WCNDT*. 2016: Munich, Germany.
127. H. YANG, et al., *In-Line Quantitative Measurement of Transformed Phase Fraction by EM Sensors during Controlled Cooling on the Run-Out Table of a Hot Strip Mill* in *WCNDT*. 2016.
128. ZHU, W., et al., *Development and deployment of online multifrequency electromagnetic system to monitor steel hot transformation on runout table of hot strip mill.* Ironmaking & Steelmaking, 2014. **41**(9): p. 685-693.
129. AVRAMI, M., *Kinetics of Phase Change. I General Theory.* The Journal of Chemical Physics, 1939. **7**(12): p. 1103-1112.

130. STOLZENBERG, M., et al., *EUR 25879 — Online material characterisation at strip production (OMC)*. 2013, European Comission. p. 168.
131. HERRMANN, K. and M. IRLE, *Flat-Rolled Steel Processes: Advanced Technologies*. 2009: CRC Press.
132. PARKER, S., *Personal Communication - IF Sample 4201200*, R. Hall, Editor. 2013, Tata Steel UK. p. 1.
133. NIROSTA, T., *Inspection Certificate*. 2012, THYSSENKRUPP. p. 1.
134. PARKER, S., *Personal Communication - Silicon Steel - Chemical Composition*, R. Hall, Editor. 2015: Tata Steel UK. p. 1.
135. STRUERS, *Metalog Guide*. 1992: Struers. 113.
136. ZWICK, *Product Information Vickers Hardness Tester 5030 / 6030*. 2013, Zwick / Roell: Zwick Website. p. 2.
137. ASSOCIATION, W.S. *STEEL UNIVERSITY - MET0201210. Measurement of Grain Size*. Ferrous Metallurgy 2009 [cited 2013; Available from: https://steeluniversity.lms.crossknowledge.com/candidat/product_sheet.php?trainingcontent_id=531&registration_id=16741&step_id=473.
138. ZHOU, L., *Non-Destructive Characterisation OF Steel Microstructures Using Electromagnetic Sensors*, in *School of Metallurgy and Materials*. 2014, University of Birmingham (UK). p. 239.
139. HAO, X.J., et al., *Off-line measurement of decarburization of steels using a multifrequency electromagnetic sensor.* Scripta Materialia, 2008. **58**(11): p. 1033-1036.
140. SOLARTRON. *SOLARTRON ANALYTICAL - Software Downloads*. 2012 2012 [cited 2013; Software downloads for control of Solartron frequency analysers]. Available from: www.solartronanalytical.com/downloads/index.aspx.
141. DAVIS, C., M. STRANGWOOD, and A. PEYTON, *Overview of Non-Destructive Evaluation of Steel Microstructures Using Multifrequency Electromagnetic Sensors.* Ironmaking and Steelmaking, 2011. **38**(7): p. 510-517.
142. HILL, R.J. and D.C. CARPENTER, *Modelling of nonlinear rail impedance in AC traction power systems.* IEEE Transactions on Power Delivery, 1991. **6**(4): p. 1755-1761.
143. BARDES, B., *Metals Handbook, Volume 1: Properties and Selection: Irons and Steels*. 9 ed, ed. H. Baker. Vol. 1: Properties and Selection: Irons and Steels. 1978: American Society for Metals. 793.
144. BONIARDI, M. and A. CASAROLI, *Stainless Steels*. 2014, Politecnico Di Milano: Lucefin S.p.A., I-25040 Esine (Brescia) Italy. p. 232.
145. ZHOU, H., *Effect of Stress on Relative Permeability and EM Sensor Measurements*, in *Department of Metallurgy and Materials*. 2012, University of Birmingham. p. 39.
146. ZHOU, L., *EM Sensor Model*, R. Hall, Editor. 2016: University of Birmingham. p. 1.
147. HUANG, S., et al., *Study on the lift-off effect of EMAT.* Sensors and Actuators A: Physical, 2009. **153**(2): p. 218-221.
148. MORRIS, P.R. and J.W. FLOWERS, *Texture and Magnetic Properties.* Texture of Crystalline Solids, 1981. **4**(3): p. 129-141.
149. LIU, J., et al., *Magnetic characterisation of microstructural feature distribution in P9 and T22 steels by major and minor BH loop measurements.* Journal of Magnetism and Magnetic Materials, 2016. **401**: p. 579-592.
150. BARNETT, M.R. and L. KESTENS, *Formation of {111}<110> and {111<112> Textures in Cold Rolled and Annealed IF Sheet Steel.* ISIJ International, 1999. **39**(9): p. 923-929.
151. SUHARTO, J. and Y. KO, *Annealing Behavior of Severely Deformed IF Steel via the Differential Speed Rolling Method.* Materials Science and Engineering: A, 2012. **558**: p. 90-94.
152. CAPDEVILA, C., et al., *Influence of Microalloying Elements on Recrystallization Texture of Warm-Rolled Interstitial Free Steels.* MATERIALS TRANSACTIONS, 2010. **51**(4): p. 625-634.
153. ASM_INTERNATIONAL, *Practical Induction Heat Treating*, in *Theory of Heating by Induction*. 2001, ASM International: www.asminternational.org. p. 10.

154. ZHOU, L., *Personal Email - High Temperature Cylindrical Sensor Field Strength*, R. Hall, Editor. 2016: Tata Steel. p. 1.
155. SUN, Y., D. NIU, and J. SUN. *Temperature and carbon content dependence of electrical resistivity of carbon steel*. in *2009 4th IEEE Conference on Industrial Electronics and Applications*. 2009.
156. WARD, M.R., *Electrical Engineering Science*. 1971: McGraw-Hill.
157. ARA, K., *Magnetic characteristics of ferromagnetic stainless steels.* Magnetics, IEEE Transactions on, 1989. **25**(3): p. 2617-2623.
158. GROUP, L., *AISI 430MFo Datasheet*. 2012: Lucefin Group Website. p. 1.
159. YIN, W., et al., *Exploring the relationship between ferrite fraction and morphology and the electromagnetic properties of steel.* Journal of Materials Science, 2007. **42**(16): p. 6854-6861.
160. HOSFORD, W., *Physical Metallurgy*. 2nd Edition ed. 2010: CRC Press, Taylor and Francis Group, LLC.
161. MARTINEZ-DE-GUERENU, A., K. GURRACHAGA, and F. ARIZTI, *Nondestructive Characterization of Recovery and Recrystallization in Cold Rolled Low Carbon Steel by Magnetic Hysteresis Loops.* Journal of Magnetism and Magnetic Materials, 2007. **316**(7): p. 842-845.
162. RUI, B., et al. *Modeling and simulation of the strip tension in bridle roll of the continuous annealing line*. in *Control Conference (CCC), 2011 30th Chinese*. 2011.
163. SMITH, A., *Personal Communication - CAPL line tension*, R. Hall, Editor. 2015, Tata Steel UK. p. 1.
164. ZHOU, L., et al., *Quantification of the phase fraction in steel using an electromagnetic sensor.* NDT & E International, 2014. **67**: p. 31-35.

Appendix 1: Error Budget for Room Temperature EM Sensor Measurements

U-shape Sensor Measurements	**Error (%) +/-**	**Probability Distribution**	**Divisor**	**Standard Uncertainty (%)**
Error for Solartron	0.1	Assumed normal	1	0.1
Variability of repeated measurement at a single point on the same sample	0.5	Normal	1	0.5
Multiple samples repeatability error for as received and heat treated samples	3.5	Normal	1	3.5
Uncertainty error at room temperature measurements	3	Normal	2	1.5
Standard uncertainty for U-shaped sensor measurements				5.6

Cylindrical Sensor Measurements	**Error (%) +/-**	**Probability Distribution**	**Divisor**	**Standard Uncertainty (%)**
Sample location error	1.3	Normal	1	1.3
Signal error due to thermocouples on sample at room temperature	0.02	Normal	1	0.02
Uncertainty error at room temperature measurements	3	Normal	2	1.5
Standard uncertainty for measurements at room temperature				2.82